

**TENSILE-FLEXURAL BEHAVIOUR OF CARBON-FIBRE REINFORCED
POLYMER (CFRP) PRESTRESSING TENDONS SUBJECTED TO
HARPED PROFILES**

by

Trevor George Quayle

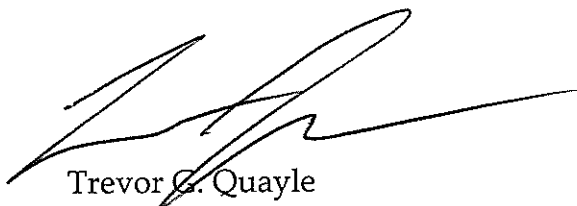
A thesis
presented to the University of Waterloo
in fulfillment of the
thesis requirement for the degree of
Master of Applied Science
in
Civil Engineering

Waterloo, Ontario, Canada, 2005

© Trevor George Quayle 2005

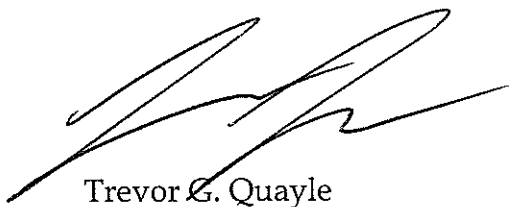
I hereby declare that I am the sole author of this thesis.

I authorize the University of Waterloo to lend this to other institutions or individuals for the purpose of scholarly research.



Trevor G. Quayle

I further authorize the University of Waterloo to reproduce this thesis by photocopying or by other means, in total or in part, at the request of other institutions or individuals for the purpose of scholarly research.



Trevor G. Quayle

ABSTRACT

External post-tensioning can provide an effective structural reinforcement system for the design of new concrete structures and for the strengthening of existing structures. In most cases, the structural effectiveness of the external tendon is increased by using a deviated or harped tendon profile. Carbon-fibre reinforced polymer (CFRP) reinforcement has emerged as an alternative to steel because it is non-corroding and fatigue resistant. However, its use in external post-tensioning has been limited due to a lack of knowledge regarding the tensile-flexural behaviour of the tendons under typical harped profiles. Limited test data has shown a reduction in the tendon capacity resulting from the combination of tensile and flexural stresses at the deviator locations. Existing models for predicting the capacity of a deviated tendon appear to be either unconservative or excessively conservative, limiting the application of CRFP tendons as external post-tensioning.

This thesis describes an experimental research study of the tensile-flexural behaviour of post-tensioned CFRP tendons subjected to harped profiles. The program studied the effect of tendon size, deviator size and harping angle on the tendon behaviour. The tendons were loaded to failure in a specially designed tension frame that accommodated a range of harped configurations. Both the flexural and overall behaviour of the tendon were observed and recorded throughout the tests. The experimental data illustrates the effect of harping variables on the tendon response and capacity, and reveals the potential for different failure modes dependent on the combination of variables. A comparison of the test data with existing analytical and design equations shows poor correlation between the predicted and measured values. The research program clearly points out the

inadequacies of the current analytical models and the need for an analytical model that more accurately predicts the tensile capacity of deviated CFRP tendons.

A primary and an extended model were developed within the research program based on the material properties and geometry of the tendon and structural mechanics. The new models were found to perform very well and were used to develop design equations for the reduced tensile strength of harped CFRP tendons as well as failure mode control guidelines for the avoidance of undesirable failure modes.

ACKNOWLEDGEMENTS

I would like to give my sincerest thanks and gratitude to my supervisors, Dr. J. S. West and Dr. K. Soudki from Civil Engineering at the University of Waterloo, for their guidance during the research program. I would also like to thank the Civil Engineering Laboratory, Engineering Machine Shop and Student Machine Shop technicians for all their assistance and expertise. Additional help and support from my fellow graduate students was greatly appreciated, especially Adil Al-Mayah for his expertise on anchorages for CFRP tendons.

Financial assistance for this research program was provided by the Natural Sciences and Engineering Research Council of Canada (NSERC) through an Industrial Postgraduate Scholarship (IPS), sponsored by Larry McCuaig and Canadian Construction Controls Ltd. of Breslau, Ontario. Additional financial assistance was provided through research funding from Dr. West and Dr. Soudki.

I would finally like to thank my family for their patience and support.

To Géraldine and Lochlainn

TABLE OF CONTENTS

Abstract	iii
Acknowledgements	v
Table of Contents	vii
List of Tables.....	xi
List of Figures	xii
1 Introduction	1
1.1 General.....	1
1.2 Objectives	2
1.3 Thesis Arrangement	2
2 Background and Literature Review	4
2.1 Introduction	4
2.2 Prestressed Concrete.....	4
2.3 Fibre Reinforced Polymer (FRP) Tendons.....	6
2.3.1 FRP as Harped External Prestressing Tendons	11
2.3.2 Analytical Models for Harped FRP Prestressing Tendons	15
2.3.2.1 JSCE.....	15
2.3.2.2 Ahmad et al.....	17
2.3.2.3 Gilstrap et al.....	19
2.4 Summary	20
3 Experimental Program.....	22
3.1 Introduction	22
3.2 Test Program.....	22
3.2.1 Test Program - Phase I.....	23
3.2.2 Test Program - Phase II	24

3.3	Test Specimen	24
3.3.1	CFRP Tendon.....	24
3.3.2	Material Properties	25
3.4	Test Setup	26
3.4.1	Test Frame.....	26
3.4.2	Deviators	28
3.4.3	Anchorage System	29
3.4.4	Safety Precautions.....	30
3.5	Instrumentation and Data Acquisition	32
3.5.1	Instrumentation.....	32
3.5.1.1	Load Cells.....	32
3.5.1.2	Tilt Sensors	32
3.5.1.3	LVDT.....	33
3.5.1.4	Strain Gauges.....	33
3.5.2	Data Acquisition.....	33
3.5.2.1	Hardware	33
3.5.2.2	Software.....	34
3.6	Test Procedure.....	35
3.6.1	Specimen Preparation.....	35
3.6.2	Specimen Installation	35
3.6.3	Load Testing	36
4	Experimental Data and Discussion	37
4.1	Introduction	37
4.2	Experimental Test Results.....	37
4.2.1	Observed Modes of Failure	37
4.2.2	Experimental Test Results.....	40
4.3	Discussion of Experimental Results	41
4.3.1	Observed Effect of Harping Configuration Variables	42

4.3.2	Comparison with Existing Analytical Models.....	43
5	Analytical Model.....	49
5.1	Introduction	49
5.2	Primary Analytical Model	49
5.2.1	Tendon Properties.....	50
5.2.2	Harping Profile Geometry	51
5.2.3	Axial Stress and Strain.....	51
5.2.3.1	Tension Stress and Strain	52
5.2.3.2	Bending Stress and Strain	52
5.2.3.3	Total Axial Stress and Strain	54
5.2.4	Radius of Curvature	54
5.2.5	Tendon Failure Criterion and Model Solution	57
5.2.6	Primary Model Solution Characteristics.....	60
5.3	Transition Effects and Inter-laminar Shear Deformation.....	63
5.4	Equivalent Spring Frame Model.....	65
5.4.1	Matrix Stiffness Method.....	68
5.4.1.1	Matrix of Unknown Displacements	69
5.4.1.2	Matrix of Fixed-End Moments	71
5.4.1.3	Stiffness Matrix.....	74
5.4.1.4	Solution for Unknown Displacements and Top Fibre Strain	77
5.4.2	Computation of Spring Constants.....	77
5.4.2.1	Linear Spring	78
5.4.2.2	Rotational Spring	80
5.4.3	Characteristics of Equivalent Spring Frame Model	81
5.4.4	Simplification of Equivalent Spring Frame Model Solution.....	86
5.4.5	Extended Analytical Model: Incorporation of Transition Effects	91
5.5	Comparison of Models with Experimental Data.....	93
5.6	Summary	97

6	Failure Mode	99
6.1	Introduction	99
6.2	Failure Mode Significance	99
6.3	Bending-Compression Failure	100
6.4	Bending-Shear Failure	108
7	Strength Design Recommendations.....	113
7.1	Introduction	113
7.2	Harping Configuration and Material Property Variables.....	113
7.3	Minimum Radius of Curvature	115
7.4	Deviator Design.....	115
7.5	Effective Harping Angle	116
7.6	Harped Tendon Tensile Capacity Reduction.....	119
7.7	Failure Mode Control	120
7.7.1	Bending-Compression Failure	120
7.7.2	Bending-Shear Failure	122
7.8	Design Procedure.....	124
7.9	Design Examples.....	124
7.9.1	Design Example 1.....	125
7.9.2	Design Example 2.....	135
8	Conclusions and Recommendations	139
8.1	Introduction	139
8.2	Conclusions.....	140
8.3	Recommendations.....	143
Appendix A: Shop Fabrication Drawings for Test Frame.....		145
Appendix B: Failure Data for Configurations with Multiple Specimens		153
References.....		154

LIST OF TABLES

Table 2-1: General Properties and Commercial Availability of FRP Types	8
Table 2-2: Typical Material Properties of FRP and Steel Reinforcing.....	9
Table 2-3: Effect of Harping Angle and Cushioning on CFCC 1x7 Tendons	14
Table 2-4: Effect of Harping Angle and Torsion on CFRP Tendons.....	15
Table 3-1: Test Program Phase I Variable Matrix	23
Table 3-2: Test Program Phase II Variable Matrix.....	24
Table 3-3: Hughes Brothers Aslan 200 Published Properties	25
Table 3-4: Guaranteed Material Properties versus Maximum Tested Properties.....	26
Table 4-1: Experimental Test Failure Stress and Mode	40
Table 5-1: Evaluation of the Influence of Transition Effects on Tensile Capacity	92
Table 5-2: Evaluation of Expected Deviance of Normalised Failure Levels.....	95
Table 6-1: Experimental Test Failure Levels For Compression and Shear Failures .	100
Table 6-2: Maximum Compressive Strain for Test Specimens	106
Table 6-3: Comparison of Compression Failure Guidelines to Test Data.....	107
Table 6-4: Maximum Longitudinal Shear Strain for Test Specimens	109
Table 6-5: Comparison of Shear Failure Guidelines to Test Data	111
Table B-1: Failure Data for Harping Configurations with Multiple Specimens	153

LIST OF FIGURES

Figure 2-1: Harped Prestressing Configurations.....	5
Figure 2-2: External Prestressing Being Used to Strengthen a Concrete Bridge.....	6
Figure 2-3: Tensile Stress-Strain Curves for FRP and Steel Tendons (Pisaniu, 1998) ..	9
Figure 2-4: Effect of Combined Axial Stresses on Harped Tendons.....	13
Figure 2-5: Test Data for JSCE Regression Equation (JSCE, 1997)	17
Figure 3-1: Configuration Variables	23
Figure 3-2: CFRP Tendon Specimen.....	25
Figure 3-3: Test Frame Schematic	27
Figure 3-4: Test Frame as Constructed.....	27
Figure 3-5: Deviator Geometric Properties.....	28
Figure 3-6: Fabricated Deviators.....	29
Figure 3-7: Anchorage System Components.....	30
Figure 3-8: Safety Enclosure	31
Figure 3-9: Anchorage Restraining Mechanism	31
Figure 3-10: Instrumentation Arrangement	32
Figure 3-11: DAQ Interface.....	34
Figure 3-12: Pre-seating Rig.....	36
Figure 4-1: Illustration of Tensile-Flexural Failure Modes.....	37
Figure 4-2: Strain-Load Plot Illustrating Failure Modes.....	39
Figure 4-3: Effect of Harping Angle on Tensile Capacity	42
Figure 4-4: Effect of Deviator Size on Tensile Capacity.....	43

Figure 4-5: Correlation Plot for JSCE Model Using Characteristic Strength	44
Figure 4-6: Correlation Plot for JSCE Model Using Design Strength	45
Figure 4-7: Correlation Plot for Gilstrap Model	46
Figure 4-8: Correlation Plot for Ahmad Model with Increased Strain Capacity	46
Figure 4-9: Correlation Plot for Ahmad Model with Guaranteed Strain Capacity	47
Figure 5-1: Assumed General Tendon Profile.....	51
Figure 5-2: Axial Stress and Strain Distribution across Tendon Cross Section.....	51
Figure 5-3: Curved Section of CFRP Tendon	53
Figure 5-4: Bending Moment Arm.....	55
Figure 5-5: Predicted Failure Level vs. Harping Angle.....	61
Figure 5-6: Predicted Failure Level vs. Deviator Radius.....	62
Figure 5-7: Top Fibre Bending Stress Distribution under Elastic Bending Theory	63
Figure 5-8: Top Fibre Bending Stress Distribution with Transition Effects.....	64
Figure 5-9: Equivalent Spring Frame Model.....	65
Figure 5-10: Elemental Representation in Equivalent Spring Frame Model.....	66
Figure 5-11: Spring Frame Model Element Variables	67
Figure 5-12: Reaction Forces Acting on Element n	69
Figure 5-13: Kinematically Determinate Fixed-End Primary Structure.....	71
Figure 5-14: Typical Element in Curved Segment of Fixed-End Primary Structure ..	71
Figure 5-15: Transition Point Element of Fixed-End Primary Structure.....	72
Figure 5-16: Typical Element in Straight Segment of Fixed-End Primary Structure .	73
Figure 5-17: Reconfigured Determinate Fixed-End Primary Structure	74
Figure 5-18: Unit Displacement at Typical Element	75

Figure 5-19: End Conditions of a Spring Frame System with i Elements	76
Figure 5-20: Representation of Linear Spring	78
Figure 5-21: Representation of Rotational Spring	80
Figure 5-22: Typical Top-Fibre Axial Bending Strain Distribution along Tendon	82
Figure 5-23: Effect of Transition Point Location on Bending Strain Distribution.....	83
Figure 5-24: Effect of Transition Point Location on Maximum Bending Strain.....	84
Figure 5-25: Effect of Harping Variables on Top Fibre Strain Distribution.....	85
Figure 5-26: Typical Out-of-Plane Rotation along Harped Tendon	86
Figure 5-27: Simplifying the Equivalent Spring Frame Model – Stage 1 and 2	88
Figure 5-28: Simplifying the Equivalent Spring Frame Model – Stage 3 and 4	88
Figure 5-29: Simplifying the Equivalent Spring Frame Model – Stage 5 and 6	89
Figure 5-30: Model vs. Experimental Data for Varying Harping Angle.....	94
Figure 5-31: Model vs. Experimental Data for Varying Deviator Size.....	94
Figure 5-32: Correlation Plot for Primary Analytical Model	96
Figure 6-1: Typical Load History Graph for a Harped CFRP Tendon	102
Figure 7-1: Harping Configuration Variables	113
Figure 7-2: Minimum Tendon Radius of Curvature	115
Figure 7-3: Deviator Design.....	116
Figure 7-4: Bending Stress and Strain Distribution Along Tendon At Deviator	117
Figure 7-5: Effective Harping Angle for Single Harped Tendon	118
Figure 7-6: Effective Harping Angle for Double Harped Tendon	118
Figure 7-7: Flowchart for Design Procedure	124
Figure 7-8: Initial Harping Configuration for Design Example 1	125

Figure 7-9: Strain vs. Loading Graph for Design Example 1	127
Figure 7-10: Strain vs. Loading Graph with Increased Deviator Size	130
Figure 7-11: Harping Configuration for Design Example 1 - Alternative 2	131
Figure 7-12: Strain-Loading Graph with Decreased Effective Harping Angle	135
Figure 7-13: Initial Harping Configuration for Design Example 2	135
Figure 7-14: Strain vs. Loading Graph for Design Example 2	138
Figure A-1: Anchor Pivot Axle Fabrication.....	146
Figure A-2: Anchor Pivot Base Fabrication	147
Figure A-3: Deviator Forks Fabrication	148
Figure A-4: Main Beam Fabrication	149
Figure A-5: Deviator Fabrication.....	150
Figure A-6: Anchor Pivot Assembly	151
Figure A-7: Deviator Fork Assembly	152

1 INTRODUCTION

1.1 GENERAL

External post-tensioning can be used as an effective reinforcement system for the design of new structures and for the strengthening of existing structures. Carbon fibre reinforced polymer (CFRP) reinforcement presents a promising alternative to steel in external prestressing applications because of its high strength-to-weight ratio, and high resistance to corrosion and fatigue. CFRP tendons also have the additional benefit of being non-metallic, which can be useful for construction in magnetically sensitive environments, such as hospitals housing MRI machines.

The use of CFRP tendons in external post-tensioning has been limited because of a lack of knowledge regarding the tensile-flexural behaviour of the tendons when used in the harped or deviated configuration typical of external post-tensioning applications. Limited test data has shown a reduction in the tendon capacity that results from the combination of axial and flexural tension stresses at the deviator locations exceeding the tensile capacity of the CFRP materials. Existing models for predicting the capacity of deviated tendons appear to be either unconservative or excessively conservative, limiting the application of CFRP tendons for external post-tensioning in harped configurations. Thus, although CFRP pre-stressing tendons are commercially available, structurally efficient and cost-effective deviated CFRP tendon systems are needed to exploit the benefits of CFRP materials and better facilitate their acceptance as an alternative to steel reinforcing in external post-tensioning applications in concrete construction and rehabilitation. A key aspect to developing these systems is gaining a better understanding of the tensile-flexural behaviour of CFRP tendons, including development of accurate models for

predicting the failure capacity of a deviated tendon and associated design guidelines.

1.2 OBJECTIVES

The overall objective of this research program is to investigate the behaviour of carbon fibre reinforced polymer (CFRP) tendons when placed in externally prestressed harped configurations (tensile-flexural behaviour). This objective will be achieved by:

- 1) Experimentally investigating the tensile-flexural and failure behaviour of CFRP tendons under various harping configurations,
- 2) Deriving analytical models that can predict the tensile-flexural behaviour of harped CFRP prestressing tendons, and
- 3) Developing design recommendations and procedures for the use of externally prestressed CFRP tendons

1.3 THESIS ARRANGEMENT

In Chapter 2, a review of the literature and background information related to external prestressing of concrete structures and the use of fibre reinforced polymer (FRP) materials in external post-tensioning is presented. Chapter 3 describes the experimental program for the testing of CFRP prestressing tendons in various harping configurations. The test setup and equipment, the variables investigated, the instrumentation and data acquisition system, and the testing procedures are described. In Chapter 4, the data obtained in the experimental program is presented and analysed, including a comparison of the experimental data to the existing analytical models and design equations that were presented in the literature review.

Chapter 5 describes the derivation of a primary and an extended analytical model that were developed in this research program. The model predictions are compared to the experimental data and discussed. Chapter 6 discusses the significance of the three different failure modes observed for the harped CFRP prestressing tendons tested in this experimental program. Design guidelines involving failure mode control are also derived and presented in this chapter. Chapter 7 summarizes the design recommendations for harped CFRP prestressing tendons based on the models and guidelines developed in Chapters 5 and 6. The conclusions and recommendations for the research program are presented in Chapter 8.

2 BACKGROUND AND LITERATURE REVIEW

2.1 INTRODUCTION

Reinforced concrete is one of the most prevalent building materials in the world. One of the major issues being faced is the need to repair or rehabilitate reinforced concrete structures because of damage from corrosion of the steel reinforcement. Fibre reinforced polymer (FRP) reinforcement presents a promising alternative to steel reinforcement, particularly because of its resistance to corrosion.

This chapter presents background information on prestressing and harped prestressing configurations, the use and development of FRP reinforcement in construction, and the existing research and design recommendations for the harping of FRP prestressing tendons.

2.2 PRESTRESSED CONCRETE

Prestressing is often used in concrete construction in conjunction with or as an alternative to non-prestressed reinforcement. It is an active reinforcing system whereby reinforcing tendons have a tensile force in them before any loading of the structure occurs. Prestressing of concrete elements may be done either by pretensioning or by post-tensioning. With pretensioned prestressing, prestressing tendons are cast inside the concrete element and are fully bonded with it. Post-tensioned prestressing, on the other hand, is performed after casting and curing of the concrete element and may be either internal or external. With external prestressing, the tendons are located completely outside the concrete. This has an added advantage of allowing for smaller concrete cross-sections, and not placing a limitation on the amount of prestressing because of concrete cover and spacing

requirements. Normally, external prestressing is performed using a harped configuration for the tendon. This is done by depressing the tendon with one or more deviators as illustrated in Figure 2-1. Gravity load moments are typically highest at the mid-span and lowest at the ends for simply supported beams. Harping of the prestressing tendon allows the eccentricity of the applied prestressing force to vary along the beam and more closely match the moments due to gravity loads. Harping of the tendons also provides additional shear resistance; the tendon prestressing force contains a vertical component that typically acts opposite to shear forces that result from loading.

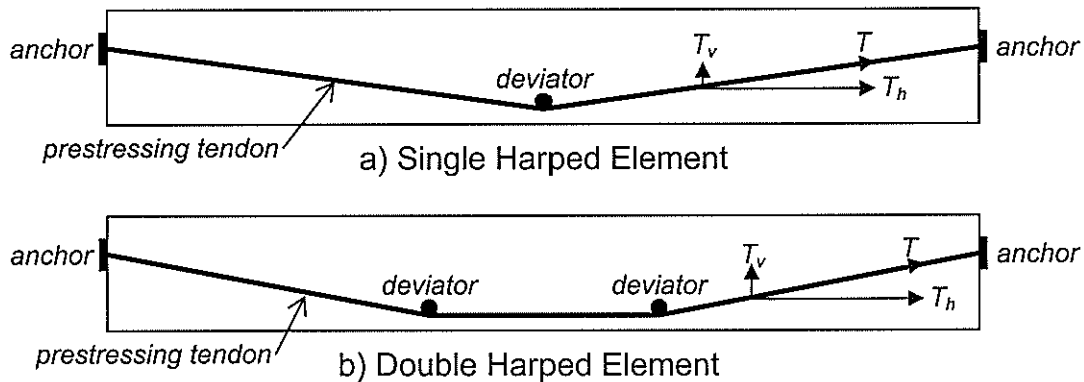


Figure 2-1: Harped Prestressing Configurations

External prestressing can be used as reinforcement for new structures as well as a strengthening technique for existing structures, increasing both the shear and flexural capacity of the structure. External prestressing can be used effectively for the repair and rehabilitation of structures that have been subjected to damage or deterioration. This may be short-term damage such as an impact or an overload, or long-term damage, such as fatigue or reinforcement corrosion. External prestressing can help recover the loss of structural strength and integrity of a structure due to damage or deterioration or provide additional structural strength to overcome design deficiencies or a change in the usage of the structure. In repair and rehabilitation of such structures with external prestressing, the vertical component

of the prestressing force can also help recover excessive elastic or plastic deflections that have occurred. Figure 2-2 shows a bridge that has been strengthened using harped external post-tensioned prestressing. This example uses steel tendons and, as can be seen in the photograph, they are situated inside ducts, which are needed to help inhibit corrosion.

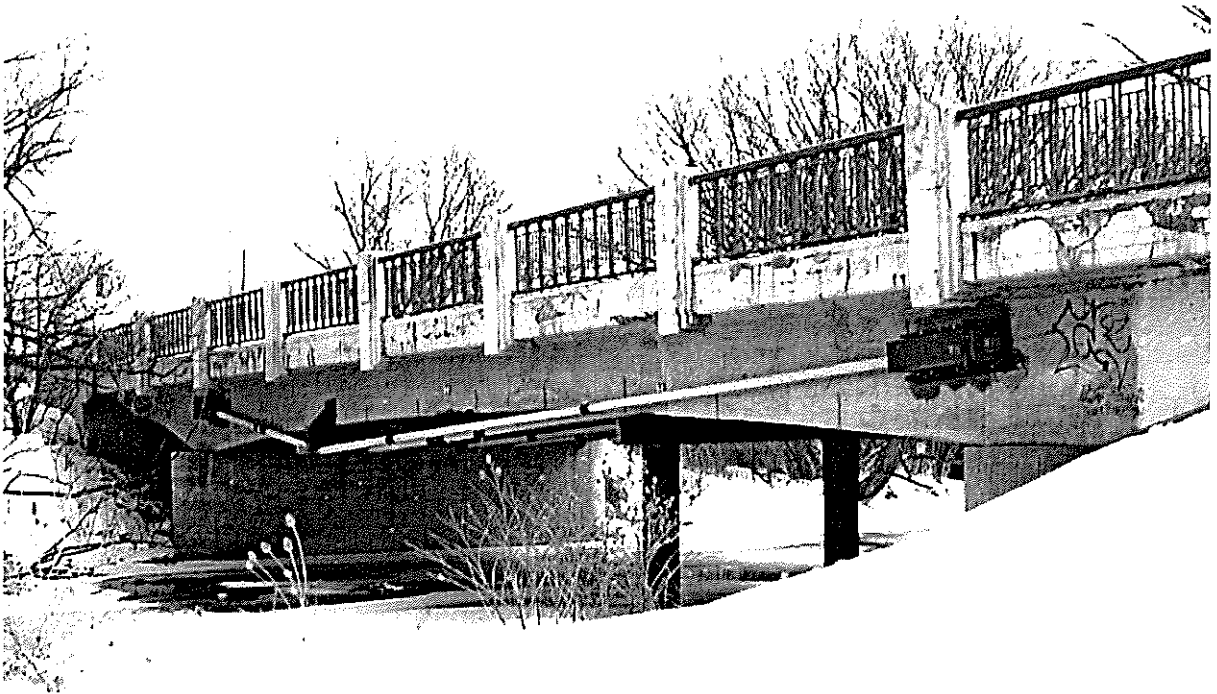


Figure 2-2: External Prestressing Being Used to Strengthen a Concrete Bridge

2.3 FIBRE REINFORCED POLYMER (FRP) TENDONS

When steel reinforcing or prestressing is used, the steel is vulnerable to corrosion. The ongoing presence of corrosion in reinforced and prestressed concrete is a major problem for infrastructure throughout the world. For example, in the U.S. it was estimated that at least 160,000 bridges are affected by corrosion with an estimated repair cost of US\$20 billion dollars (Clarke, 1993). It is apparent that steel corrosion gives rise to a large financial cost for repair and rehabilitation, and that there is a need for more durable reinforcement materials, especially in the area of corrosion.

Advanced composite materials, in the form of fibre reinforced polymers (FRP), have emerged as an alternative construction material. FRP used in construction comes in many different forms including pultruded structural shapes, material for use as externally bonded reinforcement in the form of woven sheets and solid strips, and internal concrete reinforcement (Bakis et al, 2002) as well as prestressing tendons. FRP tendons have many desirable properties including an excellent resistance to corrosion. They also have a high strength and a high elastic modulus, are lightweight and have non-conductive and non-magnetic properties that can be advantageous in design situations where steel tendons are less effective (Gilstrap et al, 2001).

FRP tendons are comprised of high-strength fibres in a polyester, vinylester or epoxy matrix and are typically manufactured using a pultrusion process. Other processes for manufacturing tendons include braiding, filament winding, vacuum compaction, and matched die molding (Gilstrap et al, 2001). Typically, the volume fraction of the fibres in FRP tendons is 60 to 65%. The matrix does not contribute significantly to the overall tensile capacity of the tendon and strength calculations typically ignore it. Thus, the effective strength of the tendon is equal to the strength of the individual fibres multiplied by the volume fraction of the fibres. The effective elastic modulus is also determined in a similar manner (Dolan, 1999).

Three different types of FRP tendons, based on the type of fibre used, are most common: glass FRP (GFRP), which comes in C-glass, S-glass and E-glass varieties, aramid FRP (AFRP), and carbon FRP (CFRP). All three types of FRP provide high strength-to-weight ratios and are resistant to corrosion. Each fibre type has its own advantages and disadvantages which make them suitable in different applications. Table 2-1 lists the individual strengths and weaknesses of each FRP type as well as some commercially available products.

Table 2-1: General Properties and Commercial Availability of FRP Types
(Gilstrap et al, 2001, El Refai et al, 2004)

Fibre Type	Relative Cost	Strengths	Weaknesses	Commercial Availability
GFRP	Low	chemical resistance electrical resistance acid resistance	poor alkaline resistance poor humidity resistance poor fatigue resistance	Isorod (Canada) C-bar (USA) Plalloy (Japan)
AFRP	Medium	fatigue resistance impact resistance thermal resistance	weak flexural and compressive properties low transverse stiffness poor UV resistance poor moisture resistance	Arapree (Italy) Fibra (Japan) Technora (Japan) Pillystran (USA) Parafil (UK)
CFRP	High	moisture resistance fatigue resistance thermal resistance chemical resistance	low ultimate strain poor impact resistance	Leadline (Japan) CFCC (Japan) Aslan 200 (USA)

CFRP tendons have better corrosion and fatigue resistance and a higher strength-to-weight ratio than steel. CFRP tendons may be especially useful in external prestressing applications where corrosion is a primary problem. Steel cables used in external prestressing have to be protected against corrosion, usually by using an external duct, as seen in Figure 2-2. The duct is filled with corrosion inhibiting grease or cement grout. This type of corrosion protection is not necessary when CFRP tendons are used, since they are resistant to corrosion, and the effective price increase associated with using CFRP over steel may be reduced. In comparison to steel tendons, external CFRP tendons can be readily inspected, as they are visible, and can be replaced more easily if damaged (Pisaniu, 1998).

Table 2-2 lists the material properties and Figure 2-3 shows the tensile stress-strain curves typical for the three different types of FRP, as well as those for prestressing steel for comparison. From the stress-strain curves, the linear elastic behaviour and lack of yielding or plastic behaviour of the FRP tendons can clearly be seen. From the properties exhibited in Table 2-2 and Figure 2-3, it can be seen that CFRP tendons show very similar mechanical properties to steel tendons, and thus, present

a promising alternative to steel for use in prestressing applications. However, because CFRP tendons are linear elastic to failure and do not exhibit yielding behaviour, they can be subject to brittle failure, and require special design consideration to avoid this.

Table 2-2: Typical Material Properties of FRP and Steel Reinforcing
(Nanni, 1994, Hughes Bros., 2002)

	GFRP E-Glass	AFRP Technora	CFRP Aslan 200	Steel
Elastic modulus GPa (ksi)	72-81 (10,500-11,500)	80 (11,600)	124 (18,000)	205 (29,000)
Tensile strength GPa (ksi)	3.4-3.6 (500-520)	3.1-3.4 (450-500)	2.1 (300)	1.9 (270)
Failure Strain %	3.5-5.0	4.4-4.6	1.7	7.0
Density kg/m ³ (lb/ft ³)	2,540-2,620 (159-164)	1,390 (87)	1,600 (100)	7,850 (490)

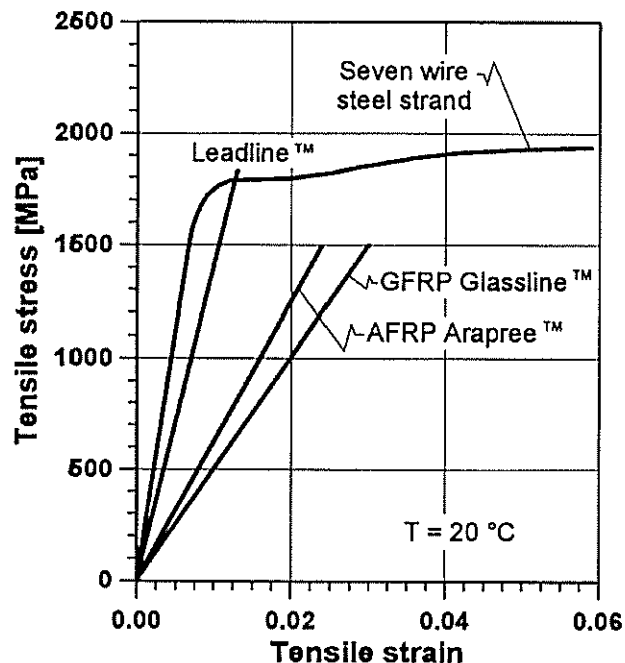


Figure 2-3: Tensile Stress-Strain Curves for FRP and Steel Tendons (Pisaniu, 1998)

The use of FRP in construction has been limited due to a lack of knowledge regarding their behaviour and performance. However, it is suggested that, as the body of knowledge on the use of FRP tendons expands and the profession becomes

comfortable with their behaviour, their use will expand, especially for saltwater and corrosive environments (Dolan, 1999). It was also put forward that the education and training of engineers, construction workers, inspectors, and owners of structures on the various relevant aspects of FRP technology and practice will be crucial in the successful application of FRP materials in construction (Bakis et al, 2002). The widespread use of FRP is also hampered by the higher short-term cost when compared to steel, which makes it unattractive for construction from an economic standpoint. However, when considering life-cycle costs, FRP may prove to be more cost-effective, especially with increased knowledge and acceptance of their usage (Hassanain et al, 2002). Externally post-tensioned concrete should be economical, provided whole-life costs and proper alternative designs are evaluated (Burgoyne, 1999).

Research and the usage of FRP have been on the increase in recent years around the world. In Europe for example, FRP has been successfully used in many different structural applications since the late 1970s, including prestressing systems, bridge stay cables, and reinforcement, as well as some structures fabricated completely out of composites (Burgoyne, 1999). In 1997 in Canada, the Taylor Bridge became the world's longest span bridge using CFRP reinforced girders. The construction of the bridge also included some CFRP deck reinforcing and GFRP barrier reinforcing (Rizkalla et al, 1998). Initiatives have also been taken around the world to develop design codes and recommendations for the usage of FRP in construction. In Canada, the Canadian Highway Bridge Design Code (CHBDC) and Network of Centers of Excellence on Intelligent Sensing for Innovative Structures (ISIS), in the United States, the American Concrete Institute (ACI) Committee 440 and Federal Highway Administration (FHWA), in Japan, the Japan Society of Civil Engineers (JSCE), and in Europe, EUROCRETE and Fédération Internationale du Béton (fib) (Bakis et al,

2002) have all been involved in the development of design codes and recommendations.

2.3.1 FRP as Harped External Prestressing Tendons

Successful usage of FRP tendons in harped external prestressing applications has been seen in the laboratory and in the field. As an example, the recently constructed Bridge Street Bridge in Southfield, Michigan utilises external CFCC prestressing tendons in addition to CFCC and CFRP flexural reinforcement and steel stirrups. Before manufacturing the beams, the design and construction method was verified by testing a full-scale beam to failure and it was observed that the ultimate flexural capacity and the cracking of the beam were about 3.4 and 1.2 times the service moment, respectively and that the tested flexural strength was about 1.6 times the calculated capacity. Failure of the beam was initiated by crushing of the concrete topping, followed by the rupture of the internal prestressing tendons, however, none of the external CFCC post-tensioning strands ruptured (Grace et al, 2003). Most notably, the project won the Harry H. Edwards Industry Advancement Award in the PCI Design Awards Program. The jury citation was as follows:

“The use of CFRP tendons in precast concrete bridges opens new potential for bridge designers to solve design problems more effectively and with faster construction. The careful and detailed work undertaken by this team of researchers, designers, and contractors holds great promise for future construction using CFRP. This project takes existing components and materials and expands on their abilities in new ways that will benefit the industry overall. These attributes define a Harry H. Edwards award winner (Grace et al, 2002).”

Previous studies involving the use of prestressed CFRP tendons in harped configurations have found that there is a reduction in the tensile capacity of the

tendon because of harping. This tensile capacity reduction does not occur with steel tendons. The bending induced in the tendon due to harping produces axial stresses additional to the axial stresses due to the tensile loading. In Figure 2-3 it was shown that CFRP tendons are linear elastic up to failure with no plastic behaviour or yielding. Steel tendons exhibit a similar initial linear-elasticity, but also have an effective yield strain, beyond which additional strain results in yielding of the steel and plastic deformation with very little increase in stress. Figure 2-4 illustrates the effect that the combined axial stresses due to bending and tension have on harped steel and CFRP tendons as loading is increased. In Figure 2-4a it is shown that when the combined top fibre strain, ϵ_{top} , exceeds the yield strain of the steel, ϵ_y , yielding of the material occurs and the tendon can continue to be loaded beyond this point. In Figure 2-4b it is shown that when the combined top fibre strain, ϵ_{top} , exceeds the tensile rupture strain of the CFRP, ϵ_u , failure occurs. The top fibre strain in the harped tendon is a result of the addition of the axial strain due to bending and the axial strain due to tensile loading, therefore, failure of the CFRP tendon will occur at a lower level than if the tendon was not harped and only axial strain due to tensile loading was present. Thus, in CFRP, the axial stresses due to bending reduce the strength available to resist stresses from the applied tensile loading, whereas in steel they do not. From this, it can be seen how the combined tensile and bending axial stresses and strains cause a reduction in the tensile capacity of CFRP tendons but not in steel tendons.

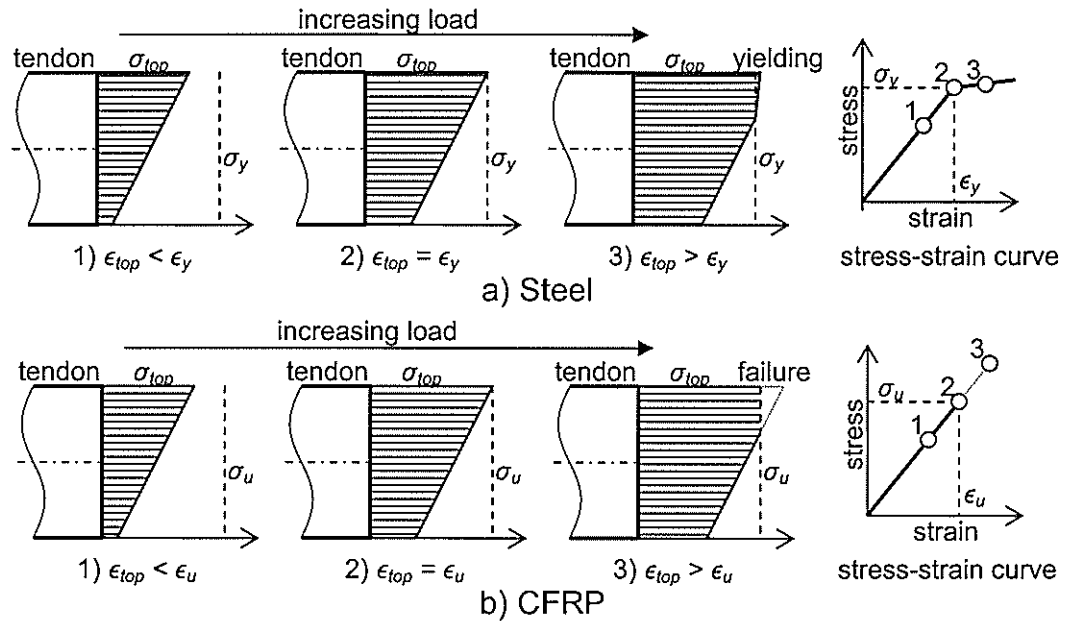


Figure 2-4: Effect of Combined Axial Stresses on Harped Tendons

Mutsuyoshi and Machida (1993) performed a study on concrete beams strengthened with externally prestressed, harped AFRP and CFRP cables. In the course of this study, they observed that the bending point of the cables at the deviator was a weak point and found that the FRP cables failed at 77-80% of their average tensile capacity. This was not the primary focus of their testing program and was not pursued further; however, they did recognize the weakness at the harping point and concluded that the design strength of FRP tendons needs to be reduced when the tendon is to be bent or deviated. It is noted that in this study, FRP cables were used rather than solid tendons, which exhibit different overall stiffness properties; however, a strength reduction due the harping was still present.

Taniguchi et al (1997) tested concrete beams using harped CFRP and AFRP tendons as external prestressing. In the course of their testing program, they observed that the harped prestressing tendons ruptured at about 70% and 90% of the nominal breaking load for CFRP and AFRP respectively. However, specific details of the deviator and harping configuration were not given.

Adachi et al (1997) performed a study on the strengthening of concrete segmental T-beam bridges using external FRP prestressing using both AFRP and CFRP tendons. When the tendons were harped at an angle of 10° over a deviator with a radius of 3000mm for their test program, a strength reduction coefficient of 0.9 was used for both tendon types to account for the strength capacity reduction in harped FRP tendons.

Grace and Abdel-Sayed (1998) performed a study of the behaviour of external prestressed, harped CFRP tendons in concrete bridges. As a part of this research, the effect of harping on the strength of prestressing tendons was studied for a limited set of variables. The effect the harping angle and deviator size, as well as the use of cushioning at the deviator was investigated for CFCC tendons (Table 2-3). CFCC tendons consist of seven individual CFRP strands twisted into a single tendon, similar to steel prestressing strands, which exhibit a lower overall stiffness in comparison to solid tendons. Still, it was observed that both increased harping angles and decreased deviator radii reduced the capacity of the tendons. They also observed that the use of cushioning at the deviator significantly reduced the strength reduction.

Table 2-3: Effect of Harping Angle and Cushioning on CFCC 1x7 Tendons (Grace et al, 1998)

Harping Angle degrees	Deviator Diameter in (mm)	Cushioning	Average Breaking Load kips (kN)	Reduction in Breaking Load
0	-	No	36.8 (163.8)	0%
3	2 (50.8)	No	29.6 (132.2)	19%
5	2 (50.8)	No	24.0 (106.5)	34%
5	20 (508)	No	32.2 (143.3)	12%
10	20 (508)	No	27.4 (121.8)	26%
5	20 (508)	Yes	36.3 (161.5)	1%
10	20 (508)	Yes	33.5 (149.1)	9%

They also investigated the effect of the harping angle as well as the introduction of a twist or torsion in the tendon for solid CFRP tendons (Table 2-4). It was again

observed that increasing the harping angle reduced the tendon capacity. It was also observed that the introduction of a twist in the tendon reduced the capacity of the tendon. Based on their observations, they recommend that cushioning at the deviator should be implemented and that the deviator should have a diameter of at least 20in (508mm) to minimise the strength reduction for harped CFRP tendons. They also recommend avoiding the introduction of twist in the tendons during post-tensioning and that a 10 percent strength reduction should be used in design to accommodate any incidental twisting that may occur.

Table 2-4: Effect of Harping Angle and Torsion on CFRP Tendons
(Grace et al, 1998)

Harping Angle degrees	Torsion	Average Breaking Load kips (kN)	Reduction in Breaking Load
0	No	48.3 (215.0)	0%
0	Yes	42.2 (188.1)	13%
4	Yes	37.6 (167.2)	22%
7	No	36.4 (161.7)	25%
7	Yes	34.8 (154.8)	28%

2.3.2 Analytical Models for Harped FRP Prestressing Tendons

Some of the previous research work on harped FRP prestressing tendons involved developing analytical models and design formulae. The three most developed models are those given by the Japan Society of Civil Engineers (JSCE), Ahmad et al, and Gilstrap et al. These three analytical models are presented here.

2.3.2.1 JSCE

The Japanese Society of Civil Engineering (JSCE, 1997) produced design recommendations for the use of FRP in the design and construction of concrete structures. The test program used several different types of FRP: carbon fibre, aramid fibre, glass fibre, and vinylon fibre. As part of these design

recommendations, a design strength formula was developed for bent or harped tendons:

$$\text{Equation 2-1: } f_{fbk} = \min \left\{ \left(0.05 \cdot \frac{r}{h} + 0.3 \right) \cdot f_{fuk}, f_{fuk} \right\} \quad (\text{JSCE, 1997})$$

$$\text{Equation 2-2: } f_{fbd} = f_{fbk} / \gamma_{mfb} \quad (\text{JSCE, 1997})$$

Where: f_{fbk} = characteristic tensile strength of bent FRP tendon

f_{fuk} = tensile capacity of the FRP

r = deviator radius

h = tendon diameter

f_{fbd} = tensile design strength of bent FRP tendon

γ_{mfb} = FRP material coefficient, generally taken as 1.3

The variable γ_{mfb} in Equation 2-2 is a material coefficient that compensates for material variability and other factors that can affect the tendon strength, much like the material factors used in steel and concrete design. Therefore, Equation 2-2 is to be used for practical design, however in actual comparisons for strength testing, the characteristic tensile strength as determined by Equation 2-1 should be considered. This equation for the design strength of a curved tendon is adopted in the CHBDC and the ACI 440 (Machida et al, 2002). This design formula was based on a regression analysis of the data from a number of tests encompassing the various types of FRP listed above. The tests also had a limited variation of harping configuration, up to a maximum r/h ratio of 10, which would represent a 100mm radius deviator for a 10mm diameter tendon. Figure 2-5 shows the test data and linear regression equation that the characteristic strength formula, Equation 2-1, was based on. The characteristic strength formula is based on the linear regression equation with an adequate margin of safety, reflected in the changing of the

coefficient from 0.09 to 0.05. It can be seen that the design formula is independent of the modulus of elasticity for the particular material and the harping angle, and is based only on the ultimate capacity of the tendon and the deviator and tendon size.

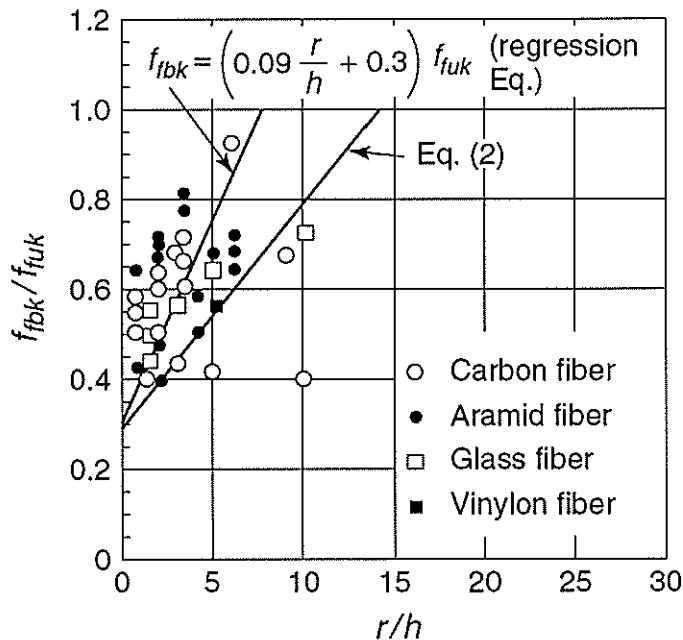


Figure 2-5: Test Data for JSCE Regression Equation (JSCE, 1997)

2.3.2.2 Ahmad et al

Ahmad et al. (1997) performed a research program on the behaviour of CFRP tendons subjected to combined axial loading and harping. The research program recognised the strength decrease in CFRP tendon strength when the tendon prestressed in a harped configuration. The material tested within this program was 8mm diameter Leadline CFRP tendons manufactured by Mitsubishi Chemical Corporation. The CFRP tendons were subjected to various harping configurations and loaded to failure.

Based on the experimental test results, design equations were developed by regression analysis:

$$\text{Equation 2-3: } P_f = \max \left\{ \begin{array}{l} \frac{21,600 - 845 \cdot \theta \cdot R^{-0.123}}{\left(\frac{1,000,000}{A \cdot E}\right) + 44 \cdot \theta \cdot R^{-0.123}} \\ \left(0.0216 - \frac{r}{R}\right) \cdot A \cdot E \end{array} \right. \quad (\text{Ahmad et al., 1997})$$

Where: P_f = failure load of the harped tendon in kips
 A = tendon cross-sectional area in in²
 E = CFRP modulus of elasticity in ksi
 R = deviator radius in inches
 r = tendon radius in inches
 θ = harping angle in degrees

Contrary to the JSCE design formula, it can be seen that this design formula does include both the modulus of elasticity for the particular material and the harping angle. The formula, however, is not dimensionally consistent and relies on the variables being in particular units of measurement. The values of 0.0216 (21,600microstrains) in the formulae are the average maximum fibre strains as measured within the program, and define the failure criterion. Though it is not stated, it should be inferred that these values should be modified to reflect the material being used. It is also noted in the paper that the average fibre failure strains for the harped tendons was much higher than those measured in uniaxial tests within the test program: approximately 0.0216 for harped tests compared to approximately 0.013 for uniaxial tests. The testing procedure used for the uniaxial tendon tests is not specified; however, it is known that factors such as tendon misalignment and stress concentrations due to the anchorages used can lead to premature failure of the tendon (Dolan et al, 2001) which can result in an inaccurate

determination of material properties. Therefore, it may be possible that the lower strain at failure determined by the uniaxial tests is a result of a premature failure of the tendons, and, therefore, may be erroneous.

2.3.2.3 *Gilstrap et al*

As part of a project funded by the US Federal Highway Administration (FHWA) to report on FRP prestressing for highway bridges, Gilstrap et al. (2001) presented a research program that studied the effect of harping on prestressed CFRP tendons. The material used in this program was a generic CFRP tendon developed specifically for the research project and referred to as the Strawman, developed by Glasforms Inc., as well as Leadline CFRP by Mitsubishi Chemical Corporation. An analytical model to predict the bending stresses in a harped tendon was developed. The formula for bending stress due to the curvature of the tendon was based on classical bending theory:

$$\text{Equation 2-4: } \sigma_h = \frac{E_f \cdot y}{R} \quad (\text{Gilstrap et al., 2001})$$

Where:

- σ_h = axial bending stress due to harping
- E_f = FRP modulus of elasticity
- y = tendon radius
- R = deviator radius

The total stress in the curved tendon is given as the sum of the bending stress and the stress due to the jacking load:

$$\text{Equation 2-5: } \sigma = \frac{P_j}{A_f} + \frac{E_f \cdot y}{R}$$

Where:

- σ = total combined bending stress at the harping point
- P_j = applied jacking load
- A_f = tendon cross-sectional area

From Equation 2-5, the failure load can be determined by setting the total combined stress variable equal to the ultimate failure stress for the tendon and solving for the jacking load, P_j . It can be seen that this model includes the elastic modulus of the CFRP material, E , but not the harping angle. Therefore, it has been assumed that the strength reduction due to harping is not influenced by the harping angle, contrary to the observations in the other literature discussed here.

The research program included an experimental program. In the experimental program, explicit tension failure testing was not performed; instead, tendons were prestressed to a given level while straight and then harped to a specified harping angle using deviators of various radii. An equation to predict the resultant loading was developed and checked against the measured loads. The analytical model was used to determine if tendon failure should be expected for the specified deviator size and predicted resultant load. For the majority of the tests, it was noted that the analytical model indicated that the total combined stress in the harped would be greater than the capacity of the tendon and, therefore, the tendon would fail. However, the researchers were able to achieve the full harping angle in all of the test configurations without tendon failure. It was concluded that shear flexibility in the matrix allows for some stress redistribution and that this may explain why the tendons exceeded the capacity predicted by the model. The overall conclusion of this program was that until more research is performed on the effect of harping tendons, any tendon that is to be used in a harped configuration should be first field-tested.

2.4 SUMMARY

CFRP may prove to be a promising alternative material to steel for use in prestressed concrete because of its advantageous material and mechanical properties. However,

because of the significantly higher cost involved, and the lack of knowledge of its mechanical behaviour, particularly when placed in harped configurations, its widespread usage in construction currently remains unattractive. In order to increase its acceptance as an alternative construction material, knowledge concerning its use and its cost needs to be improved and promoted. Increasing the knowledge of the mechanical behaviour of harped CFRP prestressing tendons has the twofold effect of improving the reliability of its design for strength and increasing its cost effectiveness through more efficient designs. The increased usage should create a higher demand for CFRP, leading to a reduction in its cost.

3 EXPERIMENTAL PROGRAM

3.1 INTRODUCTION

An experimental program was developed to investigate the behaviour of a Carbon Fibre Reinforced Polymer (CFRP) tendon when loaded in tension to failure under various harping configurations. Various parameters including harping angle, deviator size and tendon size were investigated. This chapter describes the test specimen, the test program, the equipment, the instrumentation and the test procedure used.

3.2 TEST PROGRAM

Three different parameters were varied to capture a large spectrum of harping configurations: tendon diameter, deviator radius and harping angle. These parameters are illustrated in Figure 3-1. To optimize the data acquired and minimize the number of specimens needed, the test program was performed in two segments. Phase I of the test program was set up to encompass a broad range of the variables investigated. Further test configurations that would best supplement the data from phase I and fill in desired data points were determined for phase II of the test program following an analysis of the data acquired in phase I.

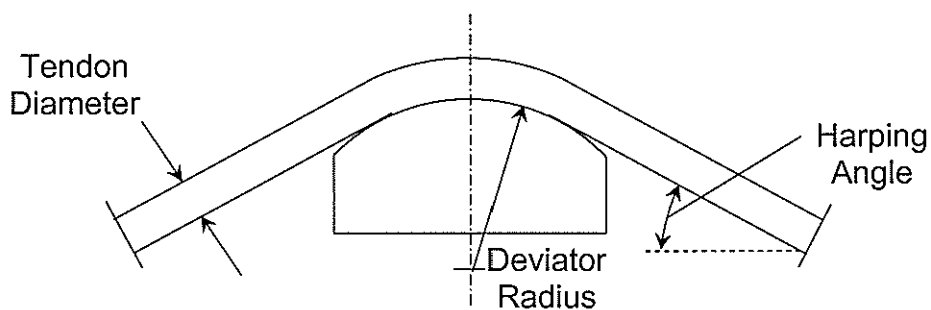


Figure 3-1: Configuration Variables

3.2.1 Test Program - Phase I

The primary test program utilized five different harping angles: 2°, 3°, 5°, 10° and 15°, five different deviator radii: 50mm (2in), 100mm (4in), 250mm (10in), 500mm (20in) and 1000mm (40in), and two different rod sizes: 6mm (1/4in) and 9mm (3/8in). A test matrix using these variables was constructed as shown in Table 3-1.

Table 3-1: Test Program Phase I Variable Matrix

Test Group	Specimen #	Tendon Size (diameter)	Deviator Size (radius)	Harping Angle
I	1	9.5mm	50mm	2°
	2	9.5mm	50mm	3°
	3	9.5mm	50mm	5°
	4	9.5mm	50mm	10°
	5	9.5mm	50mm	15°
II	6	9.5mm	500mm	2°
	7	9.5mm	500mm	3°
	8	9.5mm	500mm	5°
	9	9.5mm	500mm	10°
	10	9.5mm	500mm	15°
III	3 ^A	9.5mm	50mm	5°
	11	9.5mm	100mm	5°
	12	9.5mm	250mm	5°
	8 ^A	9.5mm	500mm	5°
IV	13	9.5mm	1000mm	5°
	14	6.3mm	50mm	2°
	15	6.3mm	50mm	3°
	16	6.3mm	50mm	5°
	17	6.3mm	50mm	10°
	18	6.3mm	50mm	15°

^A Duplicate entries (multiple test groups)

Test groups I, II and IV examined the effect of increasing harping angles with a fixed deviator for a given rod size. Test group III examined the effect of various deviator sizes against a fixed harping angle. Specimens 3 and 8 each appear in two different groups in the matrix and represent the crossover points for groups I and III, and groups II and III respectively.

3.2.2 Test Program - Phase II

Additional tests were selected following an initial analysis of the data acquired from Phase I. The Phase II matrix of variables is shown in Table 3-2.

Table 3-2: Test Program Phase II Variable Matrix

Test Group	Specimen #	Tendon Size (diameter)	Deviator Size (radius)	Harping Angle
II-b	19	9.5mm	500mm	6°
	20	9.5mm	500mm	9°
V	21	9.5mm	250mm	2°
	22	9.5mm	250mm	3°
	12 ^A	9.5mm	250mm	5°
	23	9.5mm	250mm	10°
VI	2 ^A	9.5mm	50mm	3°
	24	9.5mm	100mm	3°
	22 ^A	9.5mm	250mm	3°
	7 ^A	9.5mm	500mm	3°

^A Duplicate entries (multiple test groups)

Test group II-b extended group II by adding in two additional angles. Test group V was similar to groups I and II, using an additional deviator size. Test group VI reuses specimens from groups I, II and V, in addition to the new specimen 24, and is similar to group III from Phase I.

3.3 TEST SPECIMEN

The specimen tested in each test was a solid round CFRP tendon about 2m (6.6ft) long with an appropriate anchorage system affixed to each end.

3.3.1 CFRP Tendon

The CFRP tendon used in the experimental program was the Aslan 200 CFRP Rebar manufactured by Hughes Brothers as shown in Figure 3-2. These tendons are traditionally used for internal reinforcement and have a peel-ply surface treatment

that enhances concrete bonding properties, which can be seen in Figure 3-2. Tendons of two different sizes were used: #2 (6.3mm, 1/4in dia) and #3 (9.5mm, 3/8in dia). The length of tendon used was 2m (6.6ft) with an approximate effective free-length of 1.7m (5.6ft) between anchors, with the actual length varying with the harping angle.

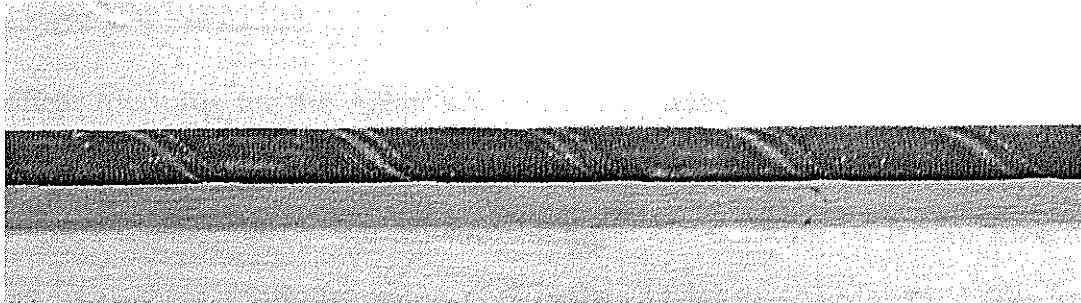


Figure 3-2: CFRP Tendon Specimen

3.3.2 Material Properties

The geometrical properties and guaranteed minimum material properties for the tendons published by the manufacturer are listed in Table 3-3.

Table 3-3: Hughes Brothers Aslan 200 Published Properties (Hughes Bros., 2002)

Bar Size	Cross Sectional Area		Nominal Diameter		Tensile Strength		Tensile Modulus of Elasticity		Ultimate Strain %	
	mm	mm ²	in ²	mm	in	MPa	ksi	GPa		ksi
#2	6	29.9	0.0464	6	0.254	2,068	300	124	18,000	0.017
#3	9	65.2	0.1010	9	0.362	2,068	300	124	18,000	0.017

Physical test data for the particular batches of tendons used were also provided by the supplier, and showed a significant scatter. Table 3-4 indicates the maximum material properties as supplied from the physical test data sheets by the supplier compared to the guaranteed minimum material properties. A significant variation of the material properties is evident. These minimum and maximum material property values can be used to determine the upper and lower bounds of an error

envelope that describes the expected deviation of the tensile-flexural and failure behaviour of different specimens resulting from the material property variability.

Table 3-4: Guaranteed Material Properties versus Maximum Tested Properties

	Tensile Strength		Tensile Modulus of Elasticity		Ultimate Strain
	MPa	ksi	GPa	ksi	%
Guaranteed Minimum Properties	2,068	300	124	18,000	0.017
Maximum Tested Properties	2,521	366	132	19,100	0.019

The shear modulus for the Aslan 200 CFRP was not tested for or provided by the supplier. However, the material properties are very similar to those of Leadline CFRP rods developed by the Mitsubishi Kasei Corporation of Japan, therefore a longitudinal shear modulus value of 7.2MPa (1,044ksi) (Al-Mayah, 1999) for the Leadline CFRP material was considered to be a reasonable estimate for the Aslan 200 CFRP for investigative purposes.

3.4 TEST SETUP

A test setup was designed and built specifically for this testing program. The testing frame was designed to allow the specimen to be anchored at each end while applying a tension loading to the specimen. The frame was designed to accommodate several harping angles and deviator sizes as required by the test matrix.

3.4.1 Test Frame

The general configuration of the test frame is shown in Figure 3-3 and Figure 3-4. The anchor pivots at either end of the frame securely restrain the tendon anchors in their longitudinal position while allowing free rotation of the anchor in a vertical plane. This free rotation allows for the various harping angles as well as the dynamically changing harp angle that occurs during the loading procedure. The

plate in the jacking end anchor pivot was threaded to accept a 180kN (20t) hydraulic jack which was used to apply a tension load to the test specimen. The hydraulic jack was fitted with an electric hydraulic pump with a variable flow valve to control the rate of loading. At the center of the frame, the deviator forks allow deviators of various sizes to be attached. The deviator forks have multiple bolt patterns to allow the deviator to be fixed in several different positions to create the desired nominal harping angles. Appendix A contains the shop drawings with detailed dimensions of the setup and fixtures.

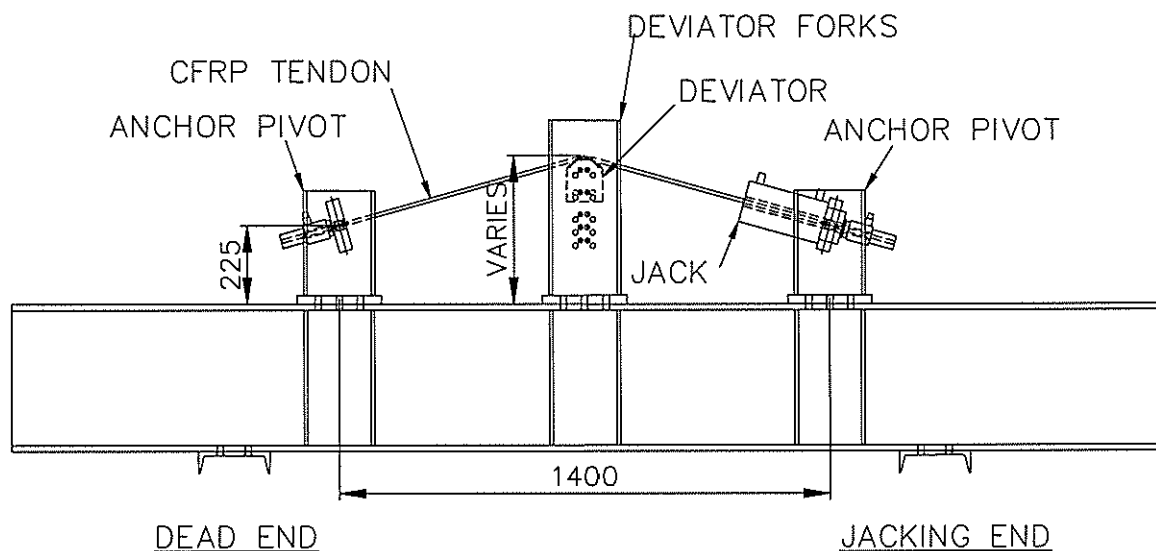


Figure 3-3: Test Frame Schematic

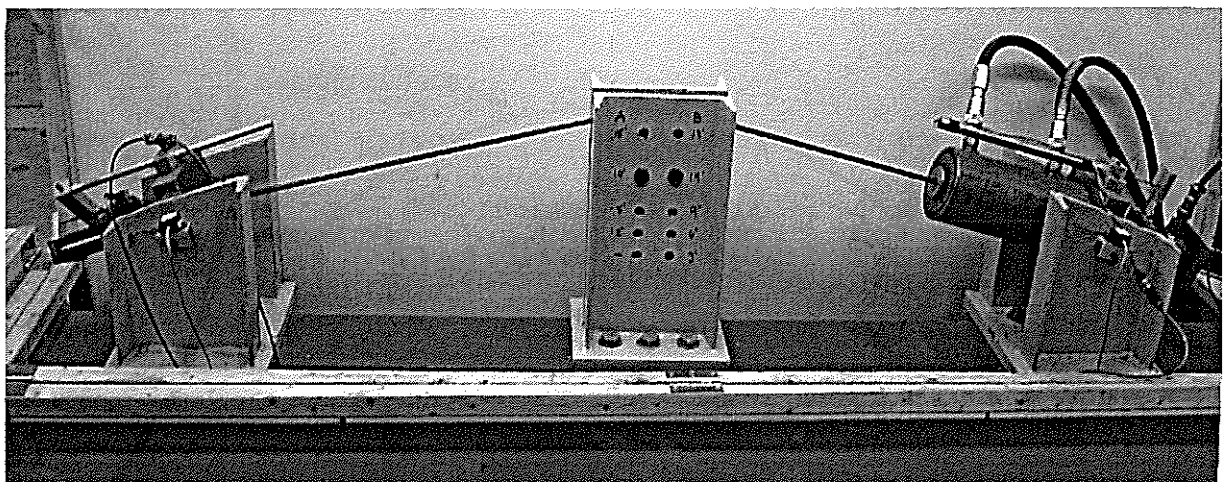


Figure 3-4: Test Frame as Constructed

3.4.2 Deviators

The deviators that were used in the experimental program were cut from 25mm (1in) thick steel plate with the geometric properties illustrated in Figure 3-5. The curved top bearing surfaces of the deviators were polished smooth in order to minimize friction with the tendon. The deviators were mounted in the testing frame with two bolts. Each deviator had two bolt patterns and these, combined with the five bolt patterns in the deviator forks, accommodated nine usable harping angles: 2°, 3°, 5°, 6°, 9°, 10°, 14°, 15° and 19°. Figure 3-6 shows the deviators fabricated for the testing program.

If the deviator is fabricated so that its tangential angle is less than the harping angle of the tendon and the tendon assumes the same curvature as the deviator radius, a sharp bending point will be induced in the tendon at the edge of the deviator. A high bending stress concentration would be created at this point that could lead to premature failure. With the exception of the 1000mm radius deviator, the deviators fabricated for this test program were designed large enough that this situation would not be encountered for any of the harping angles used. Because of size limitations, the 1000mm radius deviator was only useable for harping angles up to 6°.

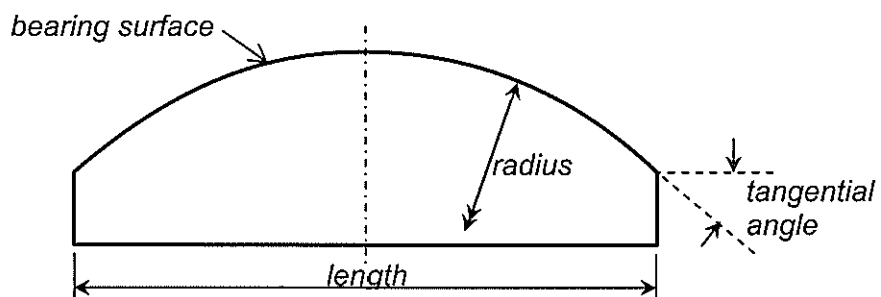


Figure 3-5: Deviator Geometric Properties

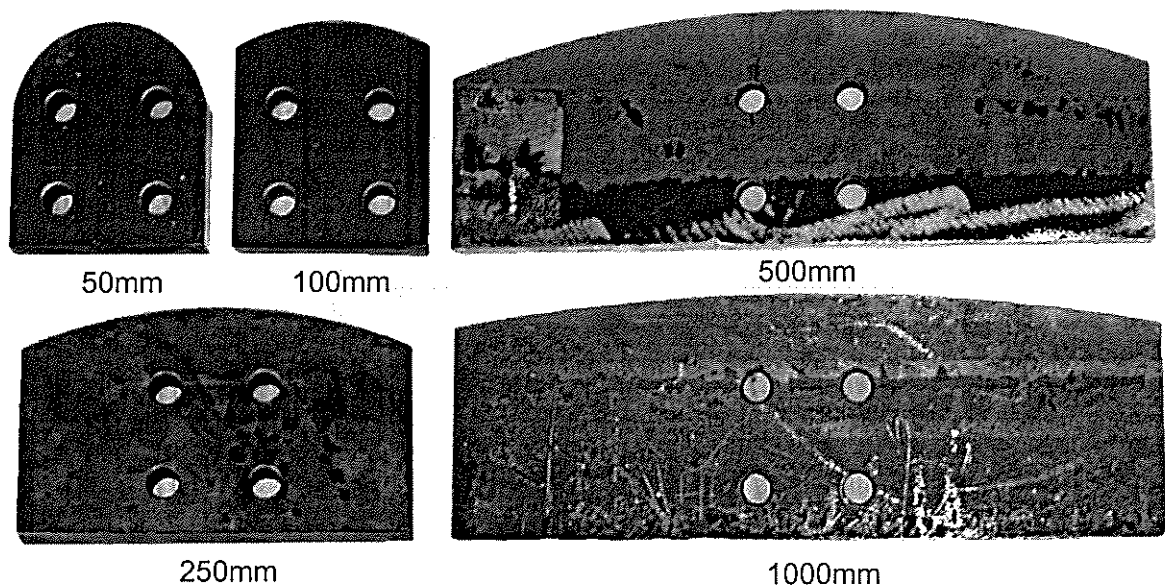


Figure 3-6: Fabricated Deviators

3.4.3 Anchorage System

A mechanical action barrel and wedge type anchor was used at each end of the tendons to anchor the specimen in the frame. The anchorage system used in the testing program was developed at the University of Waterloo, specifically for use with the Aslan tendons used in the experimental program (Al Mayah, 2003). The anchorage system consisted of a stainless steel outer barrel with four stainless steel inner wedges. A heat-softened copper tube sleeve was utilized to provide an even distribution of contact stress on the tendon. The anchorage design allowed the barrel and wedges to be reused, but new copper sleeves were required for each test specimen. The anchorage system components are shown in Figure 3-7.

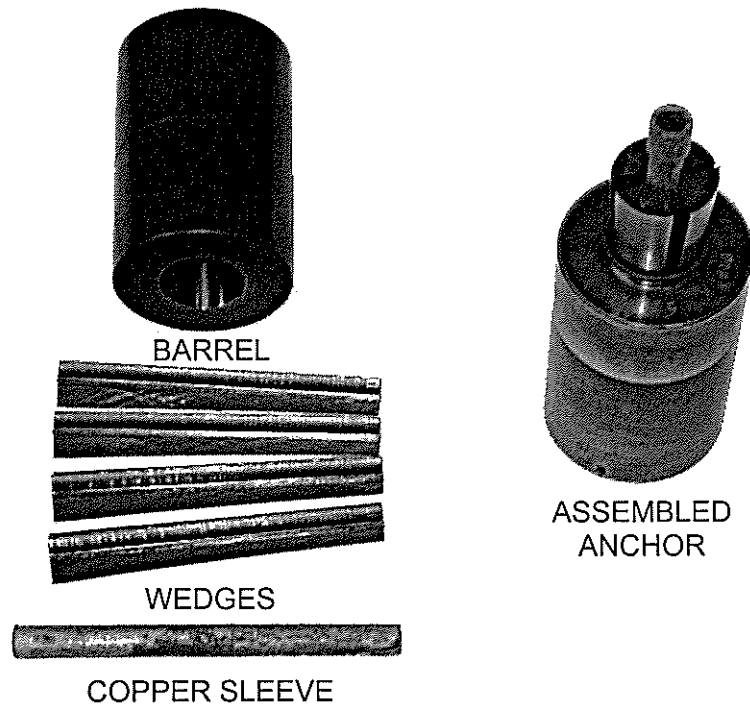


Figure 3-7: Anchorage System Components

3.4.4 Safety Precautions

The experimental program involved destructive testing of high-strength CFRP tendons. Because of the high load at which failure would occur, and the nature of this failure, several safety precautions were taken to contain the test setup and specimens. A box structure that could be completely opened and closed was built to contain the test frame, as shown in Figure 3-8. The top and front panels of the safety box were made of impact resistant clear plastic to allow visual monitoring of the test procedure. Kevlar explosion blankets were placed over the ends of the safety box to stop any specimen fragments that might penetrate the end panels. A restraining mechanism, shown in Figure 3-9, was designed to secure the anchorage systems to the anchor pivots and restrain them upon tendon failure.

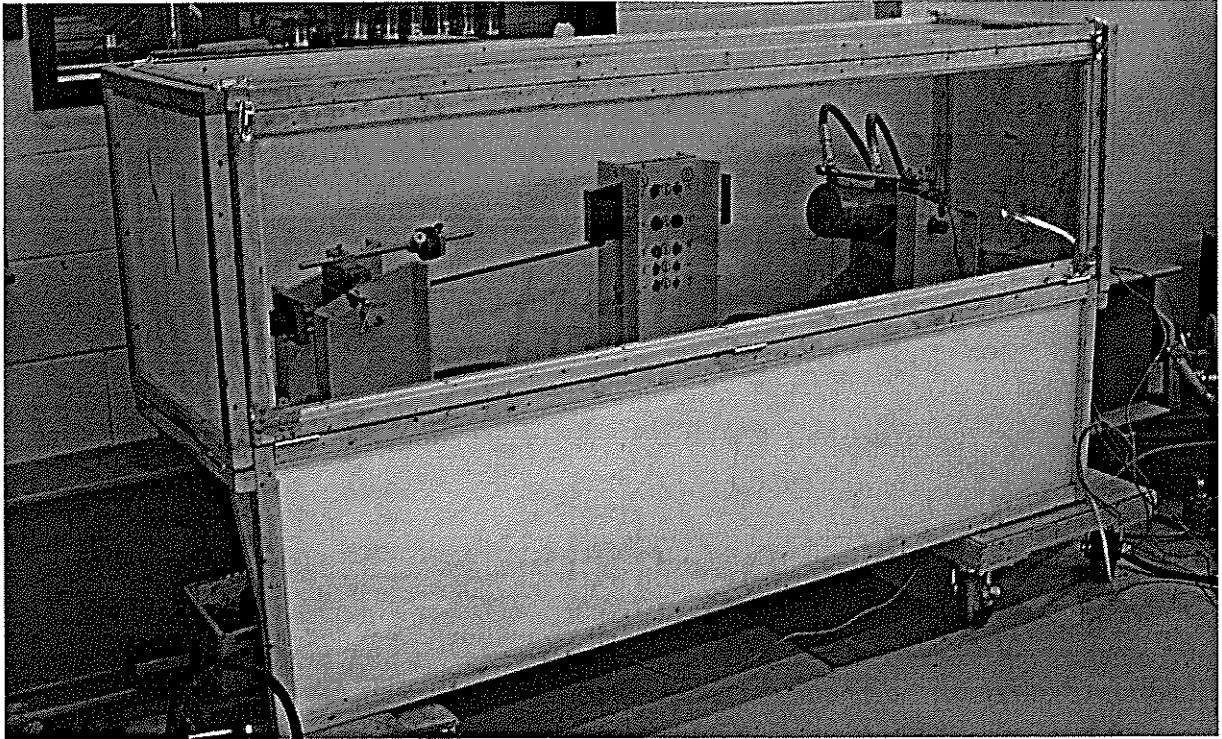


Figure 3-8: Safety Enclosure

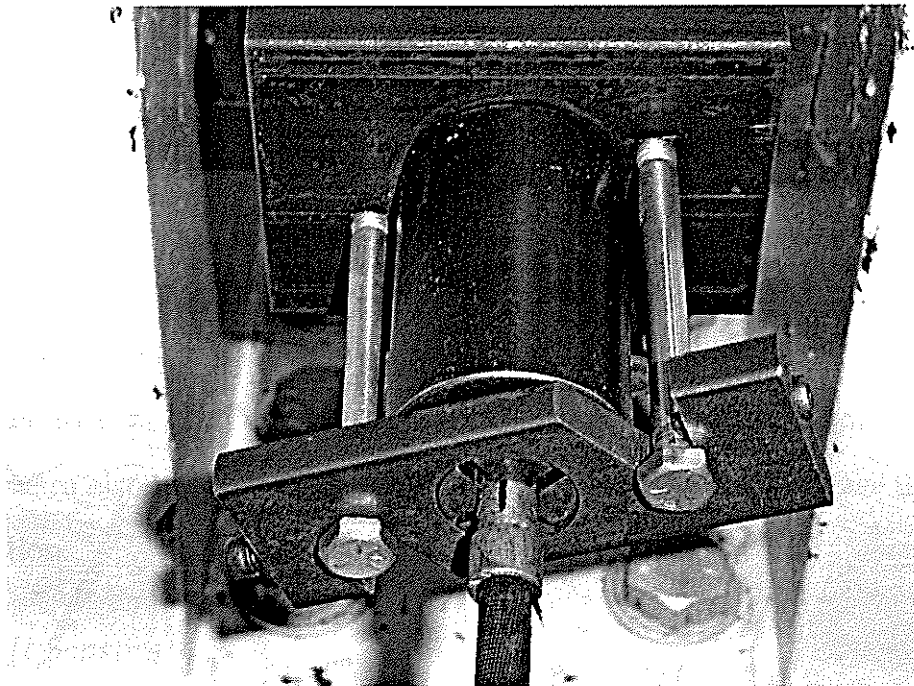


Figure 3-9: Anchorage Restraining Mechanism

3.5 INSTRUMENTATION AND DATA ACQUISITION

3.5.1 Instrumentation

Several different types of instrumentation were used to monitor important characteristics of the tendon behaviour during the test procedure. The instrumentation was arranged as illustrated in Figure 3-10.

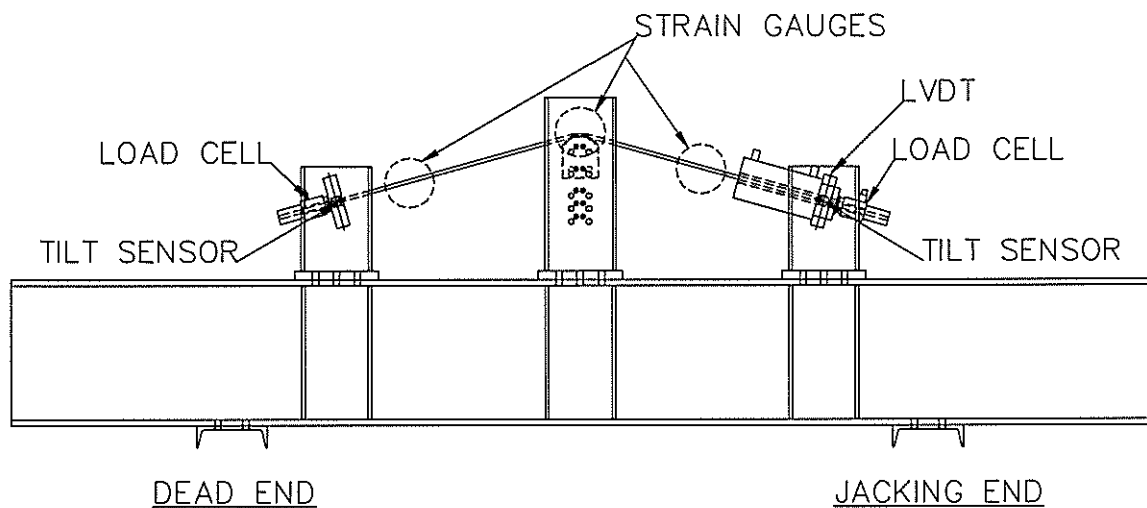


Figure 3-10: Instrumentation Arrangement

3.5.1.1 Load Cells

Two 270kN (30t) barrel-type load cells were used, one at the jacking end and one at the dead end of the tendon between the anchor and the pivot. The load cells captured the load at both ends of the specimen during the testing procedure. The load cells were also used to assess any loss of force in the tendon over the deviator due to friction.

3.5.1.2 Tilt Sensors

Two tilt sensors were used, one at either end secured to the anchor pivot. These captured the actual angle of the anchor pivots throughout the testing procedure and, thus, the effective harping angle of the tendon.

3.5.1.3 LVDT

One LVDT was secured to the jacking end anchor pivot to measure the stroke of the jack. This enabled the extension of the hydraulic jack to be monitored during testing, and allowed such problems as anchor slippage to be detected immediately.

3.5.1.4 Strain Gauges

Uniaxial 5mm Kyowa strain gauges, typically used for steel bars, were used for the program. The strain gauges were placed longitudinally at several positions along the tendon length to measure axial strains in the tendon. One strain gauge was located at the top of the tendon, at the middle of the deviator where the maximum strain was expected to occur in each test. One or two additional strain gauges were used to measure strains of interest on a test-by-test basis. Additional gauge locations included the tendon neutral axis at the deviator centre, the bottom of the tendon at the deviator centre and a position in the right or left tendon free length between the deviator and anchor pivots.

3.5.2 Data Acquisition

3.5.2.1 Hardware

A computer system equipped with a data acquisition system (DAQ) was used to collect the data from the instrumentation. The data acquisition system consisted of an internal DAQ device and an external DAQ completion box, both manufactured by National Instruments. Strain gauge completion was performed externally using a Vishay completion box. Additional power sources and signal amplifiers were also used in conjunction with the data acquisition instrumentation as needed.

3.5.2.2 Software

A data acquisition program was written using LabVIEW 6.1 software. Figure 3-11 shows a screen capture of the DAQ interface that was written specifically for this testing program. As can be seen in the figure, the interface allowed all the data to be continuously monitored during the testing program so that any problems could be detected immediately and the test halted if required. The DAQ captured the data at approximately 0.1-second intervals and recorded the raw voltages and the calibrated data directly to a text file.

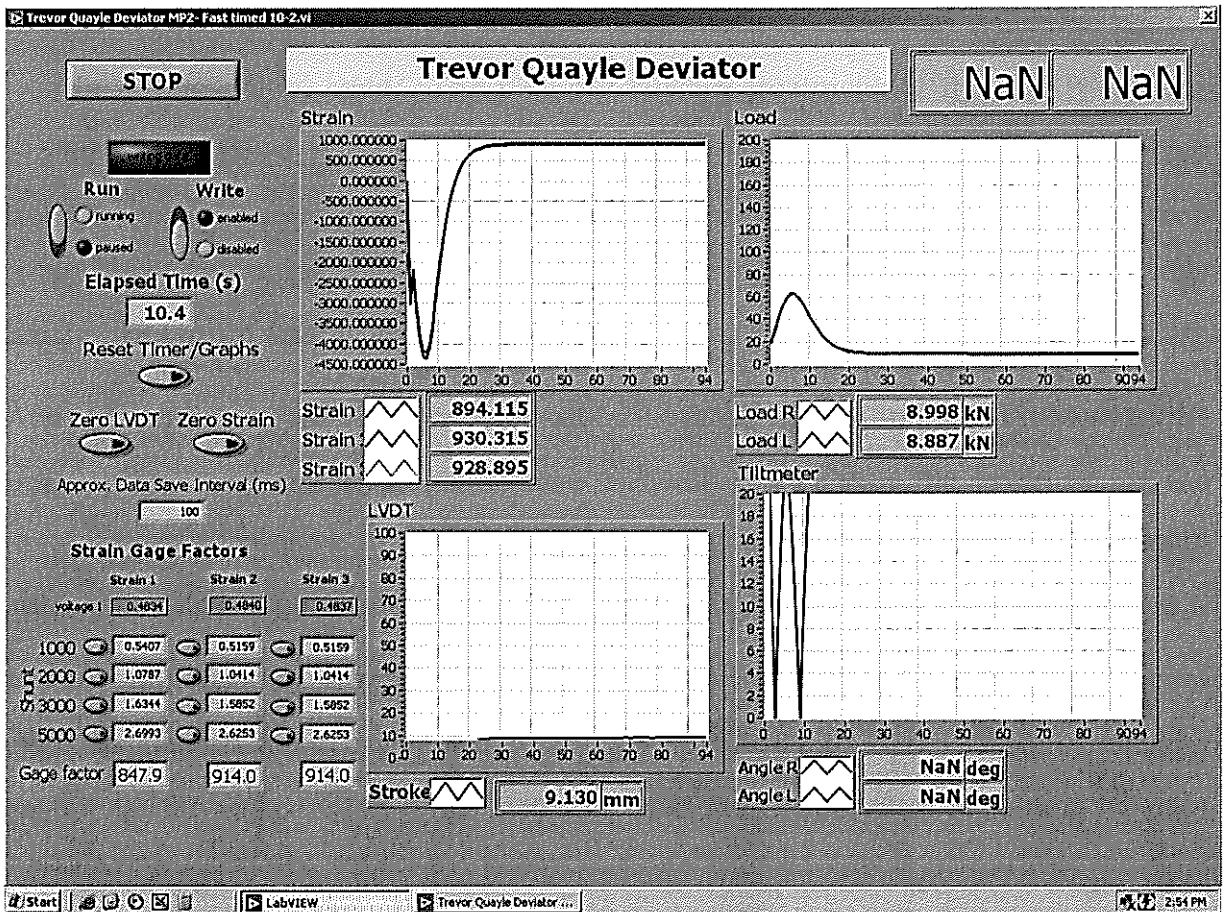


Figure 3-11: DAQ Interface

3.6 TEST PROCEDURE

This section describes the procedure required to perform each test. The test procedure consisted of three different phases: preparation of the specimen, installation of the specimen and load testing.

3.6.1 Specimen Preparation

The CFRP tendons were delivered in 6.1m (20ft) lengths and were cut to 2m (6.6ft) lengths for use in the tests using a hacksaw. The strain gauges were fixed to the tendon before installing it in the frame so they could be calibrated while the tendon was in a 'stress-free' state. The peel-ply surface treatment of the CFRP tendons provided a rough surface; therefore, the areas where the strain gages were affixed were first sanded smooth and cleaned to facilitate a proper bond with the gauge.

3.6.2 Specimen Installation

After the strain gauges were installed and calibrated, the tendon was installed in the frame. The appropriate deviator was securely bolted into the position for the harping angle required, and layer of lubricant was applied to the bearing surface to minimize any friction with the tendon. The tendon was placed over the deviator and its ends inserted through the anchor pivots. The copper sleeves were installed over the tendon at each end where the anchors were to be attached. Next, the anchor barrel and wedges were installed over the copper sleeves with a layer of metal lubricant applied between the barrel and wedge contact surfaces to facilitate seating of the wedges. To ensure that the anchors were securely affixed to the tendon and that no slippage of the anchors would occur, the anchors were pre-seated before progressing with the test. This involved using a special pre-seating rig, shown in Figure 3-12, to insert the wedges into the barrel to a load of

approximately 100kN. Pre-seating the anchors to this load ensured that premature failure of the anchorage would not occur because of slippage. After pre-seating the anchors, the anchor restraints were installed.

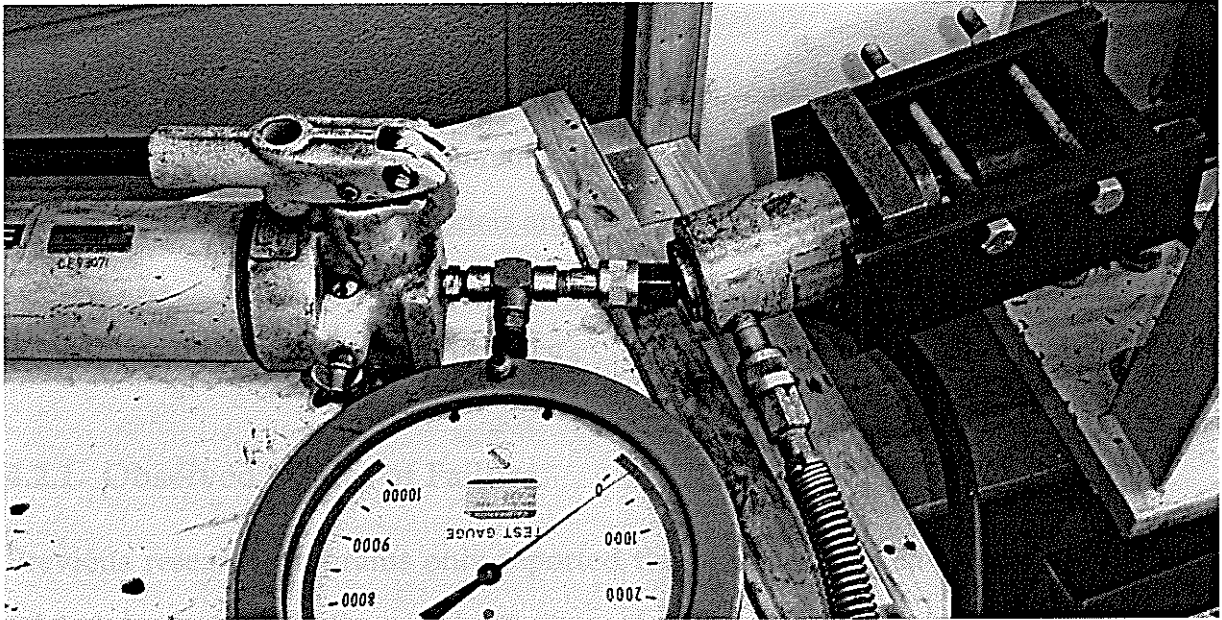


Figure 3-12: Pre-seating Rig

3.6.3 Load Testing

Once the specimen was installed and secured, the test was conducted. First, the safety cage was closed and fastened shut and the explosion blankets were placed over the ends. Any slack in the tendon was removed by loading the hydraulic jack until there was no gap between the anchors and the anchor plates at both ends. Next, the data acquisition equipment and program were started and loading of specimen was initiated. Loading was applied continuously using the electric pump, adjusting the hydraulic fluid flow to obtain a desirable loading rate. The tendon was loaded until failure was deemed to have occurred, at which point the jack was unloaded and the data file finalized.

4 EXPERIMENTAL DATA AND DISCUSSION

4.1 INTRODUCTION

In this chapter, the data obtained from the experimental program is presented. A brief discussion of the experimental data results and a performance evaluation of currently existing analytical models and design formulae follow.

4.2 EXPERIMENTAL TEST RESULTS

4.2.1 Observed Modes of Failure

Previous research programs only reported the presence of a single mode of failure related to the tensile-flexural behaviour of CFRP prestressing tendons, bending-tension failure. However, within this testing program, three distinct modes of failure were observed as illustrated in Figure 4-1:

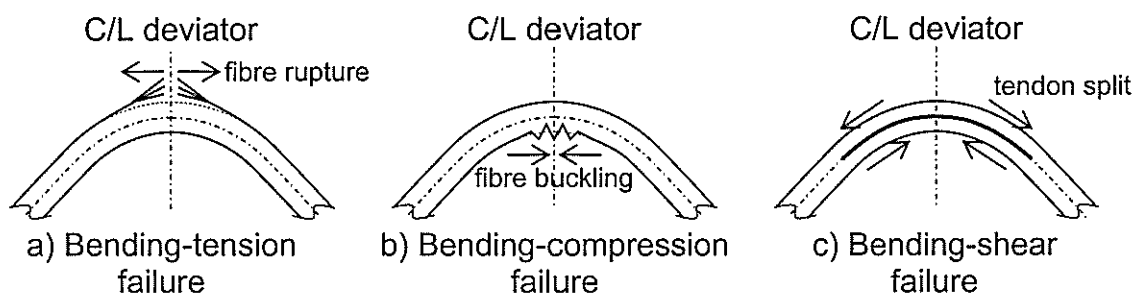


Figure 4-1: Illustration of Tensile-Flexural Failure Modes

Bending-Tension Failure (Figure 4-1a) – Herein referred to as *tension failure*. This mode of failure was the most commonly observed mode and was the only failure mode previously reported for other research programs. Tension failure is characterized by an initial rupture of the top fibres of the tendon at the centre of the deviator. Depending upon the configuration variables, the initial failure

was followed by either complete tensile failure of the entire tendon, or subsequent rupture of additional fibres propagating from the top of the tendon.

Bending-Compression Failure (Figure 4-1b) – Herein referred to as *compression failure*. Compression failure is characterized by a local buckling of the bottom fibres of the tendon at the deviator. Often, compression failure resulted in a visible sharp bend in the tendon at the location of the failure.

Bending-Shear Failure (Figure 4-1c) – Herein referred to as *shear failure*. Shear failure is characterized by a horizontal splitting of the tendon at or near its neutral axis, initiating on either one or both sides of the deviator, and propagating through the length of the tendon.

Specimens that exhibited compression or shear failure were often able to carry additional load beyond the point at which the initial failure occurs. However, the initial shear or compression failure mechanism results in a compromise of the composite action and fibre continuity of the CFRP material and the tendon's behaviour under the additional loading is unpredictable and unstable. Therefore, the load at the point of initial failure was considered to be the effective failure load for these specimens.

Often, the moment of initial tendon failure can be difficult to determine solely from visual observation, especially in the case of compression failure where the failure mechanism can be hidden from view by the testing equipment due to its location. However, along with the visual signs associated with the failure modes, inspection of the recorded strain data can give indications of the mode of failure. Figure 4-2 plots the bending strain portion of the total top fibre strain versus the applied loading as recorded for test specimens 2, 3 and 4 from test group I. Specimen 2 exhibited tension failure, specimen 3 exhibited shear failure and specimen 4

exhibited compression failure. The tension failure specimen, 2, shows a smooth, continuous strain-load plot all the way to failure. In the shear failure specimen, 3, a discontinuity can be seen in the strain-load plot at the point of where the initial shear failure occurred. The tendon is still able to carry additional loading beyond this failure point; however, the tendon exhibits a noticeable drop in stiffness as seen by the change in the trend of the strain-load plot beyond this point when compared to specimen 2. It can also be seen that the strain-load plot beyond the initial failure is no longer smooth, but exhibits an instability that results from the failure mechanism. In the compression failure specimen, 4, a discontinuity can again be seen at the point of initial failure. In this case, the discontinuity is much more significant because of failure and the sudden change in the local stiffness of the tendon in the area of the failure.

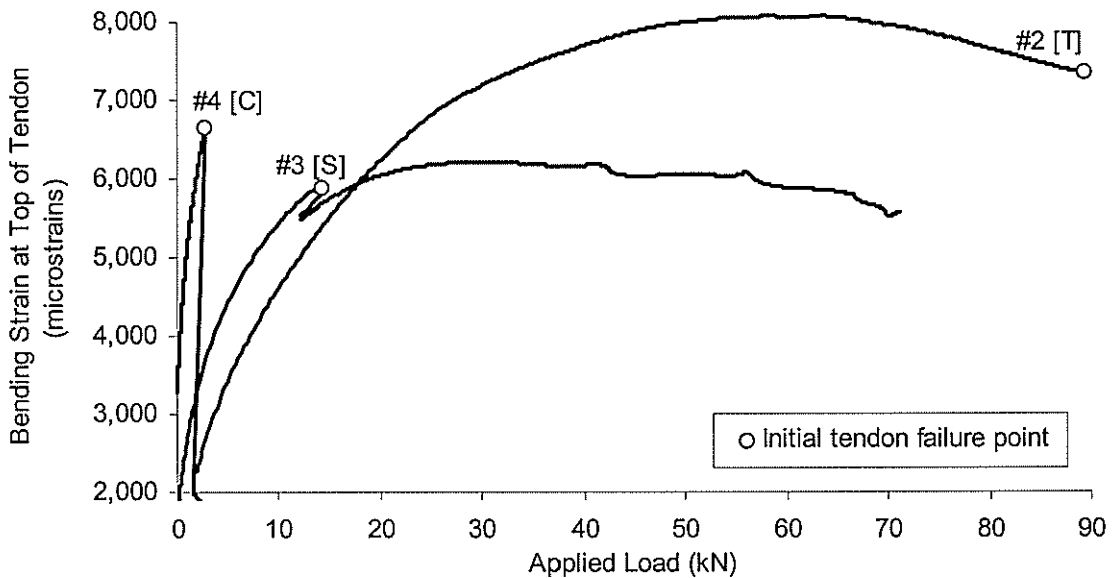


Figure 4-2: Strain-Load Plot Illustrating Failure Modes

In all the harped tests, regardless of the failure mode, it was noted that the tendon failure occurred at the location of the deviator, indicating, as should be expected, that the greatest net stresses in the harped tendon occur at this location.

4.2.2 Experimental Test Results

Table 4-1 summarizes the results of the experimental test program. The table gives the applied stress level at which effective failure of the tendon was determined to have occurred for each of the test specimens as well as the failure level as a percentage of the guaranteed tensile capacity ($f_u=2068\text{MPa}$) of the CFRP tendon.

Table 4-1: Experimental Test Failure Stress and Mode

Test Group	Specimen No.	Tendon Diameter mm	Deviator Radius mm	Harp Angle deg	Failure Stress MPa	% Ultimate ($f_u=2068\text{MPa}$)	Failure Mode ^C
I	1	9.5	50	2	1583.4	76.57%	T
	2	9.5	50	3	1255.3	60.70%	T
	3	9.5	50	5	199.4	9.64%	S
	4	9.5	50	10	38.1	1.84%	C
	5	9.5	50	15	12.5	0.60%	C
II	6	9.5	500	2	1798.2	86.95%	T
	7	9.5	500	3	1519.0	73.45%	T
	8	9.5	500	5	1335.3 ^B	64.57%	T
	19	9.5	500	6	1185.8	57.34%	T
	20	9.5	500	9	1320.4	63.85%	T
	9	9.5	500	10	1042.7 ^B	50.42%	T
III	10	9.5	500	15	20.9	1.01%	C
	3 ^A	9.5	50	5	199.4	9.64%	S
	11	9.5	100	5	284.4	13.75%	S
	12	9.5	250	5	1048.3	50.69%	T
	8 ^A	9.5	500	5	1335.3 ^B	64.57%	T
IV	13	9.5	1000	5	1633.6	78.99%	T
	14	6.3	50	2	1635.7	79.10%	T
	15	6.3	50	3	1477.7	71.46%	T
	16	6.3	50	5	963.4	46.59%	T
	17	6.3	50	10	116.0	5.61%	C
V	18	6.3	50	15	27.6	1.33%	C
	21	9.5	250	2	1751.8	84.71%	T
	22	9.5	250	3	1500.7	72.57%	T
	12 ^A	9.5	250	5	1048.3	50.69%	T
VI	23	9.5	250	10	29.2	1.41%	C
	2 ^A	9.5	50	3	1255.3	60.70%	T
	24	9.5	100	3	1165.1	56.34%	T
	22 ^A	9.5	250	3	1500.7	72.57%	T
	7 ^A	9.5	500	3	1519.0	73.45%	T

^A Duplicate entries (multiple test groups)

^B Average value (more than one specimen tested)

^C Failure mode: T = tension, C = compression, S = shear

Often, the tendon was able to take additional loading beyond the initial failure, particularly in the case of compression and shear failures, however, the failure level indicated is the initial failure level, the level at which the first failure signs were observed. For specimen 8, three specimens were tested, and for specimen 9, two specimens were tested, and the table gives the average value of the test results for these two cases. Appendix B gives the test data for the individual test specimens for these two configurations and a significant scatter can be seen. This scatter may be attributed to the variability of the material properties of the CFRP tendons. The effect of the material property variability on the experimental data is discussed later in Section 5.5. Table 4-1 also gives the mode of failure for each specimen: 'T' indicates tension failure, 'C' indicates compression failure and 'S' indicates a shear failure. It can be seen that compression failures typically occurred at larger harping angles and that shear failures typically occurred at medium angles with smaller deviator radii. Also, note that the failure stress for these failure modes is very low in comparison with tension failures.

4.3 DISCUSSION OF EXPERIMENTAL RESULTS

In this analysis of the experimental data, only the specimen tests in which tensile failure occurred are considered. Compression and shear failure were observed to occur generally at significantly lower loading levels than tension failure and design parameters giving rise to these failure modes should be avoided. The significance and impact of the mode of failure, particularly in the case of compression or shear failure, is discussed and analysed in more detail in Chapter 6.

4.3.1 Observed Effect of Harping Configuration Variables

Figure 4-3 and Figure 4-4 illustrate the effect of the harping configuration variables on the tensile capacity of the harped CFRP prestressing tendons. Figure 4-3 shows the experimental data from test groups I, II, IV and V in which the deviator size and tendon size remained constant while the harping angle was changed. The normalized failure level is plotted against the nominal harping angle for each test. The normalized failure level is calculated by dividing the measured failure stress by the guaranteed tensile stress capacity for the tendon (σ_f / σ_u). For all four of these groups, a decreasing trend can be seen. This indicates that as the nominal harping angle is increased, the tensile capacity of the harped tendon decreases.

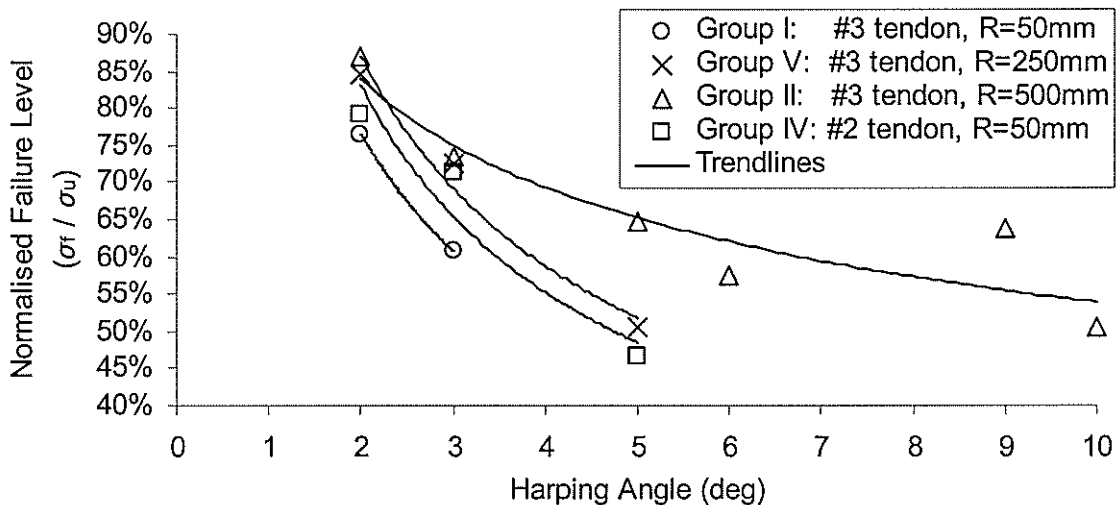


Figure 4-3: Effect of Harping Angle on Tensile Capacity

Figure 4-4 plots the experimental data for test groups III and IV in which the tendon size and nominal harping angle are held constant while the deviator size was changed. The normalized failure level is plotted against the deviator radius for each test. In both of these test groups, an increase in the capacity as the deviator size is increased can be seen. This indicates the tensile strength decreases as the deviator size decreases.

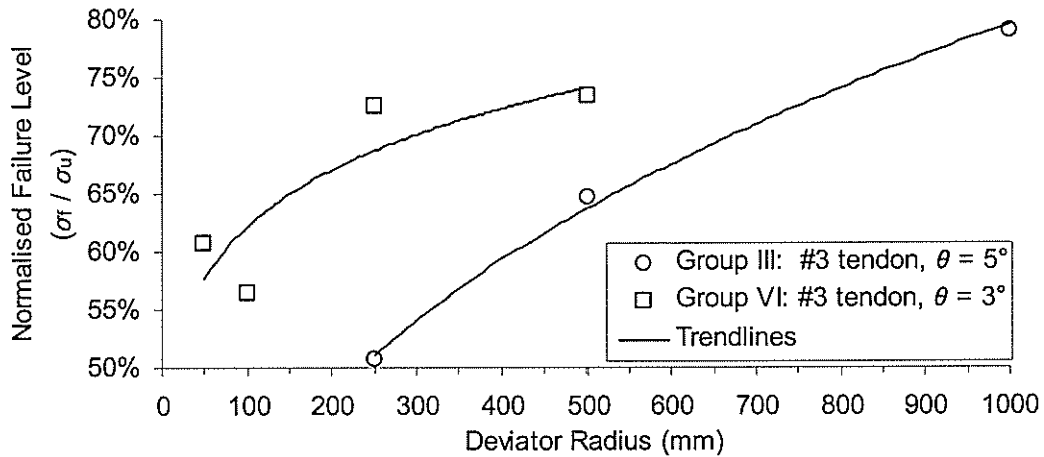


Figure 4-4: Effect of Deviator Size on Tensile Capacity

4.3.2 Comparison with Existing Analytical Models

In this section, the experimental data are compared to the three existing analytical models described in Chapter 2: the JSCE model (JSCE, 1997), the Gilstrap model (Gilstrap et al, 2001) and the Ahmad model (Ahmad et al, 1997). Figure 4-5, Figure 4-7 and Figure 4-8 illustrate the normalized correlation between each of the three models and the experimental data using the published guaranteed properties for the CFRP material. In the figures, the 1:1 correlation line represents an ideal, exact correlation where the measured and predicted failure levels are identical. Data points situated below and to the right of the 1:1 correlation line represent conservative data points where the predicted tensile strength was less than the measured tensile strength, that is, the model under-estimates the tensile strength. Data points situated above and to the left of the 1:1 correlation line represent unconservative data points where the predicted tensile strength was greater than the measured tensile strength, that is, the model over-estimates the tensile strength.

Figure 4-5 shows the normalized correlation plot for the JSCE model using the characteristic tensile strength equation for a bent FRP tendon. The majority of the data points are situated significantly on the unconservative side of the correlation

line. The majority of the failure levels predicted by the JSCE model can also be seen to be equal to 100% of the ultimate capacity while the measured values are significantly lower. This may be explained by the fact that the data used to develop the JSCE model had deviator radius to tendon diameter ratios (R_d/d_t) of up to about 10, whereas the tests in this experimental program had R_d/d_t values as high as 100. It should be noted that all of the data points that are on the conservative side are for test configurations with R_d/d_t values less than 10. The JSCE model shows a poor correlation to the measured capacity and greatly over-estimates the tensile capacity of the harped tendon. The JSCE model appears to be extremely unconservative for most cases, especially for higher R_d/d_t values where the model greatly overestimates the harped tendon's capacity, which is not desirable, as practical R_d/d_t ratios would tend to fall in this higher range.

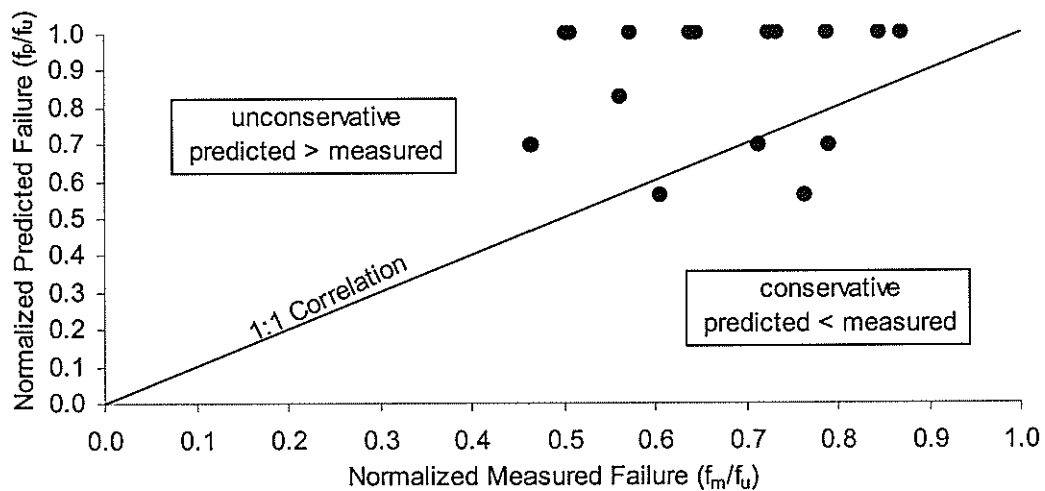


Figure 4-5: Correlation Plot for JSCE Model Using Characteristic Strength

Figure 4-6 shows the normalized correlation plot for the JSCE model using the tensile design strength equation for comparison. In this case, the data is, overall, closer to the 1:1 correlation line; however, the majority of the data is still unconservative and the margin of safety provided by the material coefficient is lost.

This further shows the overall deficiency of the JSCE model and its failure to calculate the tensile strength of harped FRP tendons safely.

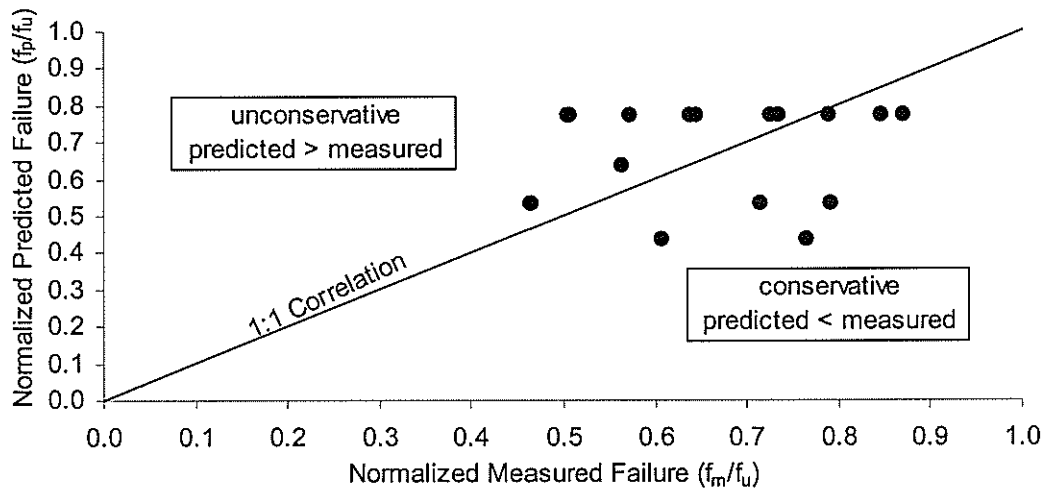


Figure 4-6: Correlation Plot for JSCE Model Using Design Strength

Figure 4-7 shows the normalized correlation plot for the Gilstrap model. The Gilstrap model exhibits a characteristic horizontal banding of data points. This occurs because the model is not influenced by the harping angle, so harping configurations with the same deviator and tendon sizes but different harping angles will produce the same strength values. All the data values for the Gilstrap model lie on the conservative side of the correlation line, however, for several of the test configurations, negative predicted values are produced (shown as zero in the figure) which suggest that the tendon cannot take any tensile loading. This was not the case, as the measured failure loads were significantly higher than zero. The Gilstrap model assumes that the tendon follows the curvature of the deviator regardless of the loading and configuration. For smaller deviator radii, this approach predicts bending stresses that can often be higher than the tensile strength of the tendon. Overall, the Gilstrap model shows very poor correlation with the measured tendon capacity. While the results of the correlation plot for the Gilstrap model are conservative, the model is often too conservative for an efficient usage of harped

CFRP tendons, as it severely limits the usable harping parameters and under-predicts the harped tendon capacity, particularly as the R/d_t ratio decreases.

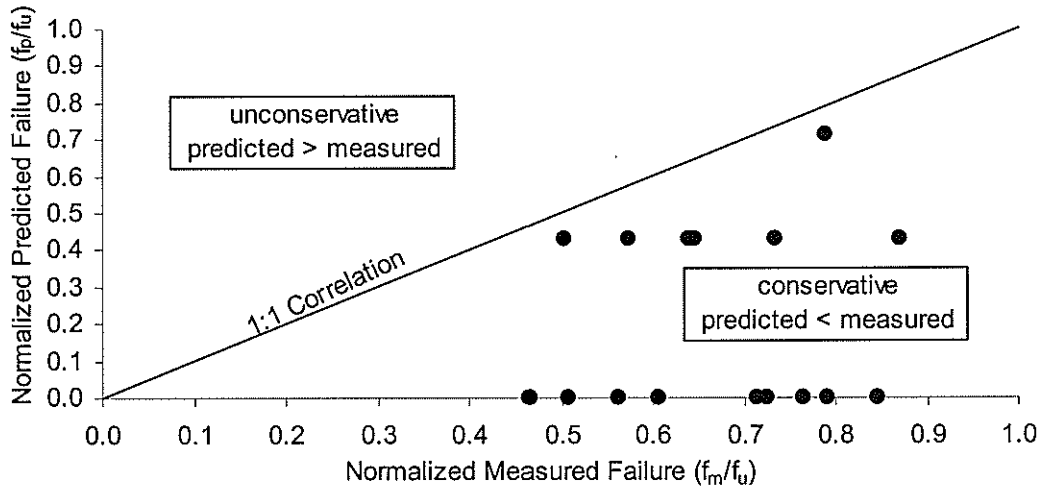


Figure 4-7: Correlation Plot for Gilstrap Model

Figure 4-8 shows the normalized correlation plot for the Ahmad model using the assumed, increased strain capacity of 0.0216 (21,600microstrain) as included directly in the model for their test program. A very poor correlation can be seen for the Ahmad model in this case. It is especially notable that all of the data points are unconservative. This may be accounted for by the fact that the strain capacity included in the model is for the specific CFRP material used in their test program.

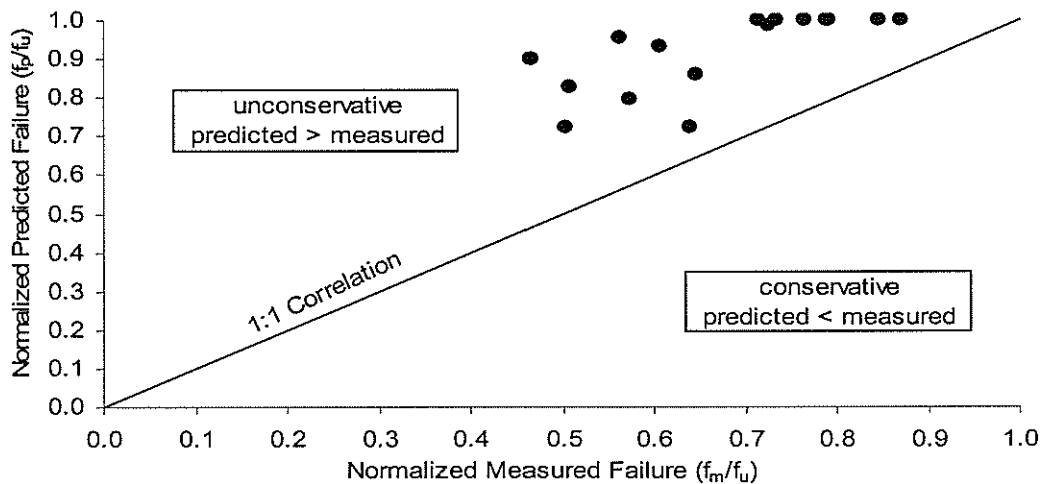


Figure 4-8: Correlation Plot for Ahmad Model with Increased Strain Capacity

To make a fairer comparison with the experimental data, the Ahmad model was modified to use the guaranteed tensile strain capacity of 16,677 microstrain for the CFRP tendons used in this research program. Figure 4-9 shows the normalized correlation plot for the modified model. Comparing Figure 4-9 to Figure 4-8, a much better correlation with the measured failure levels can be seen. A much better correlation with the measured failure levels is also seen with the modified Ahmad model than with either the JSCE or the Gilstrap model. There is some scattering of the data points, which can be expected due to the variability of the material properties. However, the scatter observed when using the Ahmad model produces several values that fall on the unconservative side. This could be corrected by the use of a material resistance factor or a factor of safety. However, an appropriate value for this factor would need to be assessed for CFRP tendons of varying material properties.

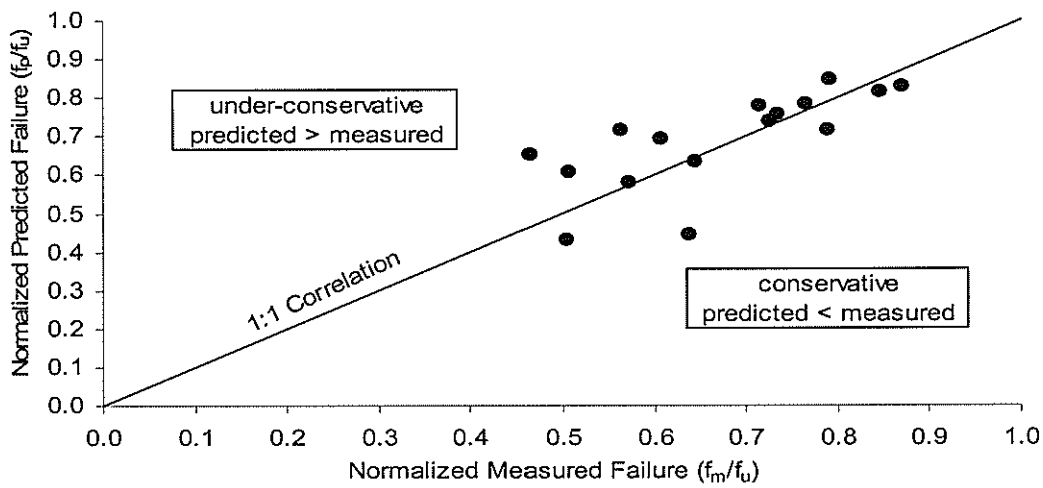


Figure 4-9: Correlation Plot for Ahmad Model with Guaranteed Strain Capacity

Overall, both the JSCE and Gilstrap models showed a very poor correlation with the measured data. It should also be noted that the JSCE and Gilstrap models are not influenced by the harping angle, whereas the experimental data, as shown in Figure 4-3, indicates that the harping angle does have an effect on the harped tendon

capacity. The Ahmad model, on the other hand, showed a much better correlation with the measured data, when modified to use the guaranteed tensile strain capacity for the CFRP material. However, the Ahmad model did still produce unconservative results. It was also found to be more difficult to use because the model is not dimensionally consistent and requires the variables to be in specific units of measure. In addition, the maximum tensile strain specific to the CFRP material used in their test program was included directly in the model rather than being specified as a variable.

Because of the problems in the existing models and design formulae for harped CFRP prestressing tendons as highlighted in this chapter, one of the objectives of this research program was to develop a new analytical model that can predict the behaviour and failure characteristics of harped CFRP prestressing tendons safely and efficiently. The next chapter presents the analytical model developed within this research program and explains its development.

5 ANALYTICAL MODEL

5.1 INTRODUCTION

The development of an analytical model that can closely predict the failure behaviour of harped CFRP prestressing tendons would allow the technology to be used much more efficiently and confidently in practical applications. As shown in the previous chapter, there are some deficiencies in existing analytical models for predicting the failure strength of the deviated tendons. The JSCE model (1997) was shown to be very unconservative when parameters beyond those used in its development were used. The model by Gilstrap et al. (2001) was shown to be too conservative in most cases. The JSCE and Gilstrap models do not include the harping angle as a variable in the models. A better correlation with the experimental data was seen with the model by Ahmad et al. (1997), however, it was still found to be unconservative in some cases. The Ahmad model was also found to be more difficult to use because the maximum tensile strain specific to their test program was included directly in the model rather than being specified as a variable, and the model is not dimensionally consistent, that is, it requires the variables to be in specific units of measure.

The objective of this portion of the research program was to develop a general analytical model based on the mechanics of the CFRP material and the statics and geometry of the tendon and harping configuration.

5.2 PRIMARY ANALYTICAL MODEL

The Gilstrap model is based on simple mechanics of materials, however, one of the main assumptions made is that the deviated CFRP tendon achieves the full

curvature of the deviator, that is, the radius of curvature of the tendon is equal to the radius of the deviator used under any loading level or harping configuration. However, experimental data reported by Gilstrap et al and by the current research program suggests that the assumption that the radius of curvature of the tendon is equal to the radius of the deviator under any condition may be erroneous. Specifically, Gilstrap et al reported that CFRP tendons were successfully loaded in configurations in which their model predicted the tendon should fail. Additionally, for several specimens from the current research program, the Gilstrap model predicted the tendon could not carry any load. This was not the case and the tendons were able to carry significant loading before failure.

The analytical model developed here is also based on mechanics and the elastic properties of the material. However, this model does not assume that the tendon achieves the curvature of the deviator. It is assumed that, because of the inherent stiffness of the tendon, it will achieve its own natural radius of curvature relative to the stiffness of the CFRP material, the harping configuration and the applied load. The model attempts to determine the natural curvature of the tendon based on its material properties, the geometry of the harped configuration and the applied load.

5.2.1 Tendon Properties

The CFRP tendon in the model is assumed to have a constant circular cross-section of radius, r . The CFRP material is assumed to be linear elastic in both tension and shear, and have the following properties:

- E : modulus of elasticity
- G : shear modulus
- ε_{ut} : tensile rupture strain
- σ_{ut} : ultimate tensile failure stress ($\sigma_{ut} = E \cdot \varepsilon_{ut}$)

5.2.2 Harping Profile Geometry

Figure 5-1 shows the general layout and configuration of the harped tendon. It is assumed that the tendon is harped symmetrically at an angle θ over point A and that a load, P , is applied axially in tension to the tendon. Between points B and C, the tendon is assumed to be bent at a constant radius of curvature, R . Beyond points B and C, the tendon is assumed to be straight ($R = \infty$). By geometry, it can be shown that angles ADB and ADC are equal to θ .

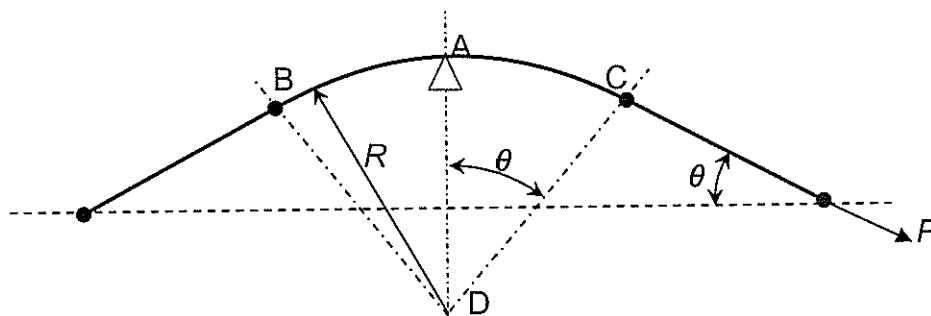


Figure 5-1: Assumed General Tendon Profile

5.2.3 Axial Stress and Strain

The mode of failure for the tendon is assumed to be a tension failure due to the total axial stresses exceeding the tensile capacity of the CFRP tendon in this model. It is also assumed that the only significant axial stresses and strains in the curved tendon are those due to tensile loading, σ_t and ϵ_t , and bending, σ_b and ϵ_b , as shown in Figure 5-2.

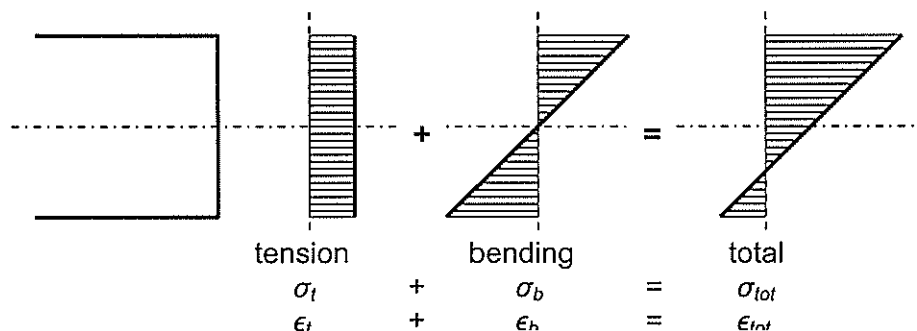


Figure 5-2: Axial Stress and Strain Distribution across Tendon Cross Section

It is acknowledged that there are other forces present in the curved tendon including normal forces perpendicular to the tendon due to bearing on the deviator and longitudinal forces due to friction between the deviator and tendon. These forces will have an effect on the axial stress in the tendon, however, the magnitude of this effect is assumed to be negligible for the purposes of this analysis.

5.2.3.1 Tension Stress and Strain

The tension stress is assumed to be uniform over the tendon cross section fibres as shown in Figure 5-2.

This stress is a direct result of the applied load P :

$$\sigma_t = \frac{P}{A}$$

For a circular cross section, $A = \pi \cdot r^2$

Equation 5-1:
$$\sigma_t = \frac{P}{\pi \cdot r^2}$$

The corresponding tension strain in the tendon is:

$$\varepsilon_t = \frac{\sigma_t}{E}$$

Equation 5-2:
$$\varepsilon_t = \frac{P}{E \cdot \pi \cdot r^2}$$

5.2.3.2 Bending Stress and Strain

Bending stress and strain are a result of the curvature induced in the tendon over the deviator. Because the material is linear elastic and the tendon cross-section is symmetric, the bending stress is assumed to vary linearly across the tendon cross section with the neutral axis at mid-depth and compression stresses occurring in the bottom fibres and tension stresses occurring in the top fibres, as shown in Figure 5-2. To calculate the axial stress and strain due to bending, the relationship between the

curvature of the tendon and the axial stress and strain needs to be determined. Figure 5-3 illustrates a section of tendon curved to radius R through angle θ .

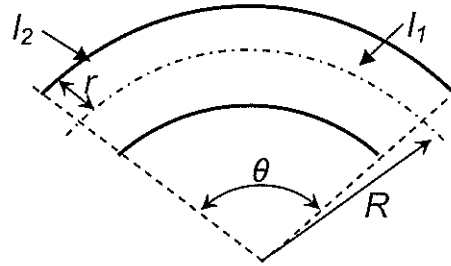


Figure 5-3: Curved Section of CFRP Tendon

The undeformed, straight length of the tendon is equivalent to the neutral axis arc length:

$$l_1 = \frac{\theta \cdot \pi}{180} \cdot R$$

The deformed length of the top fibre is:

$$l_2 = \frac{\theta \cdot \pi}{180} \cdot (R + r)$$

Therefore, the strain experienced in the top fibre is:

$$\begin{aligned} \varepsilon_b &= \frac{l_2 - l_1}{l_1} \\ \varepsilon_b &= \frac{\frac{\theta \cdot \pi}{180} \cdot (R + r) - \frac{\theta \cdot \pi}{180} \cdot R}{\frac{\theta \cdot \pi}{180} \cdot R} \end{aligned}$$

Equation 5-3: $\varepsilon_b = \frac{r}{R}$

The corresponding bending stress in the top fibre is:

$$\sigma_b = E \cdot \varepsilon_b$$

Equation 5-4: $\sigma_b = E \cdot \frac{r}{R}$

The bending stress and strain are assumed to vary linearly and symmetrically about the neutral axis; therefore, the maximum bending stress and strain in the bottom fibre of the tendon can be taken as the negative of Equation 5-4 and Equation 5-3 respectively, and will be in compression. Equation 5-4 is similar to that used by Gilstrap et al. (2001), with the difference being that the radius of curvature, R , here represents the natural radius of curvature that the tendon has assumed, which is not necessarily equal to the radius of the deviator. This will be explained further in Section 5.2.4.

5.2.3.3 Total Axial Stress and Strain

Superposition of the axial tension and bending stresses gives the total axial stress state across a given tendon cross-section, as shown in Figure 5-2.

The total axial stress is given as:

$$\text{Equation 5-5: } \sigma_{tot} = \sigma_t + \sigma_b$$

Similarly, the total axial strain is:

$$\text{Equation 5-6: } \varepsilon_{tot} = \varepsilon_t + \varepsilon_b$$

5.2.4 Radius of Curvature

To determine the total axial stress and strain state in the tendon resulting from the applied load, P , both the tension and bending stress in the tendon need to be related to P . Equation 5-1 and Equation 5-2 show the direct relationship between the tension stress and strain and the applied load. Because there is a stiffness associated with the CFRP material, the tendon will not bend to assume a sharp corner across point A. Rather, the tendon will bend to a radius of curvature that restores equilibrium of the internal and external forces, which will be termed the natural radius of curvature, R_n . It is assumed that the natural radius of curvature of the

tendon is related to the applied load, P . As shown in Equation 5-4, the axial bending stress is related to the radius of curvature of the tendon, and therefore, it follows that the axial stress and strain due to bending is related to P .

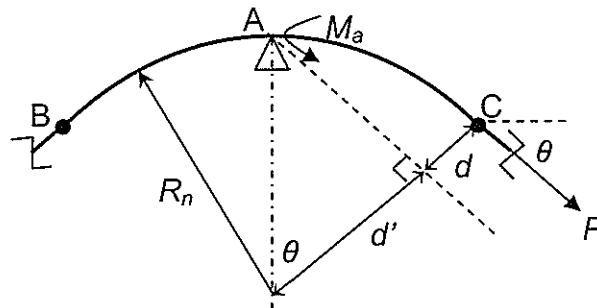


Figure 5-4: Bending Moment Arm

To determine the relationship between P and R_n , it is first assumed that the applied load, P , produces an applied bending moment, M_a , at point A because of the moment arm, d , as shown in Figure 5-4. If point A is assumed to be the bearing point, the applied moment about the point A from load P is:

$$M_a = P \cdot d$$

From geometry, the moment arm is:

$$d = R_n - d'$$

Where: $d' = R_n \cdot \cos(\theta)$

$$d = R_n \cdot (1 - \cos(\theta))$$

Therefore, the applied bending moment is:

Equation 5-7: $M_a = P \cdot R \cdot (1 - \cos(\theta))$

From classical elastic bending theory (Beer et al, 2002), beam curvature is related to the elastic bending moment by:

$$\frac{1}{R} = \frac{M}{E \cdot I}$$

Therefore, the elastic bending moment can be defined as:

$$\text{Equation 5-8: } M_e = \frac{E \cdot I}{R}$$

For equilibrium, the applied bending moment (M_a , Equation 5-7) and the elastic bending moment (M_e , Equation 5-8) at point A must be equal.

Setting these moments to be equal and solving for the applied load, P , gives:

$$M_e = M_a$$

$$\text{Therefore: } P \cdot R_n \cdot (1 - \cos(\theta)) = \frac{E \cdot I}{R_n}$$

$$P = \frac{E \cdot I}{R_n^2 \cdot (1 - \cos(\theta))}$$

For a circular tendon cross-section: $I = \frac{1}{4} \cdot \pi \cdot r^4$

$$\text{Equation 5-9: } P = \frac{E \cdot \pi \cdot r^4}{4 \cdot R_n^2 \cdot (1 - \cos(\theta))}$$

Conversely, rearranging Equation 5-9 in terms of the natural radius of curvature:

$$\text{Equation 5-10: } R_n = \frac{r^2}{2} \cdot \sqrt{\frac{E \cdot \pi}{P \cdot (1 - \cos(\theta))}}$$

These two equations show the relationship between P and R required to satisfy moment equilibrium. Equation 5-9 solves for the load, P , required to achieve a radius of curvature, R_n , in the given tendon. Equation 5-10 solves for the radius of curvature, R_n , which results in the tendon from the applied load, P . Following the initial assumption, it can be seen from these equations that the natural radius of curvature of the tendon is related to the applied load and that the radius will decrease as the load is increased.

Substituting Equation 5-10 into Equation 5-4 gives:

$$\text{Equation 5-11: } \sigma_b = \frac{2}{r} \cdot \sqrt{\frac{E \cdot P \cdot (1 - \cos(\theta))}{\pi}}$$

Similarly, substituting Equation 5-10 into Equation 5-3 gives:

$$\text{Equation 5-12: } \varepsilon_b = \frac{2}{r} \cdot \sqrt{\frac{P \cdot (1 - \cos(\theta))}{\pi \cdot E}}$$

Equation 5-11 and Equation 5-12 give the bending stress and strain, respectively, in the extreme fibres of the tendon at point A that result from the applied load P for the given harping configuration. Assuming a symmetrical stress and strain distribution, this stress and strain is equal in magnitude to that for both tension in the top fibre and compression in the bottom fibre.

5.2.5 Tendon Failure Criterion and Model Solution

In order to solve for the load at which tendon failure will occur, a failure criterion needs to be employed. Ignoring any friction effects, axial stress and strain due to tensile loading is constant along the entire tendon. On the other hand, axial stress and strain due to bending will only be present in the curved segment of the tendon. It has already been shown that, as the applied load is increased, the axial stress and strain due to tensile loading (Equation 5-1 and Equation 5-2) will increase, and that the axial stress and strain due to bending (Equation 5-11 and Equation 5-12) will increase. Thus, it follows that the maximum total axial stress and strain (Equation 5-5 and Equation 5-6) will be in the top fibre of the curved segment of the tendon, and that tendon failure will occur in this location in tension. Using the tensile rupture strain (ε_{ut}) of the material as the failure criterion, the tendon will fail in tension when the maximum total axial strain exceeds the rupture strain of the material. Therefore, Equation 5-6 can be redefined as:

$$\text{Equation 5-13: } \varepsilon_{ut} = \varepsilon_{tf} + \varepsilon_{bf}$$

The failure criterion as given by Equation 5-13 needs to be solved for the tension and bending strains that satisfy both the failure criterion and equilibrium.

Substituting Equation 5-9 into Equation 5-2:

$$\varepsilon_{yf} = \frac{\left(\frac{E \cdot \pi \cdot r^4}{4 \cdot R_{nf}^2 \cdot (1 - \cos(\theta))} \right)}{E \cdot \pi \cdot r^2}$$

$$\varepsilon_{yf} = \frac{1}{4 \cdot (1 - \cos(\theta))} \cdot \left(\frac{r}{R_{nf}} \right)^2$$

From Equation 5-3:

$$\varepsilon_b = \frac{r}{R}$$

Therefore:
$$\varepsilon_{yf} = \frac{1}{4 \cdot (1 - \cos(\theta))} \cdot (\varepsilon_{bf})^2$$

Substituting into Equation 5-13 gives a quadratic equation with bending strain, ε_{bf} , as the only unknown:

$$\varepsilon_{ut} = \frac{1}{4 \cdot (1 - \cos(\theta))} \cdot (\varepsilon_{bf})^2 + \varepsilon_{bf}$$

$$\frac{1}{4 \cdot (1 - \cos(\theta))} \cdot (\varepsilon_{bf})^2 + \varepsilon_{bf} - \varepsilon_{ut} = 0$$

Solving the quadratic for the bending strain, ε_{bf} :

Equation 5-14:
$$\varepsilon_{bf} = 2 \cdot (1 - \cos(\theta)) \cdot \left(\sqrt{1 + \frac{\varepsilon_{ut}}{(1 - \cos(\theta))}} - 1 \right)$$

Equation 5-14 gives the bending strain component of the total axial strain in the curved segment at tendon failure. This solution for the failure criterion assumes that the tendon is able to attain the natural radius of curvature corresponding to the moment equilibrium at the failure load, R_n . However, the radius of curvature of the tendon is physically limited by the radius of the deviator, R_d , that is, as the load is applied, once the tendon has reached the radius of curvature of the deviator, the

radius of curvature of the tendon will no longer be able to decrease. Therefore, the minimum radius of curvature attainable is:

$$\text{Equation 5-15: } R_{\min} = R_d + r$$

In this model, it is assumed that the tangential angle of the deviator used is greater than the effective harping angle so that a sharp bending point is not created in the tendon at the deviator edge when the tendon achieves a radius of curvature equal to R_{\min} .

Substituting Equation 5-14 into Equation 5-3, the natural radius of curvature that the tendon assumes at failure can be determined:

$$\varepsilon_{bf} = \frac{r}{R_{nf}}$$

$$R_{nf} = \frac{r}{\varepsilon_{bf}}$$

$$\text{Equation 5-16: } R_{nf} = \frac{r}{2 \cdot (1 - \cos(\theta)) \cdot \left(\sqrt{1 + \frac{\varepsilon_{ut}}{(1 - \cos(\theta))}} - 1 \right)}$$

Thus, if the natural radius of curvature, R_{nf} , given by Equation 5-16 is less than the minimum as limited by the deviator, R_{\min} , given by Equation 5-15, and then R_{\min} should be used, otherwise, R_{nf} should be used:

$$\text{Equation 5-17: } R_f = \max(R_{nf}, R_{\min})$$

The radius, R_f , can then be used to determine the both the tension and bending strain components of the total axial strain at failure:

$$\text{Equation 5-18: } \varepsilon_{bf} = \frac{r}{R_f}$$

From Equation 5-13, the tension strain component is:

$$\varepsilon_{tf} = \varepsilon_{ut} - \varepsilon_{bf}$$

Equation 5-19: $\varepsilon_{yf} = \varepsilon_{ut} - \frac{r}{R_f}$

It also follows that the tension and bending stress components of the total axial stress at failure are:

Equation 5-20: $\sigma_{bf} = E \cdot \frac{r}{R_f}$

Equation 5-21: $\sigma_{yf} = \sigma_{ut} - E \cdot \frac{r}{R_f}$

The tension stress component of the total axial stress at failure is equal to the tensile capacity of the harped tendon.

The tensile capacity of the harped tendon expressed as a percentage of the ultimate capacity of the straight tendon is:

Equation 5-22: $\sigma'_{ut} = \phi_h \cdot \sigma_{ut}$

$$\phi_h = \frac{\sigma_{ut} - E \cdot \frac{r}{R_f}}{\sigma_{ut}}$$

Equation 5-23: $\phi_h = 1 - \frac{r}{\varepsilon_{ut} \cdot R_f}$

The coefficient ϕ_h represents the tensile strength reduction factor for a harped tendon with the given configuration and properties.

From Equation 5-1, the maximum tensile load capacity for the harped tendon is:

Equation 5-24: $P_f = \sigma'_{ut} \cdot \pi \cdot r^2$

5.2.6 Primary Model Solution Characteristics

Using the primary model developed in this chapter and illustrated in Figure 5-5 and Figure 5-6, the effect that the harping configuration variables, particularly the

harping angle and deviator radius, have on the harped CFRP prestressing tendon's tensile capacity can be clearly seen.

Figure 5-5 shows the predicted tendon tensile capacity as a percent of the ultimate capacity of the CFRP tendon, in relation to the harping angle using the guaranteed minimum material properties for the CFRP material used in this research program ($E = 124\text{GPa}$ and $\epsilon_{ult} = 16,677\text{microstrain}$). It can be seen that the tendon capacity decreases as the harping angle is increased, from a maximum of 100% when the harping angle is zero or there is no harping. Also indicated in Figure 5-5 is a 'plateau' effect for deviator radii of 500mm, 1000mm and 1500mm. This effect occurs when the calculated natural radius of curvature for the tendon would be less than the specified deviator radius. The radius of curvature of the tendon becomes physically limited at the deviator radius and, therefore, the tendon capacity is not affected by any further increase of the harping angle.

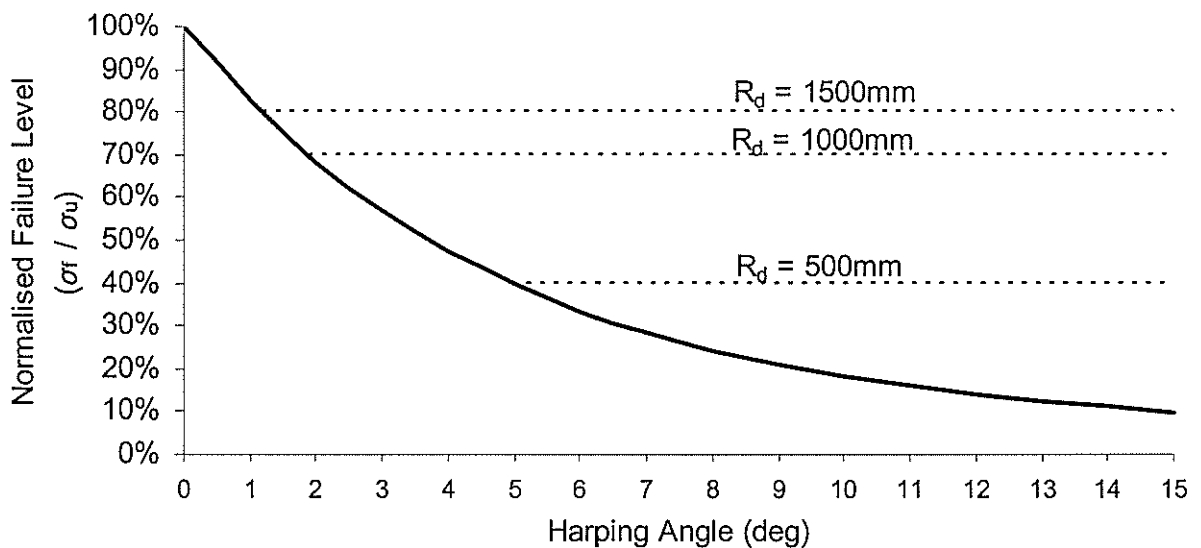


Figure 5-5: Predicted Failure Level vs. Harping Angle

Figure 5-6 shows the predicted failure level in relation to the deviator radius, using the same values for the elastic modulus and the tensile rupture strain as used for

Figure 5-5. It can be seen that the tendon capacity increases as the deviator radius is increased. The minimum failure strain curve in Figure 5-6 represents the condition where the tendon radius of curvature is equal to the deviator radius. This solution is exactly equal to that given by the Gilstrap model. However, when the natural radius of curvature for the tendon at failure is greater than that as limited by the deviator radius for the specified harping angle, the deviator radius has no effect on the tendon capacity. Examples of this condition are illustrated by the horizontal failure strain lines indicated for 2, 5 and 10 degrees. The point of intersection between the horizontal failure strain lines and the minimum failure strain curve indicates the natural radius of curvature of the tendon at failure for the given harping variables. Comparing the horizontal failure strain lines to the minimum failure strain curve, it can clearly be seen that using a natural radius of curvature, based on the tendon stiffness and equilibrium, can give a significant increase in the calculated tendon strength over using the deviator radius, especially with smaller deviators and at lower harping angles.

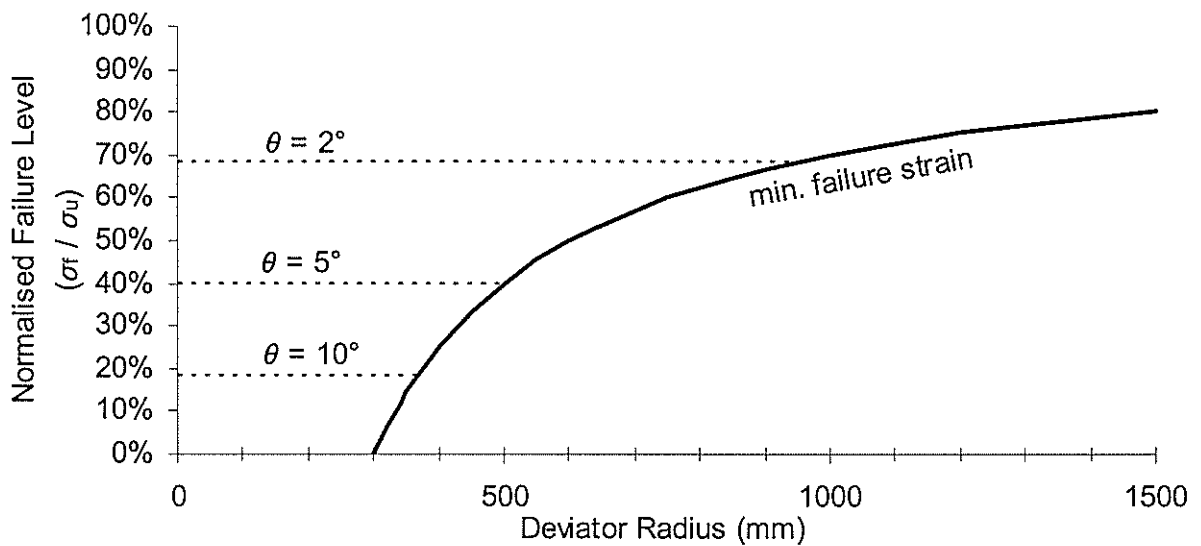


Figure 5-6: Predicted Failure Level vs. Deviator Radius

5.3 TRANSITION EFFECTS AND INTER-LAMINAR SHEAR DEFORMATION

Under the model as developed so far, the assumption is that classical bending theory applies to the tendon: plane sections remain plane and perpendicular to the neutral axis. This means that within the curved portion of the tendon where it is assumed that the radius of curvature is constant, the bending stress and strain are constant, and within the straight portions, the bending stress and strain are zero, as shown in Figure 5-7. This results in a discontinuity in the bending stress in and an unbalanced bending moment at the transition point between the curved and straight segments.

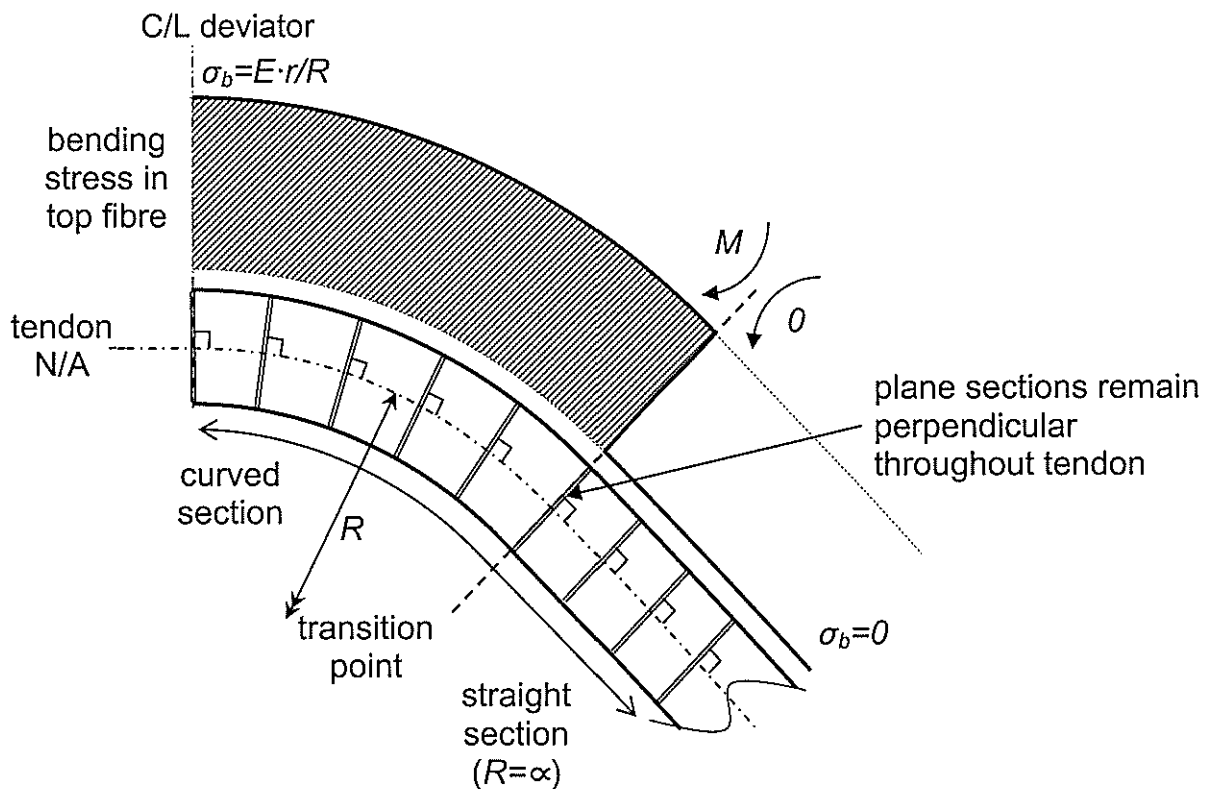


Figure 5-7: Top Fibre Bending Stress Distribution under Elastic Bending Theory

The occurrence of an unbalanced bending moment at the transition point suggests that one or more of the assumptions for classical bending theory may not be valid for this scenario. Because the CFRP material is not infinitely rigid against shear deformation, it is possible that, for some distance across the transition point, plane

sections rotate from perpendicular to the neutral axis due to inter-laminar shear deformation, as shown in Figure 5-8. This results in a relaxation of the top fibre material, which allows the resulting bending moment to transition smoothly across the transition zone. This also means that for the segment of the curved tendon that lies within the transition zone, the top fibre bending stress and strain will be lower than that given by the pure elastic theory (Equation 5-4 and Equation 5-3). If the resulting transition zone is located such that the centreline of the deviator lies within it, then the maximum bending stress and strain at this point will also be lower than that calculated by the pure elastic theory, resulting in a larger tensile capacity in the tendon.

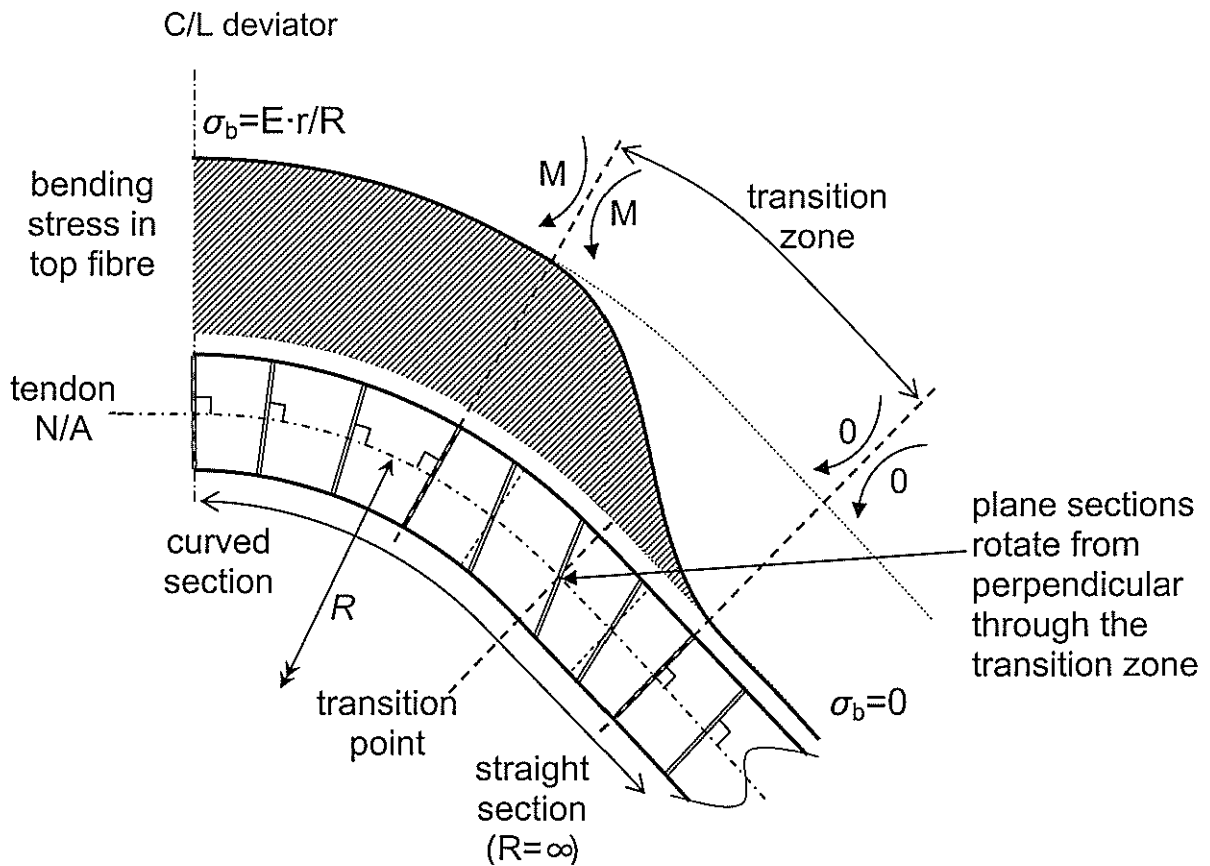


Figure 5-8: Top Fibre Bending Stress Distribution with Transition Effects

5.4 EQUIVALENT SPRING FRAME MODEL

The exact characteristics and magnitude of the transition zone and transition effect are unknown, which makes calculating this transition effect analytically using external elastic equilibrium very complex and difficult. Thus, in order to assess the significance of the transition effect, a simplified finite element analysis (FEA) was used. The CFRP tendon was transformed into an equivalent spring frame model as shown in Figure 5-9. Because the stress and strain distribution is assumed to be linear and symmetric across the neutral axis, only the top half of the tendon was modeled. In addition, because the tendon profile is symmetric across the deviator centreline, it was only necessary to model the right half of the tendon and treat the frame as fixed at the deviator centreline.

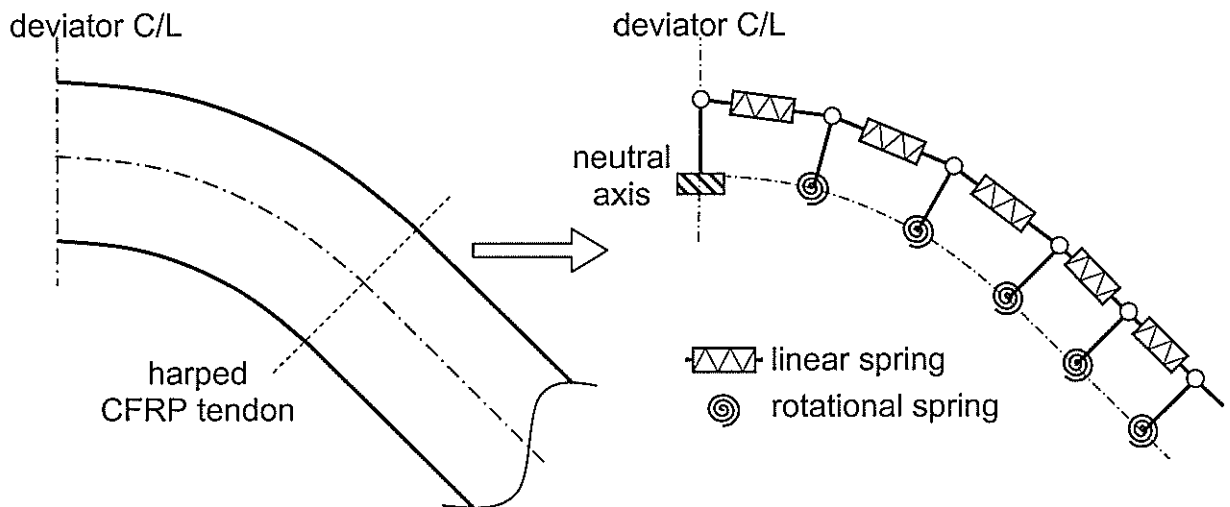


Figure 5-9: Equivalent Spring Frame Model

The tendon was discretized into frame elements with a height equal to half the tendon height and a length dependent on the level of refinement of the frame model. The horizontal frame members were represented as linear springs as shown in Figure 5-9 and Figure 5-10a. The vertical frame members were represented as a rigid body connected to the neutral axis by a rotational spring and pin-connected to

the linear springs at the top, as shown in Figure 5-9 and Figure 5-10b. It is assumed that the linear spring coefficient is related to a linear deformation of the elements and that the rotational spring coefficient is related to an inter-laminar shear deformation of the elements.

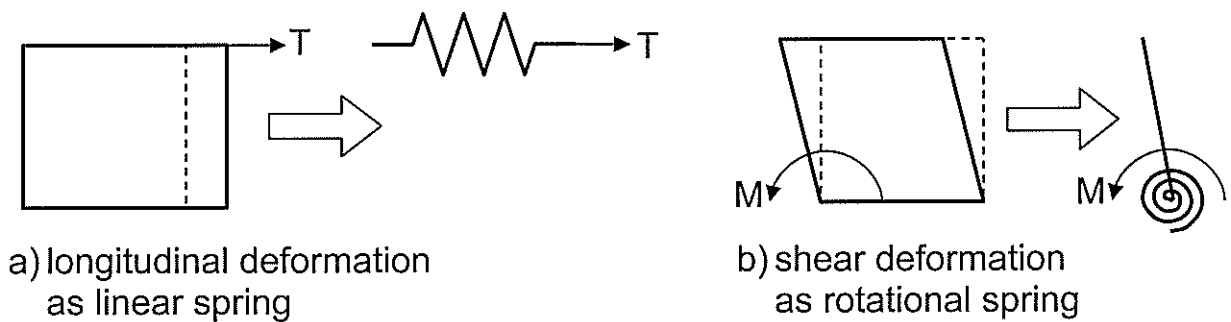


Figure 5-10: Elemental Representation in Equivalent Spring Frame Model

The axial strain resulting from the applied tensile loading is assumed to be constant both across the cross-section and along the length of the tendon, therefore, direct tension strains due to the applied load can be assumed to have no influence on the transition effect, and the spring frame needs to model only the axial bending strain. The axial bending strains are related to the deformation of the tendon because of the curvature of the tendon, therefore, the rotational springs can be assumed to be fixed in their linear position along the profile of the neutral axis, and no external loading needs to be applied to the model.

Figure 5-11 illustrates the variables of a typical element in the spring frame model. The neutral axis of the curved tendon is described by a straight line for illustrative purposes. The angle, θ_n , is used to indicate the global rotation or slope of the neutral axis of the tendon at element n due to curvature of the tendon.

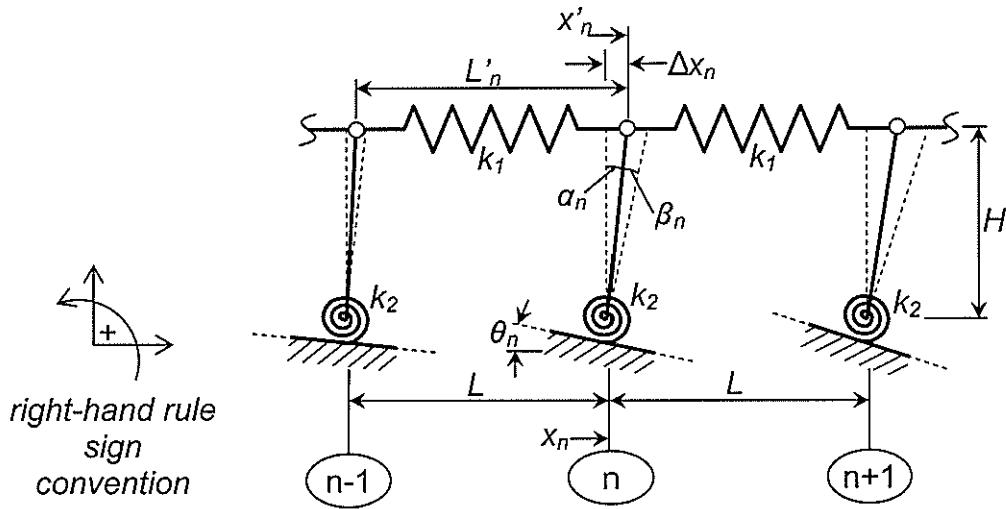


Figure 5-11: Spring Frame Model Element Variables

The frame model has the following geometric variables:

- H : element height (tendon radius, r , for circular tendon)
- L : element length
- L'_n : deformed length of element n at top fibre
- ΔL_n : net change in length of element n at top fibre (linear deformation)
- x_n : linear position of element n at the neutral axis
- x'_n : deformed linear position of element n at top fibre
- Δx_n : net change in linear position of element n at top fibre
- θ_n : global rotation or slope of neutral axis at element n due to curved tendon profile
- β_n : rotation of element n from perpendicular to neutral axis (shear deformation)
- α_n : net global rotation of element n ($\alpha_n = \theta_n + \beta_n$)
- k_1 : linear spring coefficient
- k_2 : rotational spring coefficient

Using the right-hand rule sign convention, counter-clockwise rotations are assumed to be positive. Therefore, setting up the model for the right side of the tendon profile, the global rotations, θ_n , will be negative.

Solving for geometric compatibility:

$$\Delta x_n = -H \cdot \tan(\alpha_n)$$

However, α_n is assumed small, $\therefore \tan(\alpha_n) = \alpha_n$

$$\Delta x_n = -H \cdot \alpha_n$$

$$x'_n = x_n + \Delta x_n$$

$$x'_n = x_n - H \cdot \alpha_n$$

$$L'_n = x'_n - x'_{n-1}$$

$$L'_n = (x_n - H \cdot \alpha_n) - (x_{n-1} - H \cdot \alpha_{n-1})$$

$$L'_n = (x_n - x_{n-1}) - H \cdot (\alpha_n - \alpha_{n-1})$$

But $L = (x_n - x_{n-1})$

$$L'_n = L - H \cdot (\alpha_n - \alpha_{n-1})$$

$$\Delta L_n = L - L'_n$$

$$\Delta L_n = -H \cdot (\alpha_n - \alpha_{n-1})$$

But $\alpha_n = \theta_n + \beta_n$

$$\Delta L_n = -H \cdot ((\theta_n + \beta_n) - (\theta_{n-1} + \beta_{n-1}))$$

Equation 5-25: $\Delta L_n = -H \cdot (\theta_n - \theta_{n-1} + \beta_n - \beta_{n-1})$

5.4.1 Matrix Stiffness Method

The spring frame structure can be viewed as a force-displacement equilibrium problem, with unknown forces and displacements associated with the top fibre longitudinal deformation and the out-of-perpendicular shear deformation. Therefore, to solve the spring frame structure for the unknowns, the displacement or stiffness method for analysing indeterminate structures can be utilised in a matrix form.

The system of simultaneous linear equations for the matrix stiffness method is expressed as:

$$\text{Equation 5-26: } [FEM] + [K] \cdot [D] = [M]$$

Where:

$[FEM]$: matrix of fixed-end moments: related to fixing the nodal degrees of freedom

$[K]$: stiffness matrix: matrix of forces due to unit displacements related to the unknown displacements

$[D]$: matrix of unknown displacements (degrees of freedom)

$[M]$: matrix of external moments: related to the unknown displacements

Because the spring frame model only represents the bending strain resulting from an imposed curvature, it can be assumed that there are no external applied loads on the spring-frame nodes, that is, $[M] = 0$.

$$\text{Equation 5-27: } [FEM] + [K] \cdot [D] = 0$$

5.4.1.1 Matrix of Unknown Displacements

In the spring frame model, the forces that result from the deformation of element n are shown in Figure 5-12.

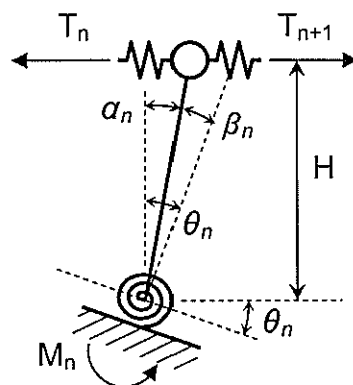


Figure 5-12: Reaction Forces Acting on Element n

For moment equilibrium, the sum of the moments about the base of the element must be equal to zero:

$$\Sigma M_{0n} = 0$$

Equation 5-28: $M_n + H \cdot T_n - H \cdot T_{n+1} = 0$

The horizontal tension force in the top member due to elongation of the linear spring is:

$$T_n = k_1 \cdot \Delta L_n$$

Incorporating Equation 5-25 gives:

Equation 5-29: $T_n = -k_1 \cdot H \cdot [(\theta_n - \theta_{n-1}) + (\beta_n - \beta_{n-1})]$

The base moment due to rotation of the rotational spring is given by:

Equation 5-30: $M_n = k_2 \cdot \beta_n$

From Equation 5-29 and Equation 5-30, since k_1 , k_2 , ΔL_n , H and θ are all known values, it can be seen that moment equilibrium (Equation 5-28) can be expressed in terms of a single degree of freedom at each element: the rotation β_n , which represents the shear deformation.

Therefore, in Equation 5-27, the matrix of unknown displacements $[D]$ can be redefined as the matrix of unknown rotations $[\beta]$:

Equation 5-31: $[FEM] + [K] \cdot [\beta] = 0$

For a structure with i elements, the matrix of unknown rotations is given by:

Equation 5-32: $[\beta] = \begin{bmatrix} \beta_1 \\ \beta_2 \\ \beta_3 \\ \vdots \\ \beta_i \end{bmatrix}$

5.4.1.2 Matrix of Fixed-End Moments

The matrix of fixed-end moments, $[FEM]$, is determined by fixing the degrees of freedom against displacement to create a kinematically determinate primary structure, as shown in Figure 5-13, and calculating the resulting fixed-end moments.

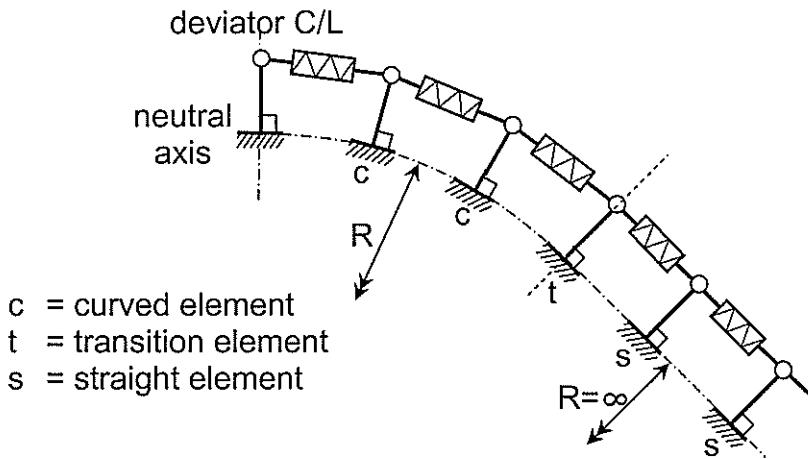


Figure 5-13: Kinematically Determinate Fixed-End Primary Structure

There are no external applied forces to cause fixed-end moments. However, the curvature induced in the straight spring frame model causes fixed-end moments due to a "lack of fit" situation whereby the horizontal spring (top member) must be stretched to fit the fixed-end structure.

Figure 5-14 shows a typical element in the curved segment of the primary structure.

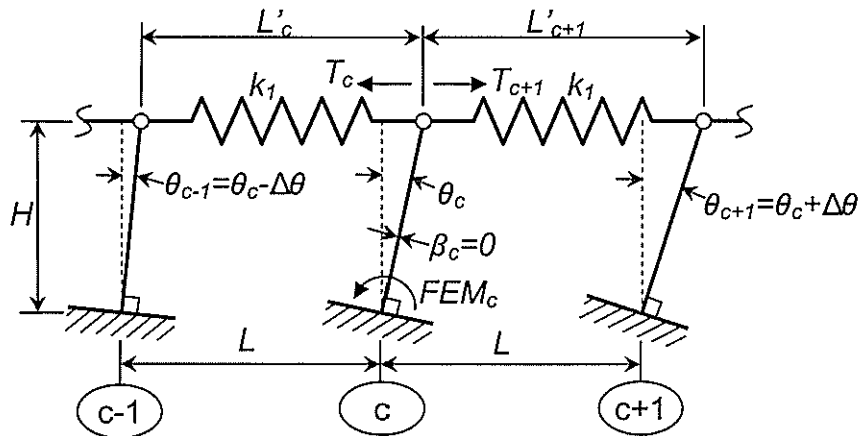


Figure 5-14: Typical Element in Curved Segment of Fixed-End Primary Structure

The fixed-end moment for node c is:

$$FEM_c = H \cdot T_{c+1} - H \cdot T_c$$

From Equation 5-29: $T_c = -k_1 \cdot H \cdot ((\theta_c - \theta_{c-1}) + (\beta_c - \beta_{c-1}))$

For the primary structure: $\beta_c = 0$

$$FEM_c = H \cdot (-k_1 \cdot H \cdot (\theta_{c+1} - \theta_c)) - H \cdot (-k_1 \cdot H \cdot (\theta_c - \theta_{c-1}))$$

$$FEM_c = -k_1 \cdot H^2 \cdot ((\theta_{c+1} - \theta_c) - (\theta_c - \theta_{c-1}))$$

$$FEM_c = -k_1 \cdot H^2 \cdot (\theta_{c+1} - 2 \cdot \theta_c + \theta_{c-1})$$

Within the curved section, $\Delta\theta$ is constant, $\therefore \theta_{c-1} = \theta_c - \Delta\theta$ and $\theta_{c+1} = \theta_c + \Delta\theta$

$$FEM_c = -k_1 \cdot H^2 \cdot (\theta_c + \Delta\theta - 2 \cdot \theta_c + \theta_c - \Delta\theta)$$

Equation 5-33: $FEM_c = 0$

Figure 5-15 shows the transition point element of the primary structure. This is a unique element in the primary structure since to the left of the element there is curvature, and to the right of the element there is no curvature.

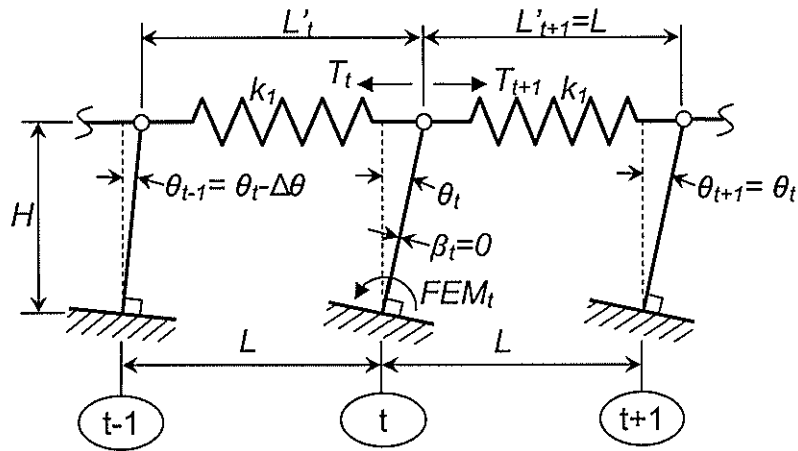


Figure 5-15: Transition Point Element of Fixed-End Primary Structure

The fixed-end moment for node t is:

$$FEM_t = H \cdot T_{t+1} - H \cdot T_t$$

$$FEM_t = -k_1 \cdot H^2 \cdot (\theta_{t+1} - 2 \cdot \theta_{t-1} + \theta_{t-1})$$

Again, within the curved section, $\Delta\theta$ is constant, $\therefore \theta_{t-1} = \theta_t - \Delta\theta$

Within the straight section, θ is constant, $\therefore \theta_{t+1} = \theta_t$

$$FEM_t = -k_1 \cdot H^2 \cdot (\theta_t - 2 \cdot \theta_t + \theta_t - \Delta\theta)$$

$$FEM_t = k_1 \cdot H^2 \cdot \Delta\theta$$

From the geometry of the structure: $L = -\Delta\theta \cdot R$

Equation 5-34: $FEM_t = -k_1 \cdot H^2 \cdot \frac{L}{R}$

Figure 5-16 shows a typical element in the straight segment of the primary structure.

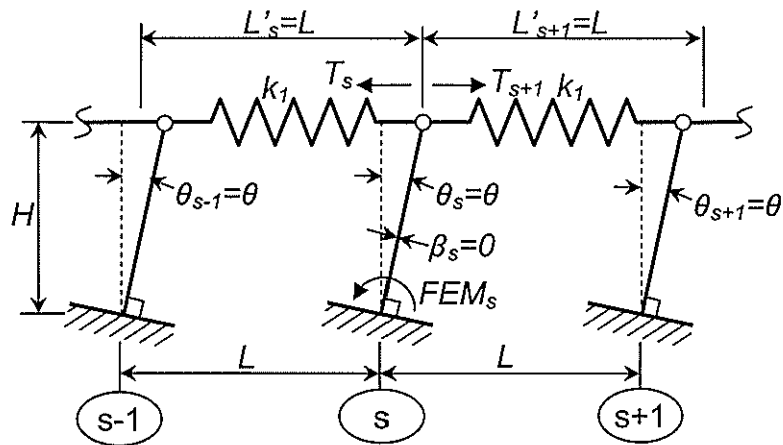


Figure 5-16: Typical Element in Straight Segment of Fixed-End Primary Structure

Because the straight segment elements of the primary structure have no curvature, there is no deformation of the elements and it can be inferred that, therefore, there is no resulting fixed-end moment:

Equation 5-35: $FEM_s = 0$

From Equation 5-33, Equation 5-34 and Equation 5-35, it can be seen that in the fixed-end moments in the primary structure are equal to zero everywhere except at the transition point, element t .

Assembling the matrix of fixed-end moments for a structure of i elements gives:

$$\text{Equation 5-36: } [FEM] = \begin{bmatrix} 0 \\ 0 \\ 0 \\ \vdots \\ -k_1 \cdot H^2 \cdot \frac{L}{R} \\ \vdots \\ 0 \\ 0 \\ 0 \end{bmatrix}$$

5.4.1.3 Stiffness Matrix

The stiffness matrix defines the force-displacement relationship for each element of the structure and is independent of any applied loading, including that from the lack of fit. Therefore, to simplify calculations, the primary structure from Figure 5-13 can be treated as straight, as shown in Figure 5-17.

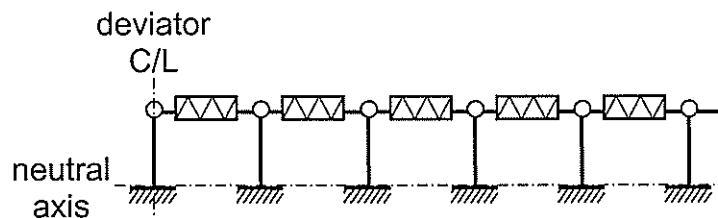


Figure 5-17: Reconfigured Determinate Fixed-End Primary Structure

The stiffness matrix is formed by releasing each node independently and applying a unit displacement in the direction of the unknown displacement. The reaction forces from the unit displacements make up the stiffness matrix. Figure 5-18 illustrates a unit displacement at a typical element, n .

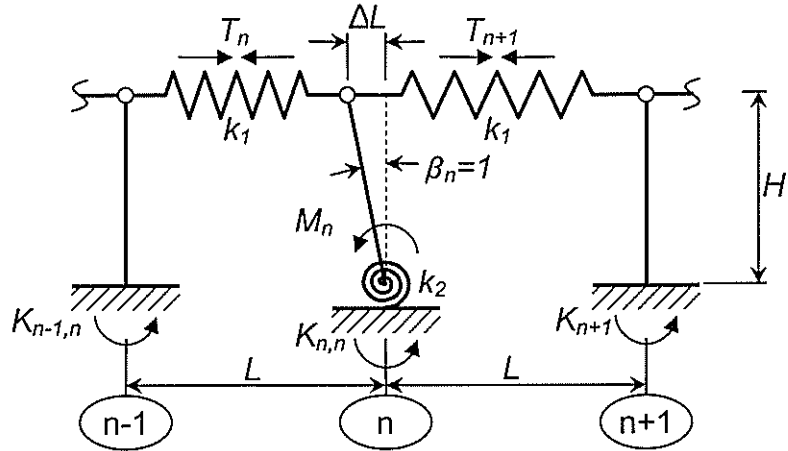


Figure 5-18: Unit Displacement at Typical Element

For the typical element as shown in Figure 5-18:

$$\theta_{n-1} = \theta_n = \theta_{n+1} = 0, \beta_{n-1} = \beta_{n+1} = 0, \beta_n = 1$$

The resultant forces from the unit displacement are calculated as:

$$\text{From Equation 5-29, } T_n = -k_1 \cdot H \cdot (\theta_n - \theta_{n-1} + \beta_n - \beta_{n-1})$$

$$\therefore T_n = -k_1 \cdot H \text{ and } T_{n+1} = k_1 \cdot H$$

$$\text{From Equation 5-30, } M_n = k_2 \cdot \beta_n$$

$$\therefore M_n = k_2$$

Calculating the reaction forces at each node:

node $n-1$:

$$K_{n-1,n} = H \cdot T_n$$

$$K_{n-1,n} = -k_1 \cdot H^2$$

node n :

$$K_{n,n} = H \cdot T_{n+1} - H \cdot T_n - M_n$$

$$K_{n,n} = k_1 \cdot H^2 - (-k_1 \cdot H^2) - k_2$$

$$K_{n,n} = 2 \cdot k_1 \cdot H^2 - k_2$$

node $n+1$:

$$K_{n+1,n} = -H \cdot T_{n+1}$$

$$K_{n+1,n} = -k_1 \cdot H^2$$

Therefore, the sub-matrix for the stiffness at node n is:

$$K_n = \left\{ -k_1 \cdot H^2 \quad 2 \cdot k_1 \cdot H^2 - k_2 \quad -k_1 \cdot H^2 \right\}$$

Equation 5-37:
$$K_n = k_1 \cdot H^2 \cdot \left\{ -1 \quad 2 - \frac{k_2}{k_1 \cdot H^2} \quad -1 \right\}$$

At either end of the spring frame structure, the structure is assumed to be fixed as illustrated in Figure 5-19.

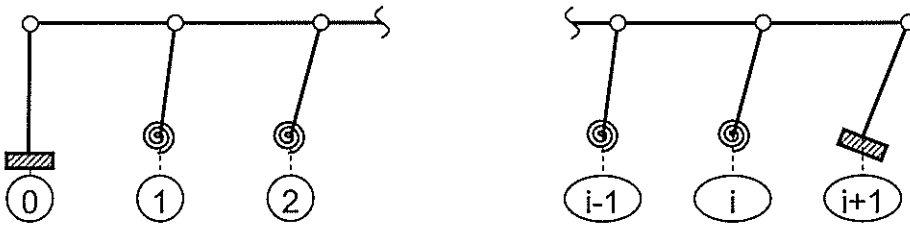


Figure 5-19: End Conditions of a Spring Frame System with i Elements

For a structure of i elements, nodes $n=0$ and $n=i+1$ have known displacements, $\beta_0 = \beta_{i+1} = 0$, and, thus, can be removed from the stiffness matrix:

Equation 5-38:
$$K_1 = k_1 \cdot H^2 \cdot \left\{ 2 - \frac{k_2}{k_1 \cdot H^2} \quad -1 \right\}$$

Equation 5-39:
$$K_i = k_1 \cdot H^2 \cdot \left\{ -1 \quad 2 - \frac{k_2}{k_1 \cdot H^2} \right\}$$

Assembling the stiffness matrix for a structure of i elements gives:

Equation 5-40:
$$[K] = \begin{bmatrix} \lambda & -1 & 0 & \cdots & 0 & 0 & 0 \\ -1 & \lambda & -1 & \cdots & 0 & 0 & 0 \\ 0 & -1 & \lambda & \cdots & 0 & 0 & 0 \\ \vdots & \vdots & \vdots & \ddots & \vdots & \vdots & \vdots \\ 0 & 0 & 0 & \cdots & \lambda & -1 & 0 \\ 0 & 0 & 0 & \cdots & -1 & \lambda & -1 \\ 0 & 0 & 0 & \cdots & 0 & -1 & \lambda \end{bmatrix} \cdot k_1 \cdot H^2$$

Where:
$$\lambda = 2 - \frac{k_2}{k_1 \cdot H^2}$$

5.4.1.4 Solution for Unknown Displacements and Top Fibre Strain

Recall from Equation 5-31 that the system of simultaneous linear equations for the spring frame structure using the matrix stiffness method is expressed as:

$$[FEM] + [K] \cdot [\beta] = 0$$

Using the assembled component matrices ($[\beta]$: Equation 5-32, $[K]$: Equation 5-40 and $[FEM]$: Equation 5-36) for a system of i elements, in Equation 5-31, the matrix of unknown displacements, $[\beta]$, for the structure can be calculated. The matrix of unknown displacements signifies the rotation of the vertical members from perpendicular in the spring frame. This corresponds to the inter-laminar shear deformation in the harped CFRP tendon that the spring frame represents.

Once the matrix $[\beta]$ has been calculated, Equation 5-25 can be used to determine the matrix $[\Delta L]$, which represents the net change in length at the top of each element in the balanced state. This also corresponds to the net linear deformation at the top of each element of the harped CFRP tendon. The strain in the top fibre of each element can then be determined by:

$$\text{Equation 5-41: } [\varepsilon_t] = \frac{[\Delta L]}{L}$$

The matrix, $[\varepsilon_t]$, corresponds to the bending strain distribution in the top fibre of the harped CFRP tendon along the tendon length with transition effects applied.

5.4.2 Computation of Spring Constants

To be able to use the spring frame model for the CFRP tendon, the spring constants need to be determined. Because the CFRP material is assumed to be linear elastic in both tension and shear, it is assumed that k_1 is directly related to the elastic modulus, E , and that k_2 is directly related to the shear modulus, G .

The spring constants can be defined as:

Equation 5-42: $k_1 = \kappa_1 \cdot E$

Equation 5-43: $k_2 = \kappa_2 \cdot G$

5.4.2.1 Linear Spring

The linear spring constant, k_1 , is assumed to be related to the linear deformation of the top fibre of the element, ΔL_t , and the total linear force on the element transposed to the top fibre, P_t , as shown in Figure 5-20.

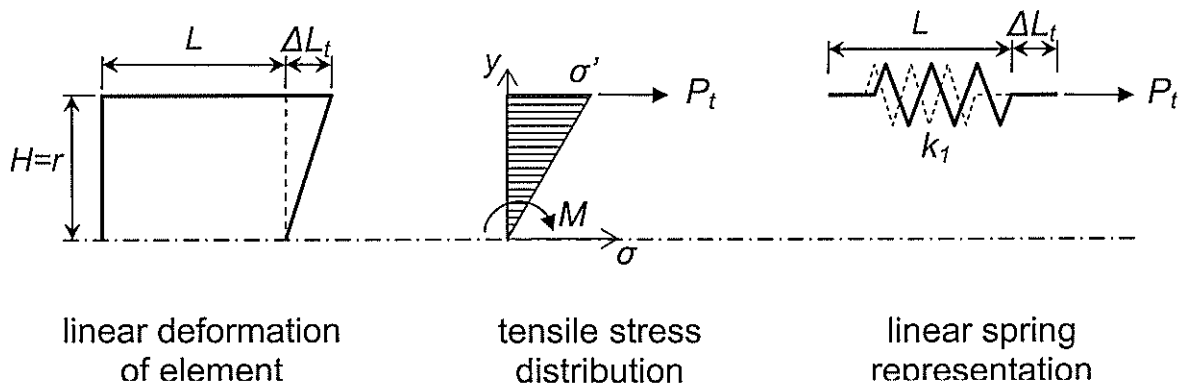


Figure 5-20: Representation of Linear Spring

For a linear spring:

Equation 5-44: $P_t = k_1 \cdot \Delta L_t$

The stress/strain distribution across the cross section is assumed to be linear:

$$\sigma(y) = \frac{y}{r} \cdot \sigma'$$

The total moment at the neutral axis resulting from this stress distribution is:

$$M = \int_0^r \sigma(y) \cdot w(y) \cdot y \cdot dy$$

For a circular cross section with radius r : $w(y) = 2 \cdot \sqrt{r^2 - y^2}$

$$M = 2 \cdot \frac{\sigma' r}{r} \int_0^r \sqrt{r^2 - y^2} \cdot y^2 \cdot dy$$

$$M = \frac{\pi}{8} \cdot \sigma' \cdot r^3$$

Transposing this moment to a force at the top of the element:

$$P_t = \frac{M}{r}$$

Equation 5-45: $P_t = \frac{\pi}{8} \cdot \sigma' \cdot r^2$

The stress in the top fibre of the element can be defined as:

$$\sigma' = E \cdot \varepsilon'$$

The top fibre strain can be expressed as:

$$\varepsilon' = \frac{\Delta L_t}{L}$$

Therefore:

$$\sigma' = E \cdot \frac{\Delta L_t}{L}$$

Substituting this into Equation 5-45 gives:

Equation 5-46: $P_t = \frac{\pi}{8} \cdot \frac{r^2}{L} \cdot E \cdot \Delta L_t$

Therefore, comparing Equation 5-46 and Equation 5-44 it can be seen that:

Equation 5-47: $k_1 = \frac{\pi}{8} \cdot \frac{r^2}{L} \cdot E$

From Equation 5-47 and Equation 5-42:

Equation 5-48: $\kappa_1 = \frac{\pi}{8} \cdot \frac{r^2}{L}$

5.4.2.2 Rotational Spring

The rotational spring constant, k_2 , is assumed to be related to the average shear deformation, β , along the element and the total moment due to inter-laminar shear differential, M , across the element as shown in Figure 5-21.

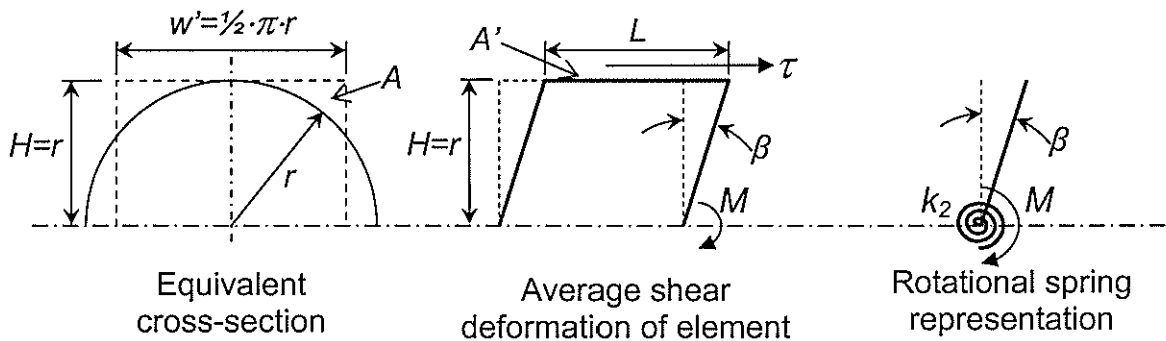


Figure 5-21: Representation of Rotational Spring

The semicircular half-tendon cross-section is idealized for simplicity into a rectangular cross-section with an equivalent area and the same height as shown in Figure 5-21. If the semi-circular and equivalent rectangular cross sections are equal, the width of the rectangular cross section can be determined to be:

$$A = \frac{\pi}{2} \cdot r^2 = w' \cdot r$$

Equation 5-49: $w' = \frac{\pi}{2} \cdot r$

To determine the spring constant, a relationship between the total shear stress, τ , and the moment, M , needs to be derived. The total shear stress, τ , is the shear stress distributed along the top surface of the element that produces the total shear deformation, β :

Equation 5-50: $\tau = G \cdot \beta$

The moment at the neutral axis resulting from this shear stress is:

$$M = \tau \cdot A' \cdot r$$

The top surface area of the element is: $A' = w' \cdot L$

$$M = \tau \cdot w' \cdot L \cdot r$$

Substituting in Equation 5-49 and Equation 5-50:

$$\text{Equation 5-51: } M = \frac{\pi}{2} \cdot r^2 \cdot L \cdot G \cdot \beta$$

Recall for a rotational spring:

$$\text{Equation 5-52: } M = k_2 \cdot \beta$$

Therefore comparing Equation 5-51 and Equation 5-52 it can be seen that:

$$\text{Equation 5-53: } k_2 = \frac{\pi}{2} \cdot r^2 \cdot L \cdot G$$

From Equation 5-53 and Equation 5-43:

$$\text{Equation 5-54: } \kappa_2 = \frac{\pi}{2} \cdot r^2 \cdot L$$

5.4.3 Characteristics of Equivalent Spring Frame Model

The spring frame model was programmed into MathCAD, software for mathematical calculation, in the form of the matrix stiffness method described previously. This enabled a frame model with a large number of elements, to be assembled and calculated. Variables could be changed and the new solution obtained quickly and accurately. Figure 5-22 illustrates the distribution of tensile strain due to bending in the top fibre of a tendon for the harping configuration variables indicated in the figure, as calculated using MathCAD. For the calculation of this figure, 500 frame elements were used with an approximate size equal to 0.05radians, as determined by a 500mm radius of curvature, or an approximate linear length of 0.436mm.

The transition zone, characterised by the smooth transition across the transition point, can clearly be seen and is similar to that illustrated in Figure 5-8. The figure

shows the transition zone to have a finite length. However, theoretically, the transition zone does not have a finite length as shown in the figure. The axial bending strain curve is asymptotic with a limit of ϵ_{blim} towards the deviator, and a limit of zero towards the tendon straight length. However, beyond a certain distance along the tendon length on either side of the transition point the effects are so minute that they can be ignored. It is notable that the limiting maximum possible bending strain is equal to the elastic bending strain defined by Equation 5-3, ϵ_{blim} .

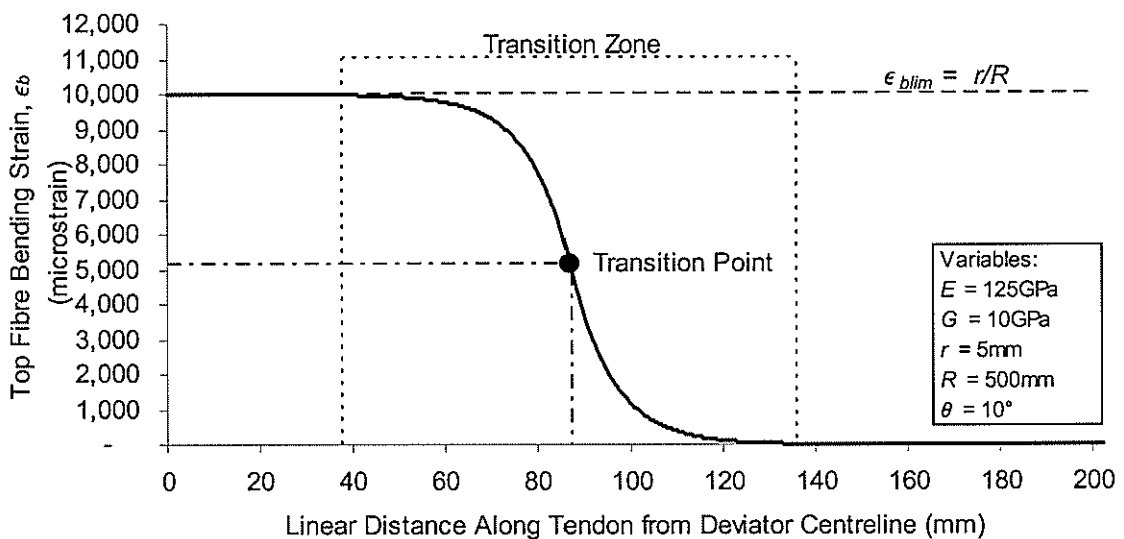


Figure 5-22: Typical Top-Fibre Axial Bending Strain Distribution along Tendon

Figure 5-23 plots a series of bending strain distributions for several harping angles when all other variables are held constant. By changing the harping angle, the location of the transition point and transition zone relative to the centreline of the deviator changes. Decreasing the harping angle has the effect of moving the transition zone closer to the deviator centreline. As can be seen in the figure, the location of the transition zone relative to the deviator centreline has a noticeable effect on the top-fibre bending strain distribution and the maximum top-fibre bending strain, located at the deviator centreline. For harping angles equal to 5, 10 and 15 degrees, the effective transition zone is located such that it does not overlap

the deviator centreline. It can be seen that for these distributions, there is no significant influence on the maximum top-fibre bending strain and that the top-fibre bending strain distribution across the transition zone is virtually identical, but shifts relative to the transition point location. However, for harping angles of 0.5, 1 and 2 degrees, the effective transition zone does overlap the deviator centreline. Figure 5-24 illustrates the effect that the location of the transition point, and, therefore, the location of the transition zone, has on the maximum top-fibre bending strain. As the transition point moves closer to the deviator centreline and more of the transition zone overlaps the centreline, the maximum bending strain in the top fibre decreases. As the transition point moves further from the deviator centreline, the maximum bending strain in the top fibre increases towards the limiting maximum possible bending strain given by ϵ_{blim} .

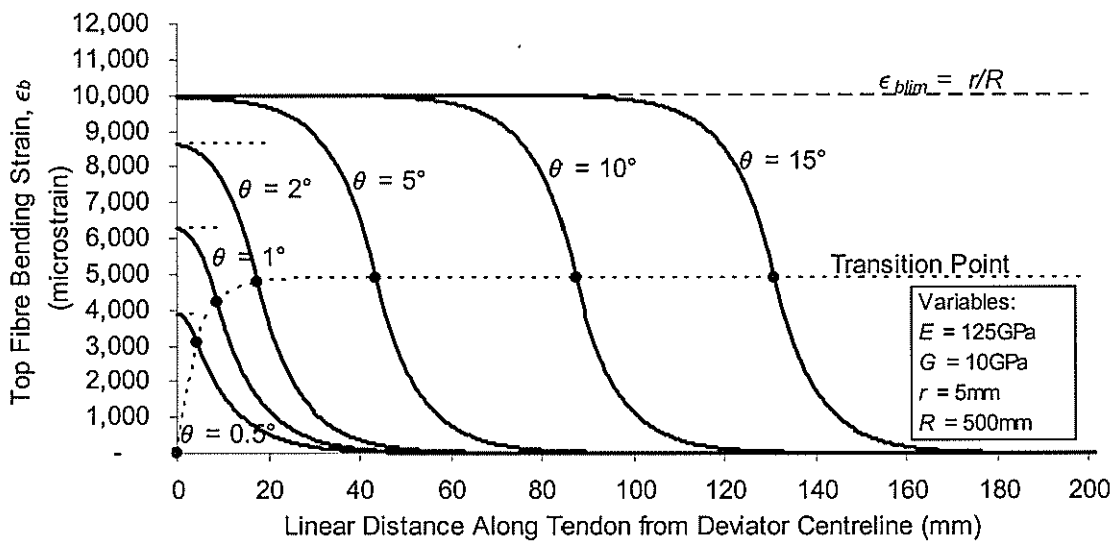


Figure 5-23: Effect of Transition Point Location on Bending Strain Distribution

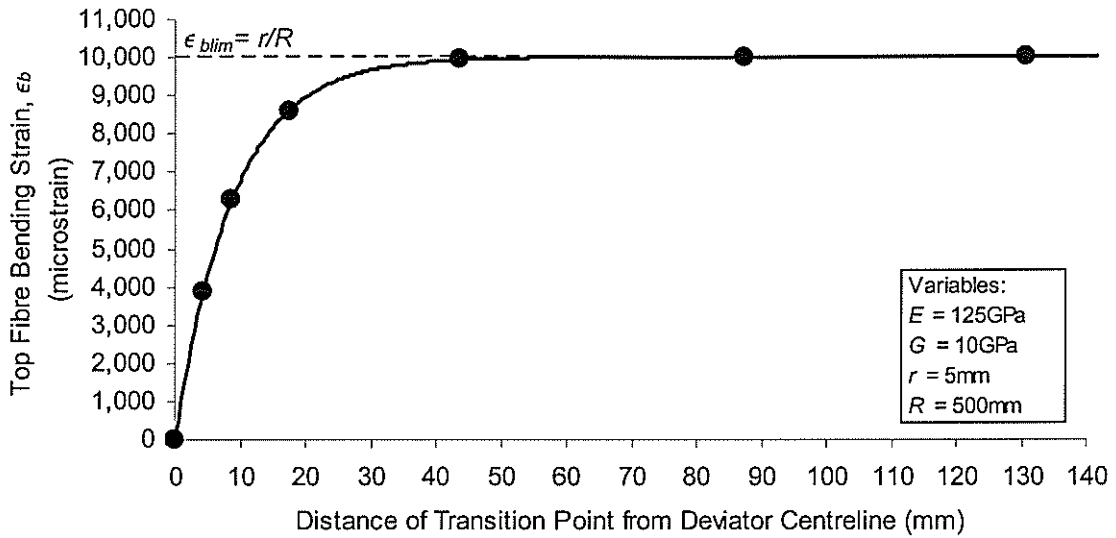


Figure 5-24: Effect of Transition Point Location on Maximum Bending Strain

Figure 5-25 illustrates the effect of the additional configuration variables on the transition zone and top fibre strain distribution, in the form of the G/E and r/R ratios. Figure 5-25a shows the effect of the G/E ratio, which represents the ratio of the shear modulus to the tensile modulus for the material. As G/E increases (increasing G or decreasing E), the transition zone gets smaller, indicating less influence from transition effects. This is because the shear stiffness is increased relative to the longitudinal stiffness, resulting in less longitudinal shear deformation.

Figure 5-25b shows the effect of the R/r ratio, which represents the ratio of the curvature of the tendon to the distance to the extreme fibres, from the tendon neutral axis. As R/r increases (increasing R or decreasing r), the transition zone gets smaller, indicating less influence from transition effects. This results because the transition effects are dependent on the relative change in curvature of the tendon between the straight section and curved section. Decreasing R/r results in a larger relative change in curvature, and, therefore, a greater influence on transition effects.

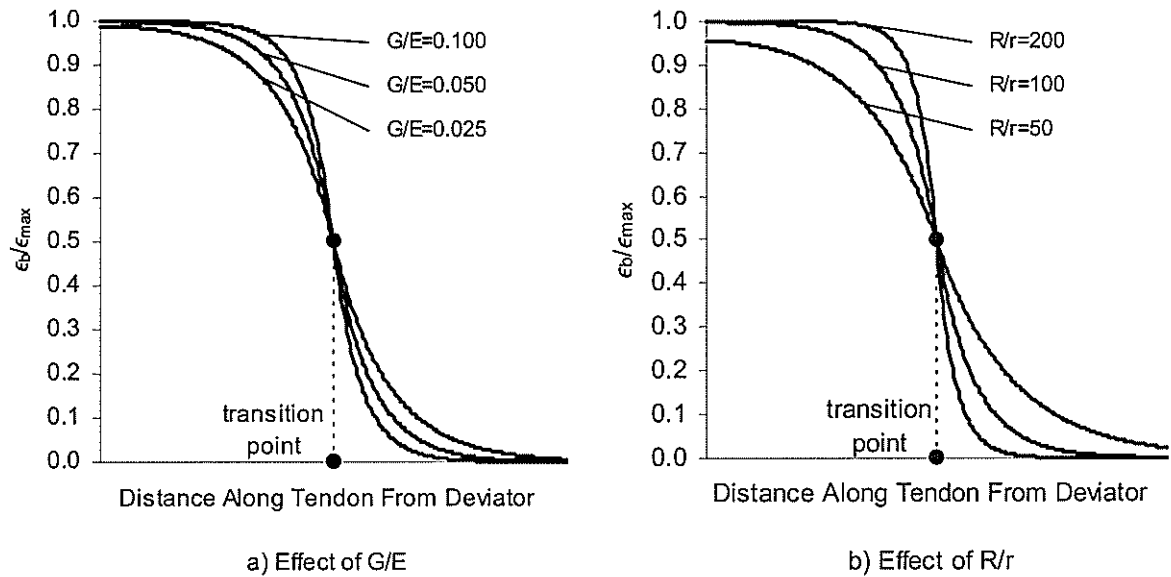


Figure 5-25: Effect of Harping Variables on Top Fibre Strain Distribution

Another unknown variable that is solved in the process of solving the equivalent frame model is β , the out-of-plane rotation of the frame elements, which is representative of the plane section rotation and longitudinal shear deformation in the tendon as illustrated in Figure 5-8. Figure 5-26 shows the progression of this rotation along the tendon, across the transition zone for the same set of variables used for Figure 5-22, as indicated in the figure. As was expected, it can be seen that, outside the effective transition zone, the rotation is virtually zero and that the maximum rotation effectively occurs at the transition point. This is significant because this rotation or deformation can be assumed to be equivalent to the net longitudinal shear strain in the tendon and it is directly related to the tendon harping. Recalling that shear stress is proportional to the shear strain and modulus:

$$\text{Equation 5-55} \quad \tau = G \cdot \beta$$

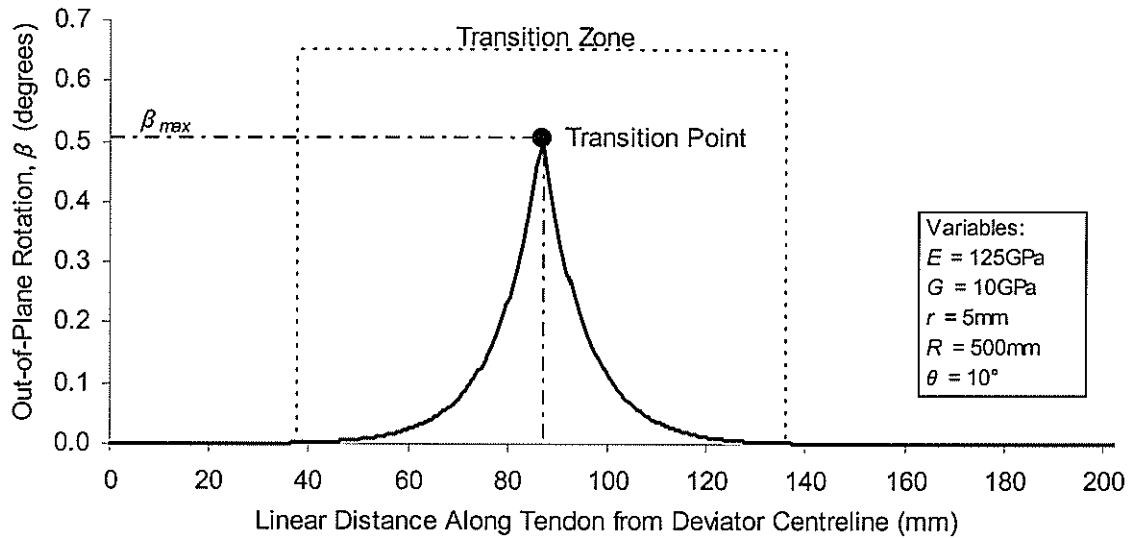


Figure 5-26: Typical Out-of-Plane Rotation along Harped Tendon

Previously developed models did not account for the possibility of shear failure, however this failure mode was observed within this research program. One of the basic assumptions of the primary model is that the tendon behaves according to traditional elastic beam theory for pure bending: plane sections remain plane and perpendicular to the neutral axis. Under this assumption there is no shear deformation, only longitudinal deformation takes place. It would follow that, because there is no longitudinal shear deformation, that there is also no longitudinal shear stress. With the inclusion of transition effects, the extended model allows for the occurrence of shear deformation. Therefore, longitudinal shear stresses are present and, thus, there is a possibility that shear failure of the tendon can occur.

5.4.4 Simplification of Equivalent Spring Frame Model Solution

Using the equivalent frame model as developed is computationally intensive, and generally cannot be done by hand. To facilitate usage of the model, closed-form formulae that closely approximate the bending strain at the centreline, or maximum bending strain, and the maximum out-of-plane rotation, or longitudinal shear strain, as calculated by the model were developed. This was done by calculating these

values, using the model programmed in MathCAD, for numerous series of configuration variables and developing a regression formula that gave a best fit to the results. Figure 5-27, Figure 5-28 and Figure 5-29 illustrate this process as used to determine maximum bending strain. In these examples, only a few data points are shown for brevity, whereas many more points were used in the actual regression to ensure good accuracy.

In the first stage (Figure 5-27a), the values of b , G , and E were kept constant while the harp angle was changed for several series of solutions to the model with constant R/r values. A regression was performed on each R/r series which determined the relationship between θ and ϕ_{te} . In the second stage, a regression is performed on R/r coefficients from the first stage regressions (Figure 5-27b), which determines the relationship between R/r and ϕ_{te} . In the third stage (Figure 5-28a), the values of b , r and R were now kept constant while the harp angle was changed for several series with constant G/E values. A regression is performed on each G/E series to gather G/E coefficients for the fourth stage. The relationship between θ and ϕ_{te} can be seen again in these regressions, and is noted to be the same as in stage 1. In the fourth stage, a regression is performed on G/E coefficients from the third stage regressions (Figure 5-28b), which determines the relationship between G/E and ϕ_{te} . This process is then performed one more time for the elasticity shape factor, b (Figure 5-29). The value of b is computed as being equal to 4 for circular cross sections as shown below. However, this variable may be used to accommodate other cross-sectional shapes, and is included here for completeness.

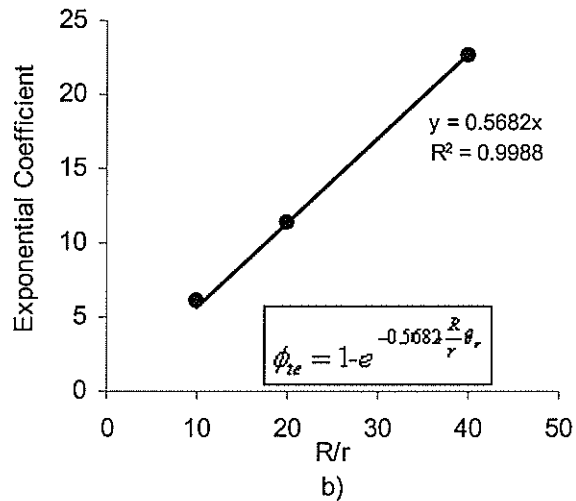
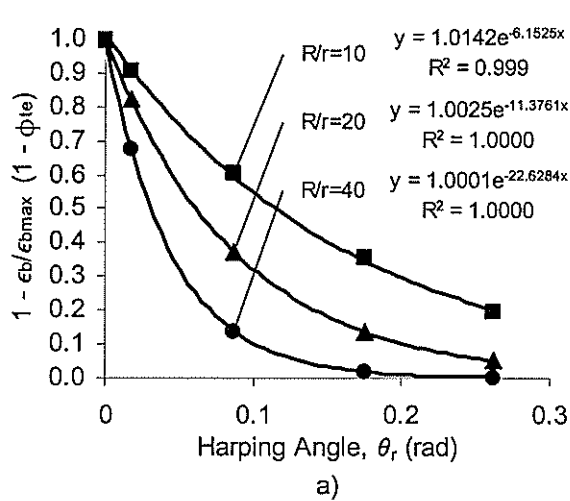


Figure 5-27: Simplifying the Equivalent Spring Frame Model – Stage 1 and 2

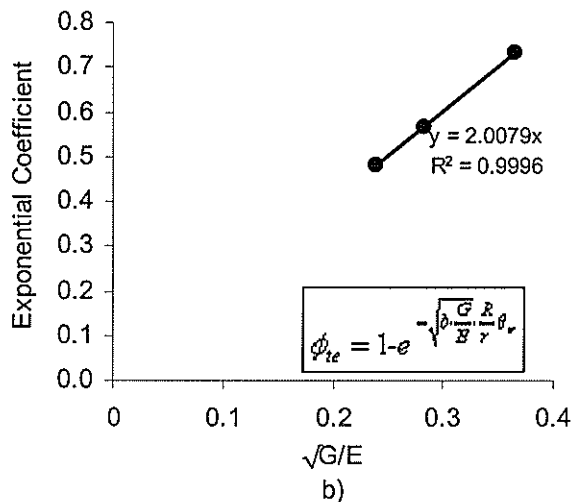
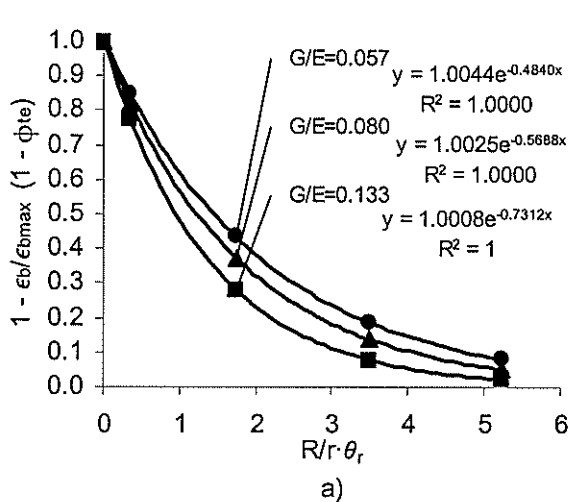


Figure 5-28: Simplifying the Equivalent Spring Frame Model – Stage 3 and 4

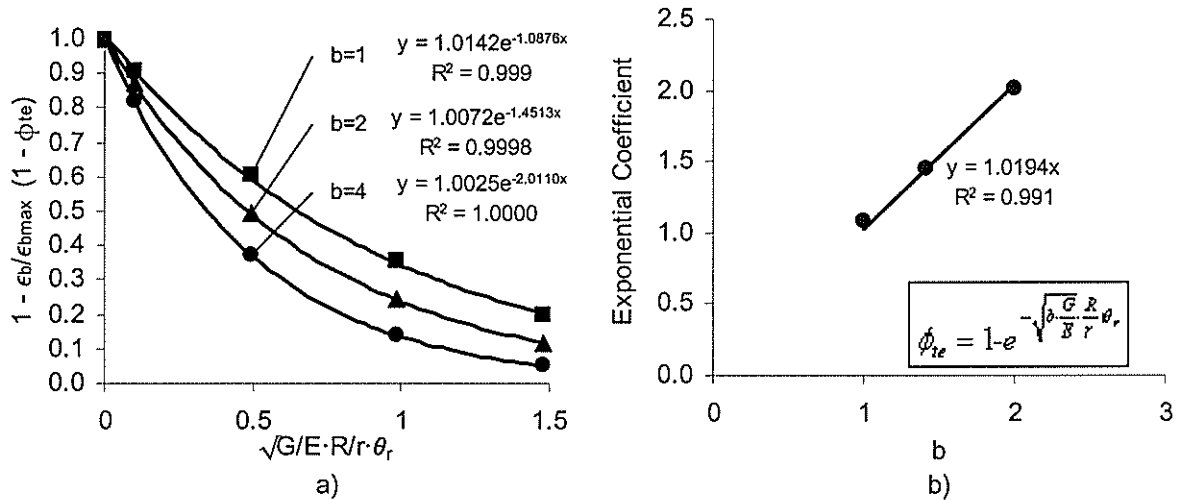


Figure 5-29: Simplifying the Equivalent Spring Frame Model – Stage 5 and 6

It can be seen in Figure 5-27, Figure 5-28 and Figure 5-29, that, even though only a few data points are used in this regression example, the correlation values (r^2) shown are very close to 1. The more data points and frame elements used in the equivalent spring frame model, the closer the correlation values get to unity. This indicates that the equations derived through the regression process are very accurate in comparison to the full frame model calculations.

For the maximum bending strain, the following formula was found:

$$\epsilon_b = \left(1 - e^{-\sqrt{\frac{G}{E}} \frac{R}{r} \theta_r} \right) \cdot \frac{r}{R}$$

Equation 5-56: $\epsilon_b = \phi_{te} \cdot \frac{r}{R}$

Equation 5-57: $\phi_{te} = 1 - e^{-\sqrt{\frac{G}{E}} \frac{R}{r} \theta_r}$

Where:

ϵ_b = Maximum top-fibre bending strain including transition effects

G = CFRP longitudinal shear modulus

E = CFRP tensile modulus

R = Radius of curvature of the tendon

r = Tendon cross-sectional height (radius for circular cross-section)

θ_r = Harping angle in radians

$b = \frac{\kappa_2}{\kappa_1 \cdot L^2}$, elasticity shape factor (4 for a circular cross-section): L = Element length, κ_1 and κ_2 are from Equation 5-48 and Equation 5-54 respectively

This formula has a correlation value that is virtually equal to one; therefore, it can confidently be used in place of the full equivalent frame method. Comparing Equation 5-56 to the equation for bending strain, Equation 5-3, the factor ϕ_{ie} as defined in Equation 5-57 can be seen to act as a reduction factor for the bending stress and strain due to transition effects. The variable b included here is essentially a shape factor for the CFRP tendon that describes the relationship between the tensile and rotational spring factors and the cross-sectional shape for the model. The variable b in Equation 5-57 is determined to be equal to 4 for a circular cross section.

The same regression method used for the maximum bending strain equation above was used in deriving a closed-form equation for the maximum longitudinal shear strain and deformation. The maximum longitudinal shear strain was found to be proportional to the maximum longitudinal shear strain when the transition zone does not overlap the centreline, which can be defined as the shear strain limit:

Equation 5-58:
$$\beta_{lim} = \frac{1}{2} \cdot \sqrt{\frac{E}{b \cdot G}} \cdot \frac{r}{R}$$
$$\beta_{max} = \left(1 - e^{-2 \sqrt{\frac{b \cdot G}{E}} \frac{R}{r} \cdot \theta_r} \right) \cdot \beta_{lim}$$

Equation 5-59:
$$\beta_{max} = \phi_{\beta} \cdot \beta_{lim}$$

Equation 5-60:
$$\phi_{\beta} = 1 - e^{-2 \sqrt{\frac{b \cdot G}{E}} \frac{R}{r} \cdot \theta_r}$$

Again, these formulae have a correlation value that is virtually equal to one, indicating they produce accurate results.

5.4.5 Extended Analytical Model: Incorporation of Transition Effects

The next step was to incorporate the bending stress reduction formula from the equivalent frame model into the primary model for the evaluation of the transition effects on the primary model. From Equation 5-56, the transition effects simply create a reduction factor, therefore the ε_b term used in the primary model can simply be replaced with the ε_b term from the equivalent frame model. This, however, does not create a simple solution for the failure criterion as the reduction factor ϕ'_h has the radius of curvature, R , included in an exponential form, and cannot be easily isolated for calculation.

The most convenient way to find a solution is to solve for the radius of curvature at failure from Equation 5-16 incorporating the bending strain reduction factor:

$$\text{Equation 5-61: } R = \frac{\phi_{te} \cdot r}{2 \cdot (1 - \cos(\theta)) \cdot \left(\sqrt{1 + \frac{\varepsilon_u}{(1 - \cos(\theta))}} - 1 \right)}$$

$$\text{Where: } \phi_{te} = 1 - e^{-\sqrt{\frac{G}{E}} \frac{R_u}{r} \theta}$$

This equation cannot be solved directly as the unknown radius R is present on both sides of the equation. An iterative process is used where a value for R is substituted into the right side and the resulting R on the left side is calculated. This is repeated until the value of the right side of the equation is equal to the substituted value of R . This value for the radius, R , can then be used in Equation 5-17 in place of R_{nf} and the failure level is calculated as before in Equation 5-18 to Equation 5-24 in section 5.2.5.

In order to evaluate the influence of the transition effects on the ultimate tensile capacity, the predicted failure radius and ultimate capacity for a number of sample variables were computed both with and without the inclusion of transition effects, as given in Table 5-1. From the calculations in the table, it can be observed that for

configurations in which the tendon curvature was not physically limited by the deviator, there was a noticeable reduction in the minimum radius of curvature of the tendon at failure when including transition effects, up to 95% of the radius calculated without transition effects. The only specimens for which there is any noticeable increase in capacity were those in which the tendon radius of curvature was physically limited by the deviator. In all the other specimens, no significant increase in capacity is observed. This may be explained by the fact that while the transition effects allow a reduction in the bending strain, this decreases the tendon stiffness and the natural radius of curvature decreases accordingly, as seen by the values of R_f and R'_f in the table. If the radius of curvature is limited by the deviator, then it is unable to decrease further physically and a maximum bending strain reduction and increase in capacity may be seen, however, the magnitude of this effect is small, with a maximum of 1.5% for the configurations assessed.

Table 5-1: Evaluation of the Influence of Transition Effects on Tensile Capacity

r (mm)	R_d (mm)	θ (deg)	Without Transition Effects		With Transition Effects		Curvature Decrease (R'_f/R_f)	Capacity Increase
			R_f (mm)	Tensile Capacity (% ultimate)	R'_f (mm)	Tensile Capacity (% ultimate)		
4.75	50	2	903.4	68.39%	860.1	68.39%	0.95	0.00%
4.75	50	3	660.9	56.79%	638.5	56.79%	0.97	0.00%
4.75	50	5	474.0	39.76%	466.3	39.76%	0.98	0.00%
4.75	50	7	399.7	28.55%	396.7	28.55%	0.99	0.00%
4.75	50	10	349.6	18.31%	348.9	18.31%	1.00	0.00%
4.75	50	15	317.0	9.93%	317.0	9.93%	1.00	0.00%
4.75	500	2	903.4	68.39%	860.1	68.39%	0.95	0.00%
4.75	500	3	660.9	56.79%	638.5	56.79%	0.97	0.00%
4.75	500	5	504.8	43.43%	504.8	44.08%	1.00	1.51%
4.75	500	7	504.8	43.43%	504.8	43.54%	1.00	0.25%
4.75	500	10	504.8	43.43%	504.8	43.43%	1.00	0.02%
4.75	500	15	504.8	43.43%	504.8	43.43%	1.00	0.00%
4.75	50	5	474.0	39.76%	466.3	39.76%	0.98	0.00%
4.75	100	5	474.0	39.76%	466.3	39.76%	0.98	0.00%
4.75	250	5	474.0	39.76%	466.3	39.76%	0.98	0.00%
4.75	500	5	504.8	43.43%	504.8	44.09%	1.00	1.52%
4.75	750	5	754.8	62.16%	754.8	62.21%	1.00	0.08%
4.75	1000	5	1004.8	71.58%	1004.8	71.58%	1.00	0.01%

From the data observed here, it may be concluded that the transition effects have very little influence on the capacity of the harped CFRP prestressing tendon, especially when the radius of curvature is not limited by the deviator. However, the model provides a mechanistic approach to describing the behaviour of the harped CFRP prestressing tendon. The model can be used to approximate and illustrate the top-fibre bending strain distribution along the tendon. The model can also be used to approximate the magnitude of the longitudinal shear stress and strain resulting from bending, for use in evaluating whether shear failure will take place.

5.5 COMPARISON OF MODELS WITH EXPERIMENTAL DATA

Figure 5-30 and Figure 5-31 plot the experimental data and a curve representing the primary model for varying harping angle and varying deviator radius respectively using both the minimum guaranteed material properties and the maximum properties for comparison. From the figures, it can be observed that the analytical model exhibits similar trends to the experimental data: the failure level decreases as the harping angle increases, and the failure level decreases as the deviator size decreases. In Figure 5-30a and Figure 5-31a, which use the guaranteed minimum material properties, all the data is situated on the conservative side of the analytical model. In Figure 5-30b and Figure 5-31b, which use the maximum material properties, the data is situated much closer to the analytical, however many of the data points are on the unconservative side.

The minimum and maximum material properties used in the figures represent the lower and upper bounds of the expected material variability. When the minimum and maximum properties are used in conjunction with the analytical model, they produce an envelope based on the expected material variability, and the data points should be expected to fall within this envelope. When comparing Figure 5-30a to

Figure 5-30b and Figure 5-31a to Figure 5-31b, it can be seen that the majority of the data points fall within the expected material variability envelope. They are all situated on the conservative side of the lower envelope bound (Figure 5-30a and Figure 5-31a), and they are predominantly on the unconservative side of the upper envelope bound (Figure 5-30b and Figure 5-31b). This shows that the analytical model describes the expected strength variability very well.

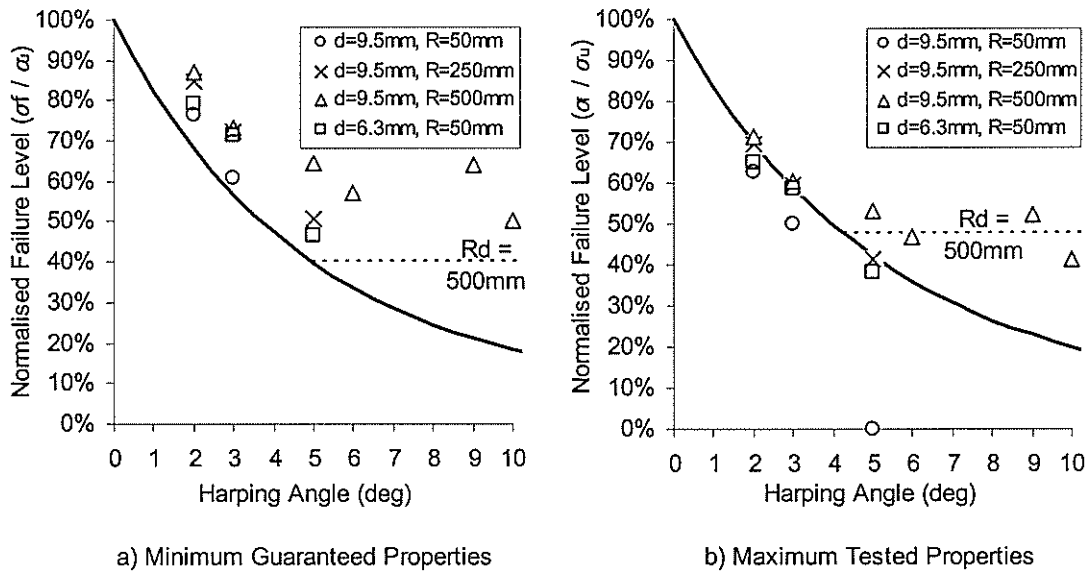


Figure 5-30: Model vs. Experimental Data for Varying Harping Angle

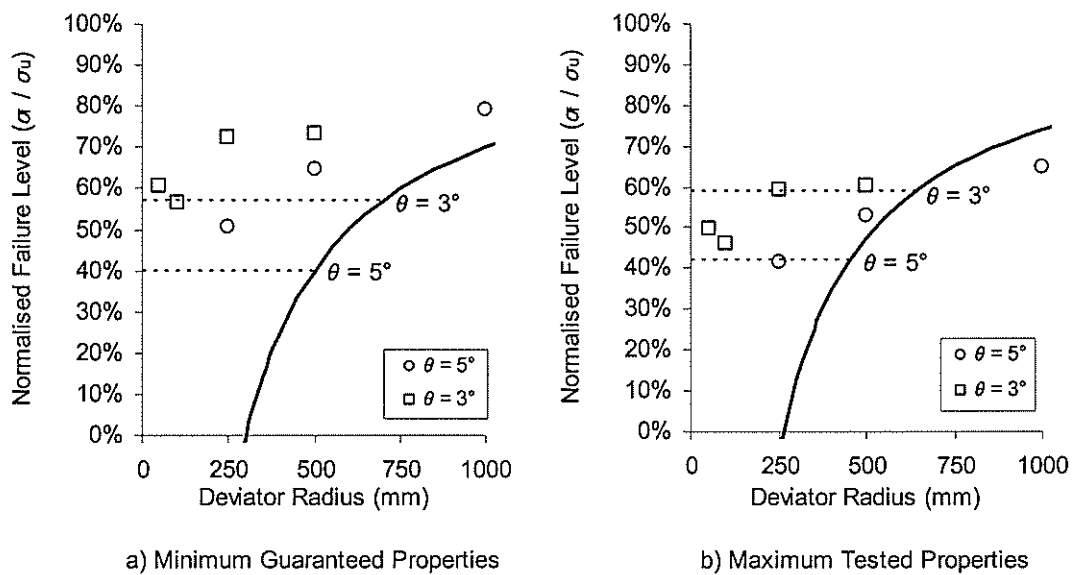


Figure 5-31: Model vs. Experimental Data for Varying Deviator Size

As has already been discussed, the CFRP material used in the testing program exhibited a large variability in material property values including the elastic modulus, E , and the tensile rupture strain, ϵ_{ult} . Table 5-2 lists a numerical evaluation of the expected deviance of the normalised failure level resulting from the known material variability: the guaranteed minimum and tested maximum material properties from the supplier. For the measured values, the expected deviance is a constant reduction of 0.82 as the normalised measured failure level is directly related to the material properties. The material properties are incorporated in the normalised predicted failure level in a much more complex manner and the expected deviance ranges from increases of 1.02 up to 1.17, depending upon the specimen configuration. The total expected deviance when comparing the measured values to the predicted values ranges from 20% to 30%.

Table 5-2: Evaluation of Expected Deviance of Normalised Failure Levels

Specimen	Normalised Measured Failure Level			Normalised Predicted Failure Level			Total Expected Deviance $1-Dev_m/Dev_p$
	f_m/f_u		Deviance _m	f_p/f_u		Deviance _p	
	Min	Max		Min	Max		
1	0.77	0.63	0.82	0.68	0.70	1.02	0.20
2	0.61	0.50	0.82	0.57	0.59	1.04	0.21
6	0.87	0.71	0.82	0.68	0.70	1.02	0.20
7	0.73	0.60	0.82	0.57	0.59	1.04	0.21
8	0.65	0.53	0.82	0.43	0.51	1.17	0.30
19	0.57	0.47	0.82	0.43	0.51	1.17	0.30
20	0.64	0.52	0.82	0.43	0.51	1.17	0.30
9	0.50	0.41	0.82	0.43	0.51	1.17	0.30
12	0.51	0.42	0.82	0.40	0.42	1.06	0.23
13	0.79	0.65	0.82	0.72	0.75	1.05	0.22
14	0.79	0.65	0.82	0.68	0.70	1.02	0.20
15	0.71	0.59	0.82	0.57	0.59	1.04	0.21
16	0.47	0.38	0.82	0.40	0.42	1.06	0.23
21	0.85	0.69	0.82	0.68	0.70	1.02	0.20
22	0.73	0.60	0.82	0.57	0.59	1.04	0.21
24	0.56	0.46	0.82	0.57	0.59	1.04	0.21

Figure 5-32 illustrates the correlation between the normalized failure level as predicted by the primary model and the normalized failure level as measured in the

experimental program for each specimen that exhibited a tension failure. The 1:1 correlation line indicates an ideal, exact correlation between the measured and predicted data, assuming the guaranteed material properties. Data points situated on the upper left side of this line would represent an unconservative prediction by the model, that the model over-estimates the harped tendon tensile capacity. Conversely, data points falling on the lower right side of this line would represent an over-conservative prediction by the model, that is, the model under-estimates the harped tendon tensile capacity. The expected maximum deviation line also indicated in Figure 5-32 represents the maximum expected deviation from the 1:1 correlation based on the material variability discussed above.

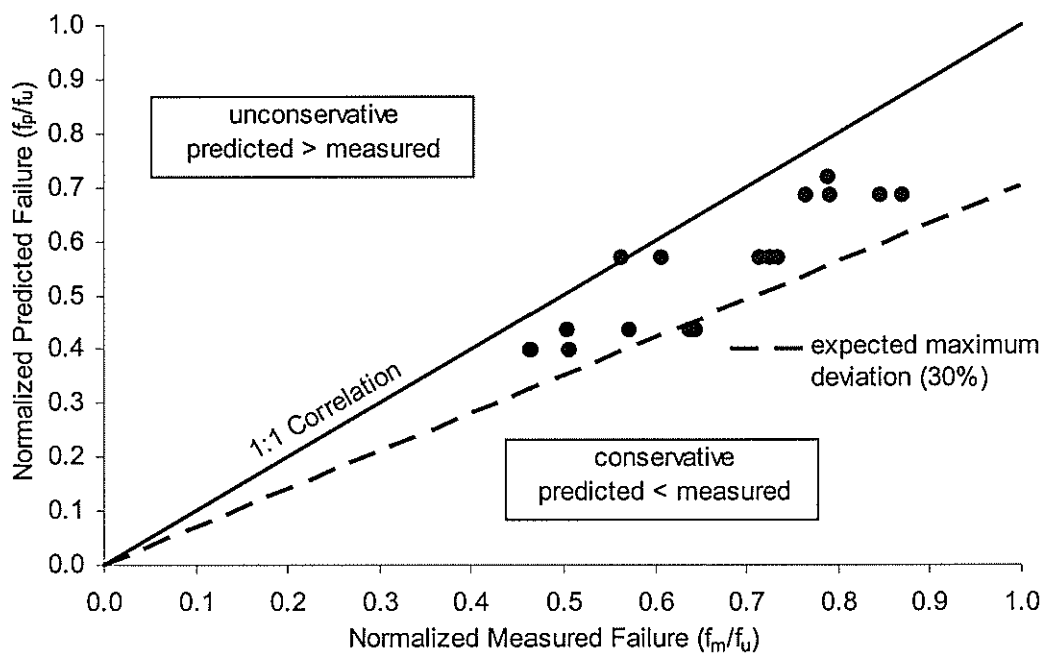


Figure 5-32: Correlation Plot for Primary Analytical Model

The correlation line and the maximum deviation line represent the upper and lower bounds for the expected data point deviance based on the material variability. It is evident from the figure that the normalized data points fall predominantly between these two lines, which indicates that the primary model gives a very good estimation of the harped tendon failure behaviour. More importantly, virtually all

of the data points fall on the conservative side when using the minimum guaranteed material properties. This means that using the primary model with guaranteed minimum material properties can give an efficient but safe estimation of the capacity of a harped CFRP prestressing tendon.

As discussed in Section 5.2.3, the analytical models neglect the effect of the normal stresses due to bearing on the deviator and the longitudinal stresses due to friction between the deviator and the tendon. From Figure 5-30, Figure 5-31 and Figure 5-32, a very good correlation is seen between the analytical models and the experimental data. The scatter evident in the figures appears to be related to the known material property variability for the CFRP tendons as discussed above. This suggests that the assumptions made in the derivation of the models, regarding the total axial stress in the curved tendon, are valid. Specifically, that the normal stresses due to bearing and the longitudinal stresses due to friction do not have a significant effect on the tensile capacity of the harped CFRP tendon.

5.6 SUMMARY

In this chapter the development of the primary and extended models for predicting the behaviour of harped CFRP prestressing tendons were developed, based on the mechanical properties of the material. The primary model is based on classic elastic beam theory. The extended model supplements the primary model by adding transition effects, which affect the stiffness of the harped tendon and introduce longitudinal shear deformations. Comparison between the primary and extended models showed that, for the configurations investigated, the extended model had very little effect on the results, especially when the tendon curvature was not physically limited by the deviator. Comparisons with the experimental data showed very good agreement in the prediction of tension failure. While this model focused

primarily on tension failure, compression and shear failure modes also need to be considered and are looked at in the next chapter.

6 FAILURE MODE

6.1 INTRODUCTION

The analysis and discussion thus far has focused primarily on tensile failure. However, as was mentioned earlier in the thesis, two additional failure modes were observed in the process of this testing program: compression failure and shear failure. In this chapter, the significance and characteristics of these additional two potential failure modes are discussed.

6.2 FAILURE MODE SIGNIFICANCE

The tendon failure level for compression and shear failures was defined as the point at which the initial signs of failure were observed as described in section 4.2.1, regardless of whether the tendon was able to carry any further load. Table 6-1 shows the applied stress levels at which initial tendon failure occurred for specimens in the experimental program that exhibited either compression or shear failure behaviour. As can be seen in the table, tendon failures for compression and shear failures were observed to occur at significantly lower applied stress levels than for tension failures. Where tension failures often resulted in a sudden, complete failure of the tendon, in compressive and shear failure this was not the case. In all cases, the tendon was still able to take additional load after the initial failure was deemed to have occurred. However, the nature of the initial compression or shear failure causes the composite action of the CFRP material to be compromised and may result in an unstable or unpredictable behaviour of the tendon under further loading. Previous research studies in the literature did not report these additional failure modes. This may be attributed to the particular test configuration limitations

and conditions within the programs. However, for the practical application of harped CFRP prestressing tendons, the possible occurrence of these failures modes need to be considered. Because of the low loading levels at which the effective failure occurs for compression and shear failure, both of these types of failure are considered undesirable and should be avoided by the design process.

Table 6-1: Experimental Test Failure Levels For Compression and Shear Failures

Specimen No.	Tendon Diameter (mm)	Deviator Radius (mm)	Harp Angle (deg)	Failure Stress (MPa)	% Ultimate ($f_u=2068\text{MPa}$)
Bending-Compression Failures					
4	9.5	50	10	38.1	1.84%
5	9.5	50	15	12.5	0.60%
23	9.5	250	10	29.2	1.41%
10	9.5	500	15	20.9	1.01%
17	6.3	50	10	116.0	5.61%
18	6.3	50	15	27.6	1.33%
Bending-Shear Failures					
3	9.5	50	5	185.1	8.95%
11	9.5	100	5	284.4	13.75%

6.3 BENDING-COMPRESSION FAILURE

Recall from Equation 5-6 that the total net axial strain is the sum of the axial strain due to direct tension and the axial strain due to bending:

$$\varepsilon_{tot} = \varepsilon_t + \varepsilon_b$$

The axial strain due to direct tension results from the applied tensile loading on the tendon and, therefore, will always be positive. As discussed previously, the bending strains in harped CFRP tendons are assumed to be symmetric and linear about the neutral axis, resulting in a positive axial strain at the top of the tendon and negative axial strain at the bottom of the tendon. The net axial strain at the top of the tendon will be additive as in Equation 5-6, and, therefore, always be positive, resulting in a net tension.

Conversely, the net axial strain at the bottom of the tendon will be subtractive as in Equation 6-1:

$$\text{Equation 6-1: } \varepsilon_{BOT} = \varepsilon_t - \varepsilon_b$$

If the magnitude of the axial bending strain is less than that of the axial tensile strain, a net tensile strain will be present in the bottom fibre. However, if the magnitude of the axial bending strain is greater than that of the axial tensile strain, a net compressive strain will be present. Because the axial bending strains at the top and bottom of the tendon are equal but opposite and the axial tensile strain is always positive, it should be obvious that the magnitude of the axial strain at the top of the tendon will always be greater than that at the bottom of the tendon. From this, it follows that if the tension and compression failure stress for the CFRP tendon were equal, the tendon would always fail in tension. However, the compressive capacity of CFRP tendons is much less than the tensile capacity (Swanson, 1990, Piggot et al, 1980), which would allow for the possible occurrence of compression failure of a harped CFRP tendon. This was confirmed by the observed compression failures in the testing program.

Recall from Equation 5-2 and Equation 5-12 that the axial tensile strain and the axial bending strain as a function of the applied load are:

$$\varepsilon_t = \frac{P}{E \cdot \pi \cdot r^2}$$

$$\varepsilon_b = \frac{2}{r} \cdot \sqrt{\frac{P \cdot (1 - \cos(\theta))}{\pi \cdot E}}$$

Using these formulae in Equation 5-6 and Equation 6-1, a strain-load graph for the harped tendon that illustrates the total axial strain at the top and bottom of the tendon as tensile loading is applied can be obtained by plotting the top and bottom axial strains versus the applied load. Figure 6-1 shows a typical strain-load graph for a harped CFRP prestressing tendon, and indicates the tension failure load

solution as computed by Equation 5-24, which occurs when the top fibre strain, ϵ_{TOP} , exceeds the tensile strain capacity of the tendon, ϵ_{ut} . From the Figure 6-1, it can be seen that the net axial strain at the top of the tendon, ϵ_{TOP} , is always positive and increases as the applied load increases. Figure 6-1 also illustrates that the net axial strain at the bottom of the tendon, ϵ_{BOT} , starts out negative or in compression, and increases to a maximum compressive strain magnitude, ϵ_{cMAX} , before beginning to decrease in magnitude and eventually exhibiting a net tensile strain.

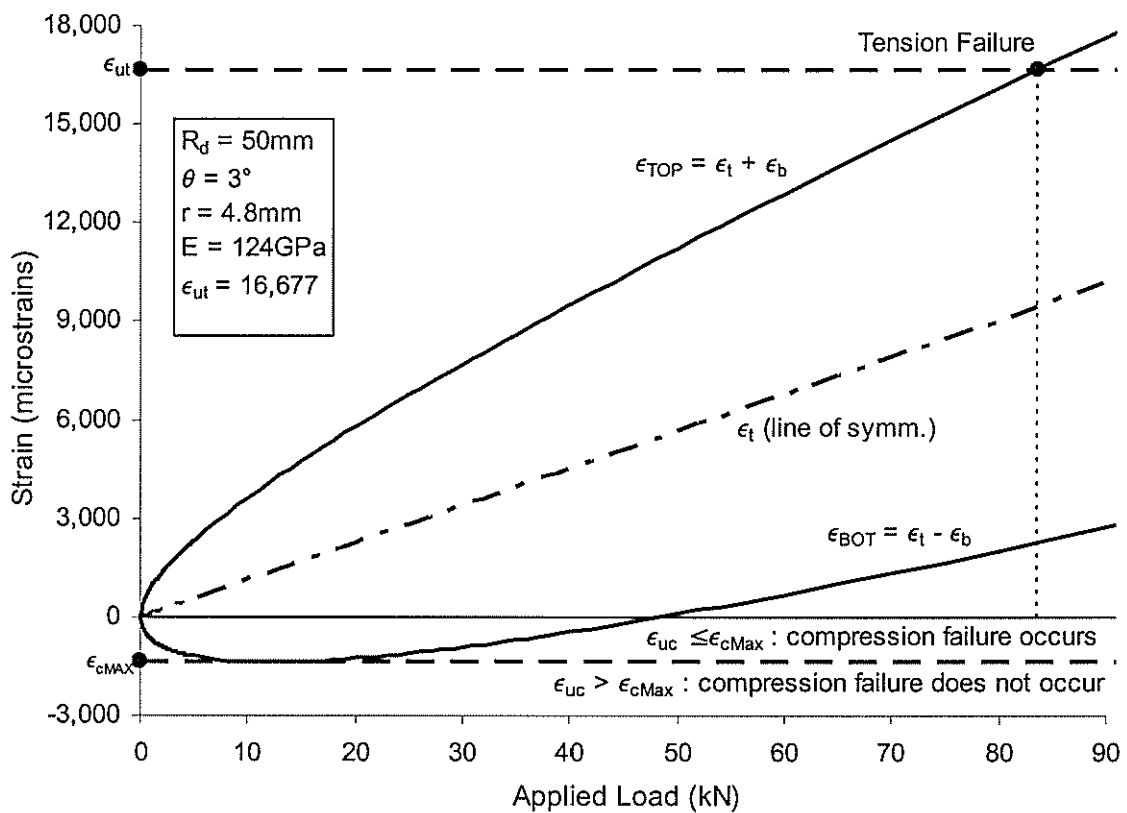


Figure 6-1: Typical Load History Graph for a Harped CFRP Tendon

Also as illustrated in Figure 6-1, if the compressive strain capacity of the CFRP tendon, ϵ_{uc} , is less than or equal in magnitude to the maximum compressive strain at the bottom of the tendon for a given configuration, ϵ_{cMAX} , a compression failure will occur, assuming that no other failure mode has already occurred. However, if the compressive strain capacity of the tendon is greater in magnitude than the

maximum compressive strain at the bottom of the tendon, then compression failure cannot occur, since the compressive strain capacity will never be reached.

If the compressive capacity for the CFRP tendon is known, a compressive failure load could be determined in a similar manner to that for tensile failure. However, since compression is not a desirable failure mode, as discussed earlier, it is only necessary to be able to determine whether compression failure will occur regardless of the applied loading at which it would occur. A simple design guideline for the effective compressive capacity was determined by observation of the experimental data obtained in the testing program. This was done by calculating the maximum compressive strain at the bottom of the tendon, ε_{cMAX} , as illustrated in Figure 6-1, for each specimen that failed in either tension or compression. By inspecting the values obtained, a compressive strain that adequately captures all the compression failures was determined, and this may be assumed to be the effective compressive capacity for design purposes.

Setting up a failure criterion equation in a similar fashion to the tensile failure criterion equation, Equation 5-13, for the bottom axial strain using an arbitrary, unknown compressive failure strain, ε_{uc} , gives:

$$\text{Equation 6-2: } \varepsilon_{uc} = \varepsilon_{tf} - \varepsilon_{bf}$$

Proceeding through a derivation similar to that described previously for tension failure in section 5.2.5, and using the compression failure criterion equation, Equation 6-2, a quadratic equation with bending strain, ε_{bf} , as the only unknown can again be obtained:

$$\text{Equation 6-3: } \frac{1}{4 \cdot (1 - \cos(\theta))} \cdot (\varepsilon_{bf})^2 - \varepsilon_{bf} - \varepsilon_{uc} = 0$$

The solution to the quadratic gives the axial bending strain component of the total axial strain in the bottom fibres of the tendon at compression failure for a given

compressive failure strain, ε_{uc} . When the quadratic in Equation 6-3 has a real solution, it means that the load history curve for the axial strain at the bottom of the tendon intersects the compression failure strain, and compression failure may occur. On the other hand, if there is no solution, it means that there is no intersection and the axial strain at the bottom of the tendon will not reach the compression failure strain, and therefore, the specimen will not exhibit a compression failure.

Recall that the general solution for a quadratic equation of the form $A \cdot x^2 + B \cdot x + C = 0$ is:

$$x = \frac{-B \pm \sqrt{B^2 - 4 \cdot A \cdot C}}{2 \cdot A}$$

In order for the quadratic equation to have a real solution, the portion inside the square root ($B^2 - 4 \cdot A \cdot C$) must be greater than or equal to zero.

The maximum value for the unknown compressive failure strain, ε'_{cu} , for which there is a solution to Equation 6-3 is equal to ε_{cMAX} , as illustrated in Figure 6-1, and is obtained when the portion inside the square-root is equal to zero:

$$B^2 - 4 \cdot A \cdot C = 0$$

Therefore: $x = \frac{-B}{2 \cdot A}$

Where: $A = \frac{1}{4 \cdot (1 - \cos(\theta))}$ and $B = -1$

Equation 6-4: $\varepsilon_{bf} = 2 \cdot (1 - \cos(\theta))$

Solving for the natural radius of curvature associated with the axial bending strain:

$$\varepsilon_b = \frac{r}{R}$$

Therefore: $\frac{r}{R_{ncMAX}} = \varepsilon_{bf}$

$$\text{Equation 6-5: } R_{ncMAX} = \frac{r}{2 \cdot (1 - \cos(\theta))}$$

As before, the tendon radius of curvature is physically limited by the size of the deviator and, therefore cannot be less than R_{min} as given by Equation 5-15:

$$R_{min} = R_d + r$$

$$\text{Equation 6-6: } R_{cMAX} = \max(R_{ncMAX}, R_{min})$$

The actual axial bending stress associated with the maximum net compressive strain can then be given as:

$$\text{Equation 6-7: } \varepsilon_{bcMAX} = \frac{r}{R_{cMAX}}$$

Setting $\varepsilon_{uc} = \varepsilon_{cMAX}$ and $\varepsilon_{bf} = \varepsilon_{bcMAX}$ in Equation 6-3 and solving for ε_{cMAX} :

$$\text{Equation 6-8: } \varepsilon_{cMAX} = \frac{1}{4 \cdot (1 - \cos(\theta))} \cdot (\varepsilon_{bcMAX})^2 - \varepsilon_{bcMAX}$$

The solution to Equation 6-8 gives the maximum compression failure strain for the CFRP material for which compression failure will occur for a specific set of variables.

Table 6-2 specifies the values of the maximum compressive strain, ε_{cMAX} , as calculated by Equation 6-8 for the experimental program specimens for which either tension or compression failure occurred. The table also gives these values as a ratio of the guaranteed tensile strain capacity of the material, ε_{ut} . As can be seen, the largest value for specimens for which tension failure occurred was 7,953 microstrain or $0.48 \varepsilon_{ut}$ and the smallest value for specimens for which compression failure occurred was 8,761 microstrain or $0.53 \varepsilon_{ut}$.

Table 6-2: Maximum Compressive Strain for Test Specimens

Specimen No.	Tendon Diameter (mm)	Deviator Radius (mm)	Harp Angle (deg)	ϵ_{cMAX} microstrain	$\epsilon_{cMAX}/\epsilon_{ut}$ ($\epsilon_{ut}=16,677$)
Bending-Tension Failures					
1	9.5	50	2	609	0.04
2	9.5	50	3	1,370	0.08
6	9.5	500	2	609	0.04
7	9.5	500	3	1,370	0.08
8	9.5	500	5	3,805	0.23
19	9.5	500	6	5,369	0.32
20	9.5	500	9	7,612	0.46
9	9.5	500	10	7,953	0.48
12	9.5	250	5	3,805	0.23
13	9.5	1000	5	3,259	0.20
14	6.3	50	2	609	0.04
15	6.3	50	3	1,370	0.08
16	6.3	50	5	3,805	0.23
21	9.5	250	2	609	0.04
22	9.5	250	3	1,370	0.08
24	9.5	100	3	1,370	0.08
Bending-Compression Failures					
4	9.5	50	10	15,192	0.91
5	9.5	50	15	34,074	2.04
23	9.5	250	10	12,925	0.77
10	9.5	500	15	8,761	0.53
17	6.3	50	10	15,192	0.91
18	6.3	50	15	33,495	2.01

By inspection of the failure results from the experimental program, a conservative value of approximately $0.45 \epsilon_{ut}$ may be used as the effective compression strain failure level for the CFRP tendons in determining whether compressive failure will occur:

Equation 6-9: $\epsilon_{uc} = \phi_{\epsilon} \cdot \epsilon_{ut}$

Where: $\phi_{\epsilon} = 0.45$

To determine if a set of harping configuration variables will produce a compressive failure, the maximum net compressive strain, ϵ_{cMAX} , is calculated using the variables for the specific harping configuration. If the magnitude of this strain is larger or equal to the effective compressive failure strain, then a compressive failure is likely to occur and the configuration should not be used. Table 6-3 compares the results of

the compression failure guideline with the behaviour observed in the experimental program. For all of the specimens in the experimental program that exhibited compression failure, the compression failure guideline also indicates a compression failure mode, which should be expected as the guideline is based on that data. For specimens 9 and 20, compression failure is given by the design guidelines while the failure mode observed was tension failure, but this is acceptable as it indicates it is very near the tension-compression failure division line and gives a conservative result. It is notable that these two specimens have large harping angles of 9° and 10° fitting with the previous observation that compression failures occur under large harping angles.

Table 6-3: Comparison of Compression Failure Guidelines to Test Data

Specimen No.	Tendon Diameter (mm)	Deviator Radius (mm)	Harp Angle (deg)	ϵ_{cMAX} microstrain	Failure Mode	
					Actual	Predicted
1	9.5	50	2	609	T	T
2	9.5	50	3	1,370	T	T
6	9.5	500	2	609	T	T
7	9.5	500	3	1,370	T	T
8	9.5	500	5	3,805	T	T
19	9.5	500	6	5,369	T	T
20	9.5	500	9	7,612	T	C
9	9.5	500	10	7,953	T	C
12	9.5	250	5	3,805	T	T
13	9.5	1000	5	3,259	T	T
14	6.3	50	2	609	T	T
15	6.3	50	3	1,370	T	T
16	6.3	50	5	3,805	T	T
21	9.5	250	2	609	T	T
22	9.5	250	3	1,370	T	T
24	9.5	100	3	1,370	T	T
4	9.5	50	10	15,192	C	C
5	9.5	50	15	34,074	C	C
23	9.5	250	10	12,925	C	C
10	9.5	500	15	8,761	C	C
17	6.3	50	10	15,192	C	C
18	6.3	50	15	33,495	C	C

$\epsilon_{ut} = 16,677$ microstrains

$\epsilon_{uc} = 7,505$ microstrains

6.4 BENDING-SHEAR FAILURE

Within the experimental program, two shear failures were observed. As already mentioned, a bending-shear failure was characterised by a horizontal, longitudinal splitting of the tendon near its neutral axis near the deviator. This type of failure occurs when the longitudinal shear stress in the tendon exceeds the longitudinal shear capacity of the tendon. The longitudinal shear stress is a result of the longitudinal shear deformation in the tendon. This cannot be predicted by the primary model, since it is based on classical bending theory for pure bending that plane sections remain plane and perpendicular to the neutral axis of the tendon. Using this assumption, no longitudinal shear deformation is present. The extended model, however, does calculate shear deformation due to transition effects. As discussed in section 5.4, in order to alleviate the unbalanced bending moment at the transition point under the primary model, under the extended model, plane sections rotate away from perpendicular through a transition zone to provide a smooth bending strain transition. This rotation of the plane sections out of perpendicular to the neutral axis is essentially shear deformation within the tendon, and results in a longitudinal shear stress and strain.

Across the tendon section, the largest resultant shear stress will be at the neutral axis, and in the longitudinal direction along the tendon length, the greatest shear stress is at the transition point as illustrated in Figure 5-26, which helps to explain the location of the initiation of shear failure. Deriving a shear failure criterion for harped CFRP prestressing tendons is difficult as very little information is given concerning the longitudinal shear properties of the material. However, a general design guideline may be established through observation of the experimental results in conjunction with the extended analytical model. This may be done by determining the maximum shear deformation that results for each specimen within

the test program that exhibited either tension or shear failure, and establishing a design guideline that can safely avoid shear failure. Recalling from section 5-4, the approximate shear deformation and strain can be determined using Equation 5-58, Equation 5-59 and Equation 5-60:

$$\beta_{\text{lim}} = \frac{1}{2} \cdot \sqrt{\frac{E}{b \cdot G}} \cdot \frac{r}{R}$$

$$\beta_{\text{max}} = \phi_{\beta} \cdot \beta_{\text{lim}}$$

$$\phi_{\beta} = 1 - e^{-2 \cdot \sqrt{\frac{G \cdot R}{E \cdot r}} \cdot \theta_r}$$

Table 6-4 indicates the values of the maximum longitudinal shear strain, β_{max} , as determined using the extended model for the experimental program specimens that exhibited either a tension or shear mode of failure.

Table 6-4: Maximum Longitudinal Shear Strain for Test Specimens

Specimen No.	Tendon Diameter (mm)	Deviator Radius (mm)	Harping Angle (mm)	R' _{min} (mm)	β_{lim} radians	ϕ_{β}	β_{max} radians
Bending-Tension Failures							
1	9.5	50	2	860	0.005745	0.998	0.005732
2	9.5	50	3	639	0.007739	0.999	0.007730
6	9.5	500	2	860	0.005745	0.998	0.005732
7	9.5	500	3	639	0.007739	0.999	0.007730
8	9.5	500	5	505	0.009789	1.000	0.009788
9	9.5	500	10	505	0.009789	1.000	0.009789
12	9.5	250	5	466	0.010596	1.000	0.010593
13	9.5	1000	5	1005	0.004918	1.000	0.004918
14	6.4	50	2	573	0.005745	0.998	0.005732
15	6.4	50	3	426	0.007738	0.999	0.007730
16	6.4	50	5	311	0.010596	1.000	0.010593
19	9.5	500	6	505	0.009789	1.000	0.009789
20	9.5	500	9	505	0.009789	1.000	0.009789
21	9.5	250	2	860	0.005745	0.998	0.005732
22	9.5	250	3	639	0.007739	0.999	0.007730
24	9.5	100	3	639	0.007739	0.999	0.007730
Bending-Shear Failures							
3	9.5	50	5	466	0.010596	1.000	0.010593
11	9.5	100	5	466	0.010596	1.000	0.010593

As can be seen, the largest assumed maximum shear strain, β_{max} , for specimens for which tension failure occurred was approximately 0.0106 radians and the smallest maximum shear strain for specimens for which shear failure occurred was also 0.0106 radians. This means that for the same assumed maximum bending shear, there were specimens that did exhibit shear failure and specimens that did not exhibit shear failure. This may be attributed to the variability in material properties. From the observations of Table 6-4, a conservative value of 0.01 radians may be used as the shear strength guideline for the tendon, based on the properties of the material used within this testing program:

Equation 6-10: $\beta_u = 0.01$

It can also be noted from Table 6-4 that shear strain reduction factor, ϕ_β , is very close to being equal to 1 for all the specimens. Indicating that, in practical harping configurations as used in the test program, the maximum shear strain, β_{max} , is, in effect, equal to the maximum limiting shear strain associated with the tendon radius of curvature, β_{lim} , and this value may be used for simplicity in lieu of calculating ϕ_β :

$$\beta_{max} = \beta_{lim}$$

Equation 6-11: $\beta_{max} = \frac{1}{2} \cdot \sqrt{\frac{E}{b \cdot G}} \cdot \frac{r}{R'_{min}}$

Where: $b = 4$ for a circular cross-section

Calculation of the minimum radius of curvature of the tendon within the extended model can be a rather lengthy procedure as stated in section 5.4.5. It was observed earlier (Table 5-1) that the minimum radius of curvature for the harped tendon, when calculated using the extended model, was reduced to up to 95% of the minimum radius of curvature calculated within the primary model. Therefore, for a simpler, but conservative shear failure design guideline, the minimum radius of

curvature can be set to be equal to 90% of the natural radius of curvature, R_{min} , from Equation 5-16:

$$\text{Equation 6-12: } R'_{min} = \max(0.9 \cdot R_{min}, R_{min})$$

To determine if a set of harping configuration variables will produce a shear failure, the maximum shear strain can be estimated using Equation 6-11 and Equation 5-17.

If the magnitude of this shear strain is larger than or equal to the shear failure strain given by Equation 6-10, then a shear failure is likely to occur and the configuration should not be used.

Table 6-5: Comparison of Shear Failure Guidelines to Test Data

Specimen No.	Tendon Diameter (mm)	Deviator Radius (mm)	Harping Angle (deg)	R'_{min} (mm)	β_{MAX} radians	Failure Mode	
						Actual	Predicted
1	9.525	50	2	813	0.006077	T	T
2	9.525	50	3	595	0.008307	T	T
6	9.525	500	2	813	0.006077	T	T
7	9.525	500	3	595	0.008307	T	T
8	9.525	500	5	505	0.009789	T	T
9	9.525	500	10	505	0.009789	T	T
12	9.525	250	5	427	0.011581	T	S
13	9.525	1000	5	1,005	0.004918	T	T
14	6.35	50	2	542	0.006077	T	T
15	6.35	50	3	397	0.008307	T	T
16	6.35	50	5	284	0.011581	T	S
19	9.525	500	6	505	0.009789	T	T
20	9.525	500	9	505	0.009789	T	T
21	9.525	250	2	813	0.006077	T	T
22	9.525	250	3	595	0.008307	T	T
24	9.525	100	3	595	0.008307	T	T
3	9.525	50	5	427	0.011581	S	S
11	9.525	100	5	427	0.011581	S	S

$\beta_u = 0.01$ radians

Table 6-5 compares the results of the shear failure guideline with the behaviour observed in the experimental program. For all of the specimens in the experimental that exhibited shear failure, the shear failure guideline also indicates a shear failure mode as expected as the guideline is based on that data. For specimens 12 and 16, shear failure is given by the design guidelines while the failure mode observed was

tension failure. This is a conservative result and, therefore, is considered acceptable. As stated above, this may be attributed to the factors stated earlier as well as the fact that the design guideline was developed as conservative. It is also notable that these two specimens have a medium harping angle of 5° and smaller deviator radii of 50mm and 250mm, which agrees with the previous observation that shear failures occur with medium harping angles and small deviator sizes.

The effective compressive strength and effective longitudinal shear strength are dependent upon the material used. The rules developed here for bending-compression and bending-shear failure mode control are based upon observation of the experimental data from this research program, therefore, they can only be considered valid for the particular material tested in this program.

7 STRENGTH DESIGN RECOMMENDATIONS

7.1 INTRODUCTION

One of the main objectives of this research program was to develop a model that can predict the tensile-flexural and failure behaviour of harped CFRP prestressing tendons. In this chapter, factors and equations for determining the design strength of harped CFRP prestressing tendons, as derived from the analytical models developed within the research program, are presented.

7.2 HARPING CONFIGURATION AND MATERIAL PROPERTY VARIABLES

Figure 7-1 illustrates the overall harping configuration and geometric variables associated with a harped prestressing tendon that are used for the strength design presented here.

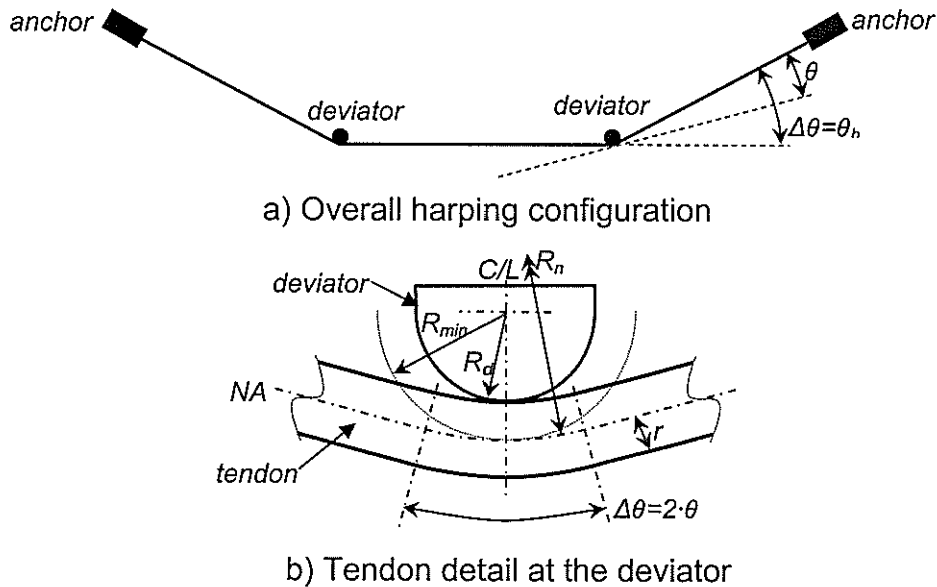


Figure 7-1: Harping Configuration Variables

The CFRP tendon material properties can typically show significant scatter, unless the specific material properties for the tendons used can be accurately determined through lab testing, it is recommended that the guaranteed minimum values be used for all design calculations. The harping configuration and material property variables that are used for the design formulae in this chapter are:

- A_t = cross-sectional area of the prestressing tendon
- b = shape factor (= 4 for circular cross-section)
- G = guaranteed minimum Shear modulus for CFRP material
- E = guaranteed minimum Young's modulus for CFRP material
- P_f = tensile load applied to the harped tendon at which failure will occur
- r = tendon cross-section radius
- R_{cMAX} = tendon radius of curvature at point of maximum net bending-compression
- R_d = deviator radius
- R_f = tendon radius of curvature of tendon at point of bending-tension failure
- R_{min} = minimum tendon radius of curvature as physically limited by the deviator
- R_{ncMAX} = tendon natural radius of curvature at point of maximum net bending-compression
- R_{nf} = natural tendon radius of curvature at point of bending-tension failure
- R_β = minimum tendon radius of curvature associated with maximum longitudinal shear strain
- β_{max} = maximum longitudinal shear strain in tendon
- β_u = effective maximum longitudinal shear strain capacity
- ε_{uc} = effective compressive strain capacity
- ε_{ut} = guaranteed minimum tensile rupture strain for CFRP material
- ε_{cMAX} = maximum net bending-compression strain at bottom of tendon
- ε_{bcMAX} = axial bending strain component of ε_{cMAX}
- ε_{tcMAX} = axial tensile strain component of ε_{cMAX}
- σ_{ut} = guaranteed minimum tensile stress capacity of tendon ($\sigma_{ut} = E \cdot \varepsilon_{ut}$)

- σ'_{ut} = reduced tensile stress capacity of harped tendon
- ϕ_h = tensile capacity reduction factor for harped tendon
- ϕ_{te} = bending stress reduction factor for transition effects
- ϕ_e = strain capacity reduction factor for compressive strain
- θ_h = overall harping angle
- θ_e = effective harping angle
- θ_r = effective harping angle in radians
- $\Delta\theta_h$ = total change in harping angle over an individual deviator

7.3 MINIMUM RADIUS OF CURVATURE

When a CFRP prestressing tendon is placed in a harped configuration and loaded, it assumes a natural radius of curvature based on the stiffness of the tendon and equilibrium. However, because the tendon is harped around a deviator of a fixed radius, the minimum radius of curvature that the tendon can assume is physically limited by the deviator size as illustrated in Figure 7-2. Therefore the minimum radius of curvature is:

Equation 7-1: $R_{min} = R_d + r$

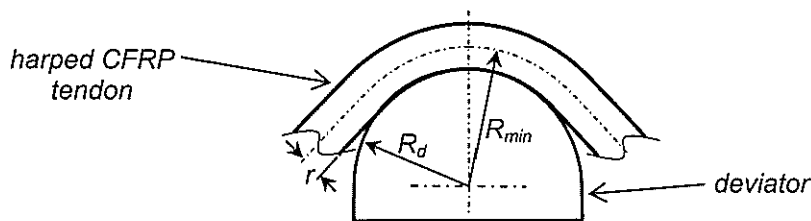


Figure 7-2: Minimum Tendon Radius of Curvature

7.4 DEVIATOR DESIGN

The strength reduction of the harped tendon is related to the minimum radius of curvature in the tendon. When the curvature of the tendon assumes the minimum

radius of curvature as limited by the deviator radius, if the deviator is designed such that its tangential angle is greater than the effective harping angle of the tendon, as shown in Figure 7-3a, the deviator radius will be the governing curvature. However, if the deviator is designed such that its tangential angle is less than the effective harping angle, a localized bending point or kink will be induced in the tendon at the deviator edge, as shown in Figure 7-3b. The curvature of the tendon at this location will be smaller than the minimum curvature defined by the deviator size and a bending stress concentration will be created. Therefore, the tensile strength reduction of the harped tendon will be greater than that calculated using the minimum radius of curvature defined by the deviator size. In order to avoid this situation, deviators should be designed so that the tangential angle, θ_t , of the deviator is larger than the effective harping angle, θ_e .

Equation 7-2: $\theta_t > \theta_e$

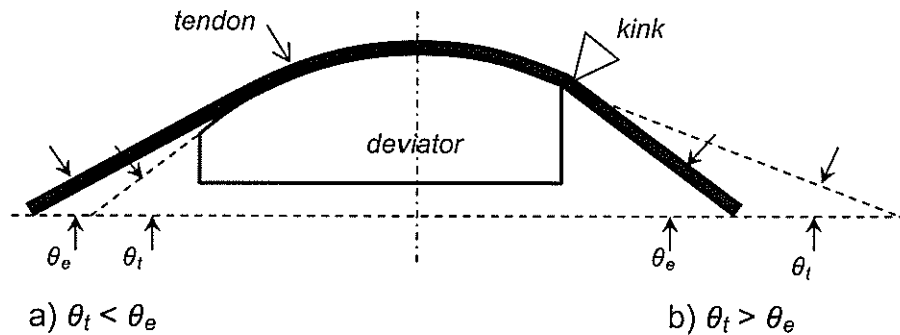


Figure 7-3: Deviator Design

7.5 EFFECTIVE HARPING ANGLE

Within the research program, only a single harped tendon configuration was used for the experimental tests and for illustrating the analytical model development. However, it is recognized that a reduced tendon strength results from the additional strains in stresses in the tendon resulting from the curvature of the tendon induced by harping. Figure 7-4 illustrates the distribution of axial bending stresses and

strains along the harped tendon in the region of the deviator. The figure shows that the axial bending stresses and strains induced in the tendon are localized around the deviator, within the curved portion of the tendon.

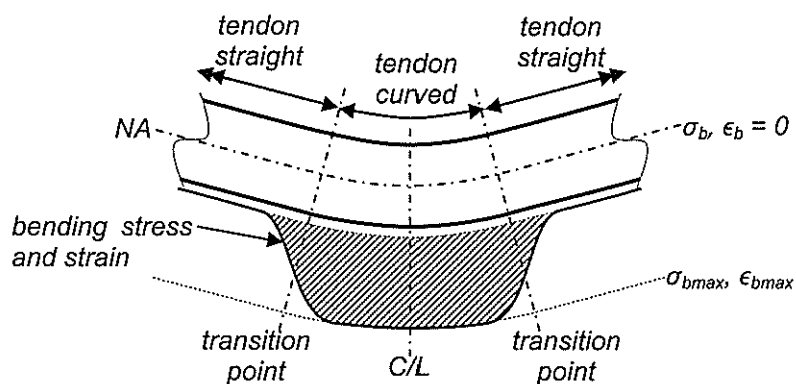


Figure 7-4: Bending Stress and Strain Distribution Along Tendon At Deviator

The fact that the bending stresses and strains are localized should be considered when determining the effective harping angle to be used within the design formulae, especially when multiple deviators are used. Figure 7-5 illustrates the configuration for a tendon with a single deviator and harping point, as used within the research program. The effective tendon harping angle, θ_e , used for determining the design strength is the same as the overall harping angle, θ_h . The total included angle or change in angle over the deviator, $\Delta\theta_h$, is equal to twice the effective harping angle. Figure 7-6 illustrates the configuration for a tendon with two deviators and harping points. In this case, because the bending stresses and strains are localised at each individual deviator, the strength reduction of the tendon at the two deviators can be considered to act independently of each other. Therefore, the effective harping angle used for strength reduction calculation should be based on a set of axes local to each deviator. In this case, the effective harping angle, θ_e , at each deviator will be equal to one-half of the overall applied harping angle, θ_h . The total

included angle or change in angle over the deviator, $\Delta\theta_h$, is equal to twice the effective harping angle.

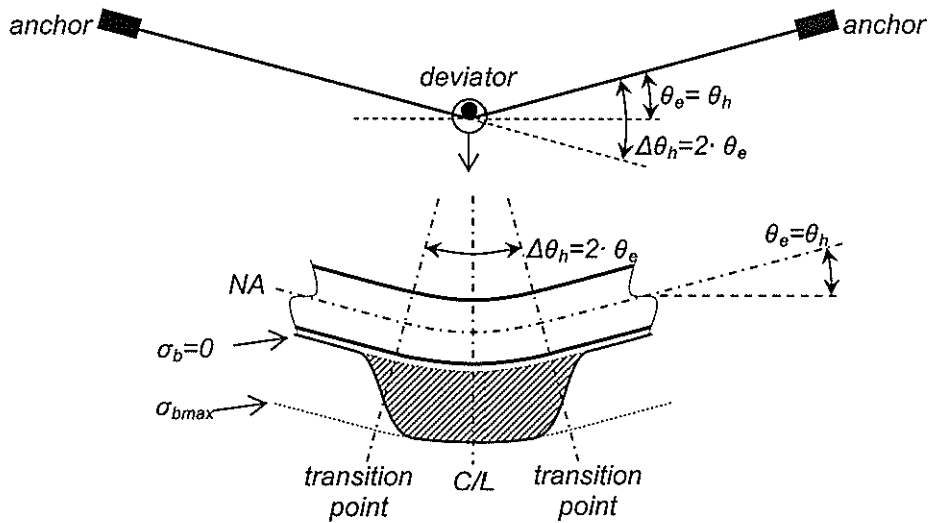


Figure 7-5: Effective Harping Angle for Single Harped Tendon

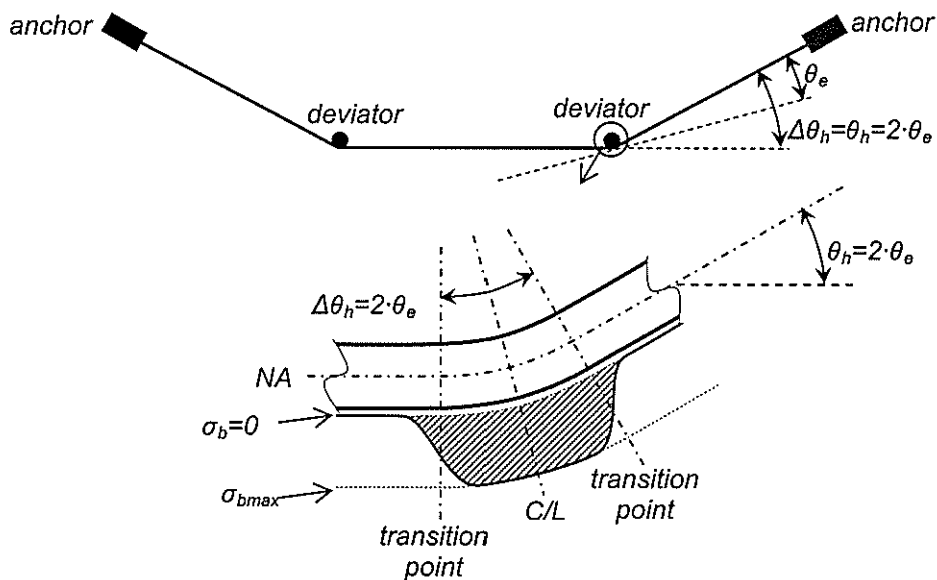


Figure 7-6: Effective Harping Angle for Double Harped Tendon

In both the cases shown above, it can be seen that the effective harping angle is not directly related to the overall harping angle, but rather the change in angle at each individual deviator. It can be reasoned that this should hold true even for tendons with more than two deviators. Therefore:

Equation 7-3: $\theta_e = \frac{1}{2} \cdot \Delta\theta_h$

Where: θ_e = effective harping angle at individual harping point
 $\Delta\theta_h$ = total change of harping angle at individual harping point

7.6 HARPED TENDON TENSILE CAPACITY REDUCTION

Two analytical models for determining the tensile capacity of harped CFRP tendons were developed within the research program: the primary model and the extended model. The extended model is based on the primary model, but with transition effects included. It was shown that the transition effects have no effect on the capacity of the harped tendon when the tendon radius is not physically limited by the deviator. When the tendon radius is physically limited by the deviator, the extended model produces slightly higher effective tendon capacities. Therefore, the extended model can be used when the radius of curvature is limited by the deviator, and the primary model can be used when it is not. The radius of curvature of the harped tendon at the point of tensile failure can be determined to be:

Equation 7-4:
$$R_{nf} = \frac{r}{2 \cdot (1 - \cos(\theta_e)) \cdot \left(\sqrt{1 + \frac{\varepsilon_{ut}}{(1 - \cos(\theta_e))}} - 1 \right)}$$

Equation 7-5: $R_f = \max(R_{nf}, R_{min})$

Depending whether the radius of curvature determined by Equation 7-5 is equal to the natural radius of curvature, R_{nf} , or the minimum physical radius of curvature limited by the deviator size, R_{min} , the tensile capacity reduction factor can be calculated as:

Equation 7-6: $\phi_h = 1 - \frac{r}{\varepsilon_{ut} \cdot R_f}$ when $R_f = R_{nf}$

$$\text{Equation 7-7: } \phi_h = 1 - \frac{\phi_{te} \cdot r}{\varepsilon_{ut} \cdot R_f} \quad \text{when } R_f = R_{\min}$$

Where:

$$\text{Equation 7-8: } \phi_{te} = 1 - e^{-\sqrt{\frac{G}{E}} \frac{R_f}{r} \cdot \theta_r}$$

The reduced tensile capacity of the harped CFRP tendon can then be calculated as:

$$\text{Equation 7-9: } \sigma'_{ut} = \phi_h \cdot \sigma_{ut}$$

The maximum tensile load that can be applied to the harped tendon before failure occurs can be defined as:

$$\text{Equation 7-10: } P_f = \sigma'_{ut} \cdot A_t$$

7.7 FAILURE MODE CONTROL

It was shown that bending-compression and bending-shear failures occur at significantly lower loading levels than for bending-tension failures, and are undesirable from a usability standpoint. Therefore, one of the most important factors when checking the design strength of a harped tendon is to ensure that it will not fail in either a bending-compression or a bending-shear.

7.7.1 Bending-Compression Failure

As discussed previously, during the process of loading a harped tendon, net compressive stresses and strains will develop in the bottom of the tendon. In order to avoid a bending-compression mode of failure, the maximum net compressive strain must be kept less than the compressive capacity of the tendon.

An effective compressive strength was developed based on an inspection of the experimental data and the analytical model, and based on the guaranteed tensile strength. The effective compressive strain capacity was determined to be:

Equation 7-11: $\varepsilon_{nc} = \phi_e \cdot \varepsilon_{ut}$

Equation 7-12: $\phi_e = 0.45$

To check the harping configuration for the possibility that bending-compression failure will occur, the assumed maximum net compressive strain at the bottom of the tendon is determined and compared to the effective compressive strain capacity. The maximum net compressive strain at the bottom of the tendon is directly related to the radius of curvature of the tendon at the point of maximum compressive strain:

Equation 7-13: $R_{ncMAX} = \frac{r}{2 \cdot (1 - \cos(\theta_e))}$

Equation 7-14: $R_{cMAX} = \max(R_{ncMAX}, R_{min})$

The maximum net compressive strain can then be calculated as:

Equation 7-15: $\varepsilon_{bcMAX} = \frac{r}{R_{cMAX}}$

Equation 7-16: $\varepsilon_{tcMAX} = \frac{1}{4 \cdot (1 - \cos(\theta_e))} \cdot (\varepsilon_{bcMAX})^2$

Equation 7-17: $\varepsilon_{cMAX} = \varepsilon_{tcMAX} - \varepsilon_{bcMAX}$

In order to avoid the occurrence of bending-compression failure, the maximum net compressive strain must be less than the effective compressive strain capacity:

Equation 7-18: $|\varepsilon_{cMAX}| < |\varepsilon_{nc}|$

If it is determined that the tendon will exhibit a bending-compression failure, the maximum net compressive strain must be decreased to a value lower than the effective compressive strain capacity. This may be done either by increasing the deviator size such that it limits the minimum radius of curvature of the tendon, or by decreasing the effective harping angle, which has the effect of increasing the minimum radius of curvature of the tendon. Decreasing the effective harping angle is done by decreasing the change of angle of the tendon over the deviator(s) by either decreasing the overall harping angle or increasing the number of harping

points. Both of these methods for decreasing the effective harping angle have the same effect on the tensile design strength of the harped tendon. However, increasing the number of harping points can allow the overall harping angle to remain the same, which may be more desirable under circumstances where the vertical loading at the deviator, resulting from harping the tendon, needs to maintain a specific magnitude.

It should be noted that this guideline for bending-compression failure control is based on the specific CFRP material used within this testing program, Aslan 200 CFRP rebar by Hughes Brothers Inc., and may not hold true for other CFRP tendons.

7.7.2 Bending-Shear Failure

Within the development of the extended model, it was shown that when determining transition effects in the curved tendon, the presence of longitudinal shear deformation is highlighted. This shear deformation results in longitudinal shear stresses and strains in the tendon. In order to avoid a bending-shear mode of failure, the maximum longitudinal shear must be kept to a value less than the longitudinal shear capacity of the tendon.

An effective longitudinal shear strength guideline was developed based on inspection of the experimental data and an analytical model. The effective longitudinal shear strain capacity was determined to be:

Equation 7-19: $\beta_u = 0.01$

To check the harping configuration for the possibility that bending-shear failure will occur, the assumed maximum longitudinal shear strain in the harped tendon is determined and compared to the effective longitudinal shear strain capacity. The maximum longitudinal shear strain in the harped tendon is related to the minimum radius of curvature that the tendon will achieve. In lieu of having to determine the

minimum natural radius of curvature of the tendon including transition effects, which is an iterative and complex process, the minimum natural radius of curvature, as determined using the primary model, is used and a reduction factor of 0.9 applied to produce a conservative result. The minimum natural radius of curvature of the tendon is equal to the radius of curvature of the tendon at the point of tensile failure:

$$\text{Equation 7-20: } R_{\beta} = \max(0.9R_{nf}, R_{\min})$$

The maximum longitudinal bending-shear strain can then be calculated as:

$$\text{Equation 7-21: } \beta_{\max} = \frac{1}{2} \cdot \sqrt{\frac{E}{b \cdot G}} \cdot \frac{r}{R_{\beta}}$$

In order to avoid the possible occurrence of bending-shear failure, the maximum longitudinal bending-shear strain must be less than the effective longitudinal shear strain capacity:

$$\text{Equation 7-22: } \beta_{\max} < \beta_u$$

If it is determined that the tendon will exhibit a bending-shear failure, the maximum longitudinal shear strain must be decreased to a value lower than the effective longitudinal shear strain capacity. When the radius of curvature of the tendon is physically limited by the deviator size, this may be done by increasing the deviator size. When the radius of curvature of the tendon is not physically limited by the deviator size, this may be done by decreasing the effective harping angle, which has the effect of increasing the radius of curvature of the tendon.

As with the bending-compression failure guidelines, this guideline for bending-shear failure control is based on the specific CFRP material used within this testing program and may not hold true for other CFRP tendons.

7.8 DESIGN PROCEDURE

From the design recommendations summarized in this chapter, a procedure for the tensile strength design of CFRP tendons in harped prestressing configurations can be assembled. The flowchart in Figure 7-7 outlines the design procedure.

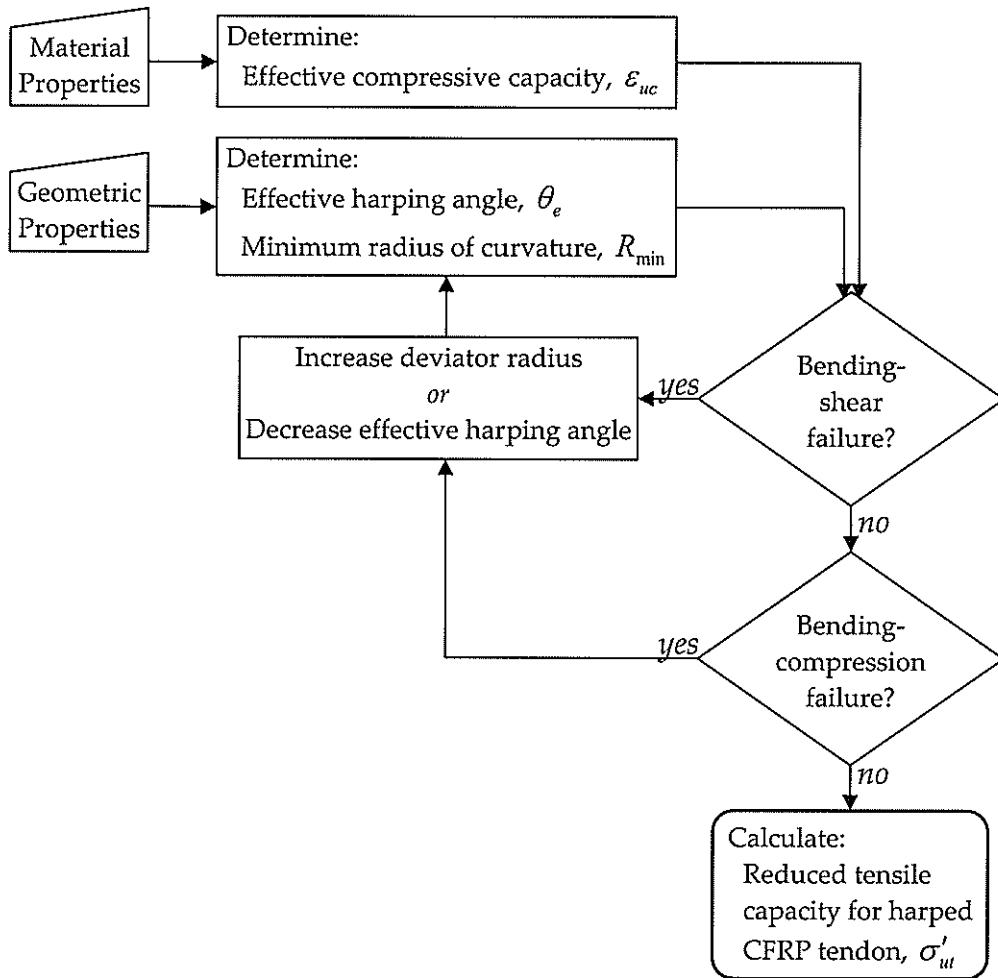


Figure 7-7: Flowchart for Design Procedure

7.9 DESIGN EXAMPLES

In this section, two design examples are given to illustrate the procedure for strength design of a harped tendon using the design formulae from this chapter. These

examples use configuration variables that illustrate most of the design circumstances that may be encountered.

7.9.1 Design Example 1

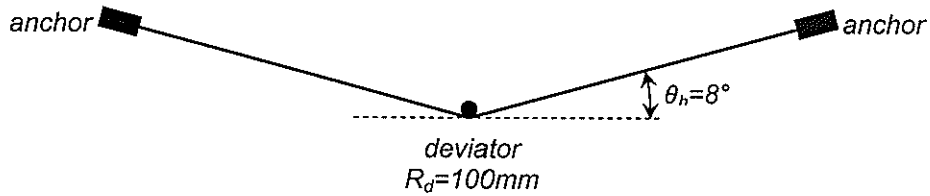


Figure 7-8: Initial Harping Configuration for Design Example 1

A 10mm diameter CFRP prestressing tendon is to be harped at an angle of 8° over a single deviator with a radius of 100mm as illustrated in Figure 7-8. Resolve any failure mode problems and determine the tensile design capacity of the tendon.

The material properties of the CFRP tendon are as follows:

$$E = 124GPa$$

$$\varepsilon_{ut} = 16,677 \text{ microstrains}$$

$$\sigma_{ut} = E \cdot \varepsilon_{ut} = 2,068MPa$$

$$G = 7.2GPa$$

The geometric harping configuration variables have been given as:

$$\theta_h = 8^\circ$$

$$r = 5mm, A_t = 78.54mm^2$$

$$R_d = 100mm$$

Therefore, the minimum physical radius of curvature of the tendon is:

$$R_{min} = R_d + r = 105mm$$

Effective Harping Angle

The tendon is given as having a single harping point with an overall harping angle of 8° . In this case, the effective harping angle would also be 8° .

Alternatively, the total change in angle at the deviator is:

$$\Delta\theta_h = 2 \cdot \theta_h = 16^\circ$$

Therefore, the effective harping angle is:

$$\theta_e = \frac{1}{2} \cdot \Delta\theta_h = 8^\circ$$

Failure Mode Control

Check for bending-compression failure:

Determine effective compressive strain capacity:

$$\varepsilon_{uc} = \phi_\varepsilon \cdot \varepsilon_{ut} = 7,505 \text{ microstrains}$$

Determine tendon radius of curvature at maximum compressive strain:

$$R_{ncMAX} = \frac{r}{2 \cdot (1 - \cos(\theta_e))}$$

$$R_{ncMAX} = 257 \text{ mm}$$

$$R_{ncMAX} > R_{\min}, \text{ therefore: } R_{cMAX} = R_{ncMAX} = 257 \text{ mm}$$

Determine the maximum net compressive strain:

$$\varepsilon_{bcMAX} = \frac{r}{R_{cMAX}} = 19,464 \text{ microstrains [C]}$$

$$\varepsilon_{icMAX} = \frac{1}{4 \cdot (1 - \cos(\theta_e))} \cdot (\varepsilon_{bcMAX})^2 = 9,732 \text{ microstrains [T]}$$

$$\varepsilon_{cMAX} = \varepsilon_{icMAX} - \varepsilon_{bcMAX} = 9,732 \text{ microstrains [C]}$$

$$\varepsilon_{cMAX} > \varepsilon_{uc}$$

The maximum net compressive strain is greater than the effective compressive strain capacity; therefore, the CFRP tendon is likely to exhibit bending-compression failure and should not be used in this configuration. Figure 7-9 illustrates the strain versus applied load graph for design example 1 and highlights the occurrence of bending-compression failure.

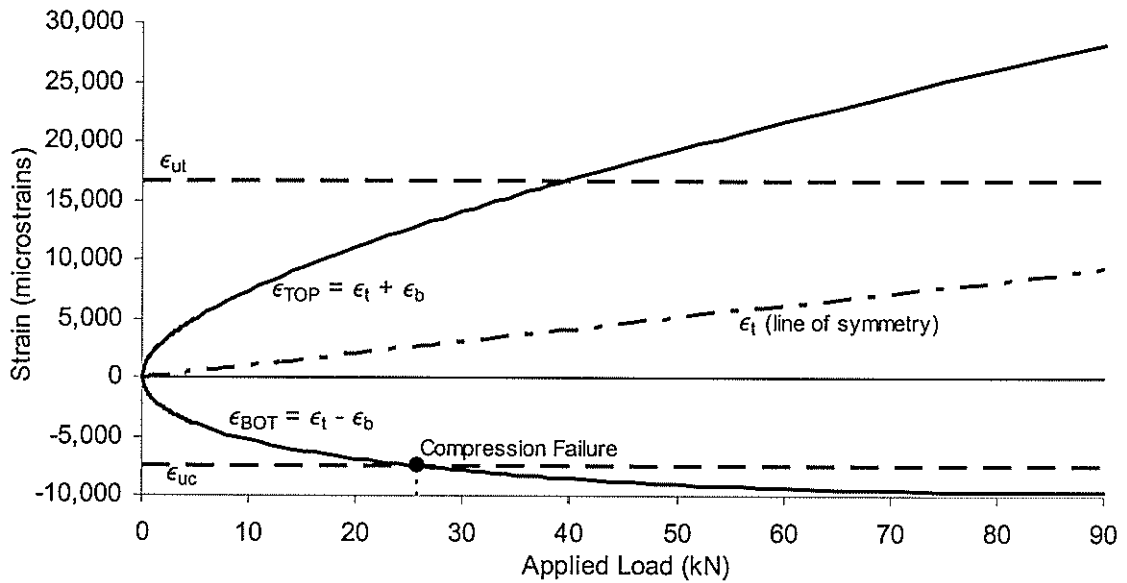


Figure 7-9: Strain vs. Loading Graph for Design Example 1

In order to be able to use a harped CFRP tendon, the occurrence of bending-compression failure needs to be resolved by either increasing the deviator radius to limit the tendon radius of curvature or decreasing the effective harping angle.

Alternative 1: Increase Deviator Radius

The harped tendon configuration is the same as before, but a larger radius deviator will be used. Try a 500mm radius deviator:

$$R_d = 500mm$$

$$R_{min} = R_d + r = 505mm$$

Effective Harping Angle

The effective harping angle is as before:

$$\theta_e = 8^\circ$$

Failure Mode Control

Check for bending-compression failure:

Effective compressive strain capacity as before:

$$\varepsilon_{uc} = 7,505 \text{microstrains}$$

Determine tendon radius of curvature at maximum compressive strain:

$$R_{ncMAX} = 257 \text{mm}$$

$$R_{ncMAX} < R_{\min}, \text{ therefore: } R_{cMAX} = R_{\min} = 505 \text{mm}$$

Determine the maximum net compressive strain:

$$\varepsilon_{bcMAX} = \frac{r}{R_{cMAX}} = 9,901 \text{microstrains [C]}$$

$$\varepsilon_{icMAX} = \frac{1}{4 \cdot (1 - \cos(\theta_e))} \cdot (\varepsilon_{bcMAX})^2 = 2,518 \text{microstrains [T]}$$

$$\varepsilon_{cMAX} = \varepsilon_{icMAX} - \varepsilon_{bcMAX} = 7,383 \text{microstrains [C]}$$

$$\varepsilon_{cMAX} < \varepsilon_{uc}$$

The maximum net compressive strain is less than the effective compressive strain capacity; therefore, the CFRP tendon will not exhibit bending-compression failure.

Check for bending-shear failure:

Effective longitudinal shear strain capacity:

$$\beta_u = 0.01$$

Determine minimum tendon radius of curvature:

$$R_{nf} = \frac{r}{2 \cdot (1 - \cos(\theta_e)) \cdot \left(\sqrt{1 + \frac{\varepsilon_{ut}}{(1 - \cos(\theta_e))}} - 1 \right)} = 397 \text{mm}$$

$$0.9R_{nf} = 357 \text{mm}$$

$$0.9R_{nf} < R_{\min}, \text{ therefore: } R_{\beta} = R_{\min} = 505 \text{mm}$$

Determine the maximum longitudinal bending-shear strain:

$$\beta_{\max} = \frac{1}{2} \cdot \sqrt{\frac{E}{b \cdot G}} \cdot \frac{r}{R_{\beta}} = 0.010272$$

$$\beta_{\max} > \beta_u$$

The maximum longitudinal shear strain is greater than the effective longitudinal shear strain capacity. Therefore, the CFRP tendon is likely to exhibit bending-shear failure and should not be used in this configuration. The minimum radius of curvature of the tendon is limited by the deviator size in this case; therefore, the deviator size should be increased.

Try a 550mm radius deviator and recheck for bending-shear failure:

$$R_d = 550mm$$

$$R_{\min} = R_d + r = 555mm$$

Determine the maximum longitudinal bending-shear strain:

$$0.9R_{nf} = 357mm$$

$$0.9R_{nf} < R_{\min}, \text{ therefore: } R_\beta = R_{\min} = 555mm$$

Determine the maximum longitudinal bending-shear strain:

$$\beta_{\max} = \frac{1}{2} \cdot \sqrt{\frac{E}{b \cdot G}} \cdot \frac{r}{R_\beta} = 0.009347$$

$$\beta_{\max} < \beta_u$$

The maximum longitudinal shear strain is less than the effective longitudinal shear strain capacity; therefore, the CFRP tendon will not exhibit bending-shear failure.

Tendon Tensile Capacity Reduction

Determine tendon radius of curvature at the point of tensile failure:

$$R_{nf} = 397mm$$

$$R_{nf} < R_{\min}, \text{ therefore: } R_f = R_{\min} = 555mm$$

The radius of curvature of the tendon at failure is equal to the minimum physical radius of curvature limited by the deviator size; therefore, the tensile capacity reduction factor can be calculated using transition effects with the extended model:

$$\phi_{te} = 1 - e^{-\sqrt{\frac{G}{E}} \frac{R_f}{r} \theta_r} = 0.9994$$

$$\phi_h = 1 - \frac{\phi_{te} \cdot r}{\epsilon_{ut} \cdot R_f} = 0.4601$$

Therefore, the tensile capacity of the tendon is reduced to approximately 46% of its ultimate tensile capacity:

$$\sigma'_{ut} = \phi_h \cdot \sigma_{ut} = 952 \text{ MPa}$$

The maximum tensile loading that can be applied to the tendon before failure can be calculated as:

$$P_f = \sigma'_{ut} \cdot A_t = 74.7 \text{ kN}$$

Figure 7-10 illustrates the strain versus applied load graph for the given harped CFRP tendon configuration with the increased deviator radius and highlights the occurrence of bending-tension failure. Comparing the strain-load curve to that for the initial configuration, it can be seen that the deviator size limits the bending strain component. By doing so, it prevents the maximum net compressive strain at the bottom of the tendon from reaching the effective compressive strain capacity.

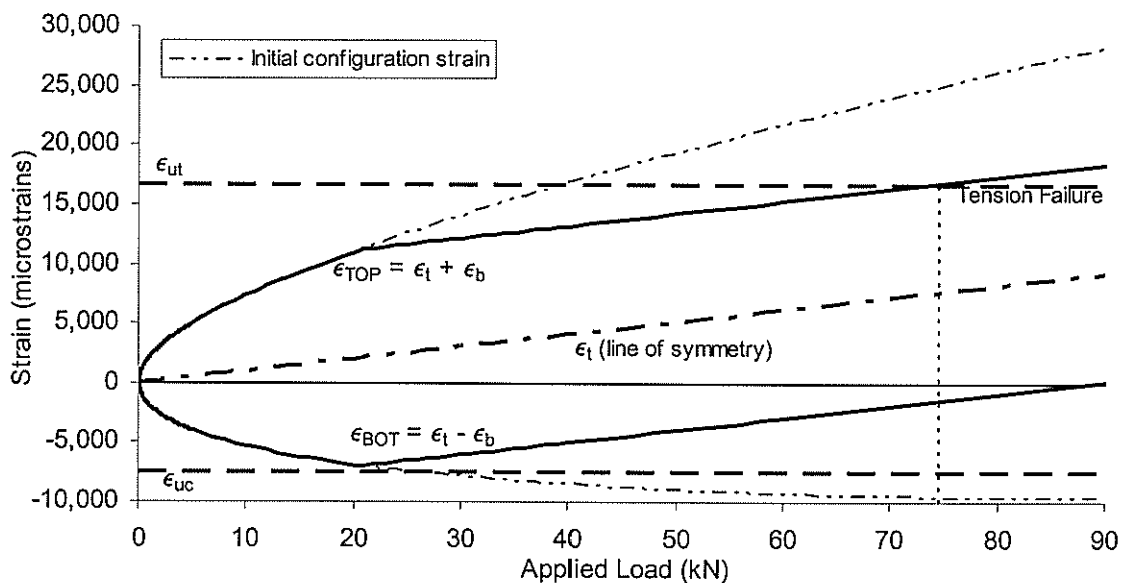


Figure 7-10: Strain vs. Loading Graph with Increased Deviator Size

Alternative 2: Decrease Effective Harping Angle

The effective harping angle is decreased by decreasing the total change in angle of the tendon at the deviator. This may be achieved in one of two ways: decreasing the overall harping angle or increasing the number of harping points. Either method will have the same effect on the design strength of the tendon. However, increasing the number of harping points can allow the overall harping angle to remain the same, which may be desirable. For this example, the overall harping angle will be kept at 8° , but two harping points will be used as illustrated in Figure 7-11.

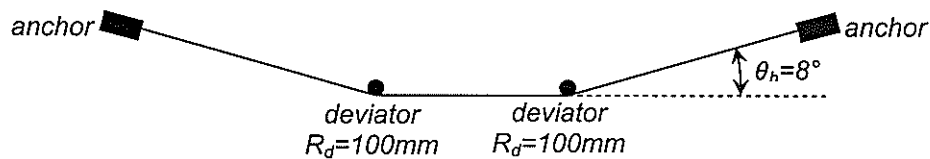


Figure 7-11: Harping Configuration for Design Example 1 - Alternative 2

Effective Harping Angle

The tendon is given as having two harping points and an overall harping angle of 8° .

The total change in angle at each deviator is:

$$\Delta\theta_h = 8^\circ$$

Therefore, the effective harping angle is:

$$\theta_e = \frac{1}{2} \cdot \Delta\theta_h = 4^\circ$$

It can be noted that this has the same effect on the design strength as keeping a single harping point and reducing the overall harping angle to 4° .

Failure Mode Control

Check for bending-compression failure:

Effective compressive strain capacity as before:

$$\varepsilon_{uc} = 7,505 \text{ microstrains}$$

Determine tendon radius of curvature at maximum compressive strain:

$$R_{ncMAX} = \frac{r}{2 \cdot (1 - \cos(\theta_e))}$$

$$R_{ncMAX} = 1026mm$$

$$R_{ncMAX} > R_{min}, \text{ therefore: } R_{cMAX} = R_{ncMAX} = 1026mm$$

Determine the maximum net compressive strain:

$$\varepsilon_{bcMAX} = \frac{r}{R_{cMAX}} = 4,872microstrains [C]$$

$$\varepsilon_{icMAX} = \frac{1}{4 \cdot (1 - \cos(\theta_e))} \cdot (\varepsilon_{bcMAX})^2 = 2,436microstrains [T]$$

$$\varepsilon_{cMAX} = \varepsilon_{icMAX} - \varepsilon_{bcMAX} = 2,436microstrains [C]$$

$$\varepsilon_{cMAX} < \varepsilon_{uc}$$

The maximum net compressive strain is less than the effective compressive strain capacity; therefore, the CFRP tendon will not exhibit bending-compression failure.

Check for bending-shear failure:

Effective longitudinal shear strain capacity:

$$\beta_u = 0.01$$

Determine minimum tendon radius of curvature:

$$R_{nf} = \frac{r}{2 \cdot (1 - \cos(\theta_e)) \cdot \left(\sqrt{1 + \frac{\varepsilon_{uf}}{(1 - \cos(\theta_e))}} - 1 \right)} = 570mm$$

$$0.9R_{nf} = 513mm$$

$$0.9R_{nf} > R_{min}, \text{ therefore: } R_{\beta} = R_{min} = 513mm$$

Determine the maximum longitudinal bending-shear strain:

$$\beta_{max} = \frac{1}{2} \cdot \sqrt{\frac{E}{b \cdot G}} \cdot \frac{r}{R_{\beta}} = 0.010115$$

$$\beta_{max} > \beta_u$$

The maximum longitudinal shear strain is greater than the effective longitudinal shear strain capacity. Therefore, the CFRP tendon is likely to exhibit bending-shear failure and should not be used in this configuration. Because the minimum radius of curvature of the tendon is not limited by the deviator size in this case, the effective harping angle should be decreased.

Try an overall harping angle of 7° .

Effective Harping Angle

The total change in angle at each deviator is:

$$\Delta\theta_h = 7^\circ$$

Therefore, the effective harping angle is:

$$\theta_e = \frac{1}{2} \cdot \Delta\theta_h = 3.5^\circ$$

Failure Mode Control

The effective harping angle has been decreased, therefore, the maximum net compressive strain will also have decreased and will still be less than the effective compressive strain capacity; therefore, the CFRP tendon will not exhibit bending-compression failure and need not be rechecked.

Check for bending-shear failure:

Determine minimum tendon radius of curvature:

$$R_{nf} = \frac{r}{2 \cdot (1 - \cos(\theta_e)) \cdot \left(\sqrt{1 + \frac{\varepsilon_{ut}}{(1 - \cos(\theta_e))}} - 1 \right)} = 623mm$$

$$0.9R_{nf} = 560mm$$

$$0.9R_{nf} > R_{\min}, \text{ therefore: } R_\beta = R_{\min} = 560mm$$

Determine the maximum longitudinal bending-shear strain:

$$\beta_{\max} = \frac{1}{2} \cdot \sqrt{\frac{E}{b \cdot G}} \cdot \frac{r}{R_{\beta}} = 0.009258$$

$$\beta_{\max} < \beta_u$$

The maximum longitudinal shear strain is less than the effective longitudinal shear strain capacity; therefore, the CFRP tendon will not exhibit bending-shear failure.

Tendon Tensile Capacity Reduction

Determine tendon radius of curvature at the point of tensile failure:

$$R_{nf} = 623mm$$

$$R_{nf} > R_{\min}, \text{ therefore: } R_f = R_{\min} = 623mm$$

The radius of curvature of the tendon at failure is not limited by the deviator size; therefore, the tensile capacity reduction factor can be calculated using the primary model:

$$\phi_h = 1 - \frac{r}{\varepsilon_{ut} \cdot R_f} = 0.5184$$

Therefore, the tensile capacity of the tendon is reduced to approximately 52% of its ultimate tensile capacity:

$$\sigma'_{ut} = \phi_h \cdot \sigma_{ut} = 1,072MPa$$

The maximum tensile loading that can be applied to the tendon before failure can be calculated as:

$$P_f = \sigma'_{ut} \cdot A_t = 84.2kN$$

Figure 7-12 illustrates the strain versus applied load graph for the given harped CFRP tendon configuration with the decreased effective harping angle and highlights the occurrence of bending-tension failure. Comparing the strain-load curve to that for the initial configuration, it can be seen that lowering the effective

harping angle decreases the maximum net compressive strain at the bottom of the tendon and prevents it from reaching the effective compressive strain capacity.

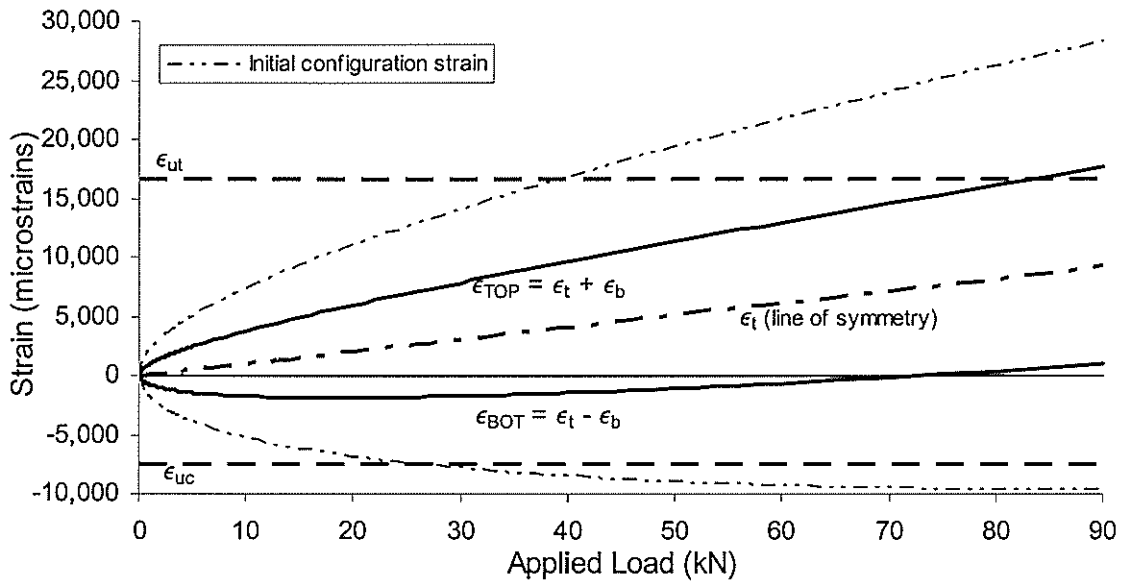


Figure 7-12: Strain-Loading Graph with Decreased Effective Harping Angle

7.9.2 Design Example 2

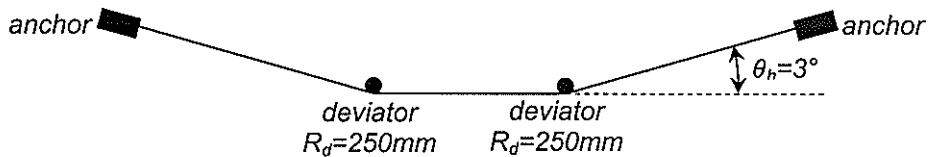


Figure 7-13: Initial Harping Configuration for Design Example 2

A 10mm diameter CFRP prestressing tendon is to be harped at an angle of 3° over two deviators with a radius of 250mm as illustrated in Figure 7-13. Resolve any failure mode problems and determine the tensile design capacity of the tendon.

The material properties of the CFRP tendon are as follows:

$$E = 124GPa$$

$$\epsilon_{ut} = 16,677 \text{ microstrains}$$

$$\sigma_{ut} = E \cdot \epsilon_{ut} = 2,068MPa$$

$$G = 7.2GPa$$

The geometric harping configuration variables have been given as:

$$\theta_h = 3^\circ$$

$$r = 5mm, A_t = 78.54mm^2$$

$$R_d = 250mm$$

Therefore, the minimum physical radius of curvature of the tendon is:

$$R_{min} = R_d + r = 255mm$$

Effective Harping Angle

The tendon is given as having two harping points with an overall harping angle of 3° . The total change in angle at each deviator is:

$$\Delta\theta_h = 3^\circ$$

Therefore, the effective harping angle is:

$$\theta_e = \frac{1}{2} \cdot \Delta\theta_h = 1.5^\circ$$

Failure Mode Control

Check for bending-compression failure:

Effective compressive strain capacity as before:

$$\varepsilon_{uc} = 7,505 \text{microstrains}$$

Determine tendon radius of curvature at maximum compressive strain:

$$R_{ncMAX} = \frac{r}{2 \cdot (1 - \cos(\theta_e))} = 7,296mm$$

$$R_{ncMAX} > R_{min}, \text{ therefore: } R_{cMAX} = R_{ncMAX} = 7,296mm$$

Determine the maximum net compressive strain:

$$\varepsilon_{bcMAX} = \frac{r}{R_{cMAX}} = 685 \text{microstrains [C]}$$

$$\varepsilon_{icMAX} = \frac{1}{4 \cdot (1 - \cos(\theta_e))} \cdot (\varepsilon_{bcMAX})^2 = 343 \text{microstrains [T]}$$

$$\varepsilon_{cMAX} = \varepsilon_{icMAX} - \varepsilon_{bcMAX} = 343 \text{microstrains [C]}$$

$$\varepsilon_{cMAX} < \varepsilon_{uc}$$

The maximum net compressive strain is less than the effective compressive strain capacity; therefore, the CFRP tendon will not exhibit bending-compression failure.

Check for bending-shear failure:

Effective longitudinal shear strain capacity:

$$\beta_u = 0.01$$

Determine minimum tendon radius of curvature:

$$R_{nf} = \frac{r}{2 \cdot (1 - \cos(\theta_e)) \cdot \left(\sqrt{1 + \frac{\varepsilon_{ut}}{(1 - \cos(\theta_e))}} - 1 \right)} = 1,206mm$$

$$0.9R_{nf} = 1,086mm$$

$$0.9R_{nf} > R_{min}, \text{ therefore: } R_\beta = R_{min} = 1,086mm$$

Determine the maximum longitudinal bending-shear strain:

$$\beta_{max} = \frac{1}{2} \cdot \sqrt{\frac{E}{b \cdot G}} \cdot \frac{r}{R_\beta} = 0.00346$$

$$\beta_{max} < \beta_u$$

The maximum longitudinal shear strain is less than the effective longitudinal shear strain capacity; therefore, the CFRP tendon will not exhibit bending-shear failure.

Tendon Tensile Capacity Reduction

Determine tendon radius of curvature at the point of tensile failure:

$$R_{nf} = 1,206mm$$

$$R_{nf} > R_{min}, \text{ therefore: } R_f = R_{min} = 1,206mm$$

The radius of curvature of the tendon at failure is not limited by the deviator size; therefore, the tensile capacity reduction factor can be calculated using the primary model:

$$\phi_h = 1 - \frac{r}{\epsilon_{ut} \cdot R_f} = 0.7515$$

Therefore, the tensile capacity of the tendon is reduced to approximately 75% of its ultimate tensile capacity:

$$\sigma'_{ut} = \phi_h \cdot \sigma_{ut} = 1,655 \text{MPa}$$

The maximum tensile loading that can be applied to the tendon before failure can be calculated as:

$$P_f = \sigma'_{ut} \cdot A_t = 130.0 \text{kN}$$

Figure 7-14 illustrates the strain versus applied load graph for design example 2 and highlights the occurrence of bending-tension failure.

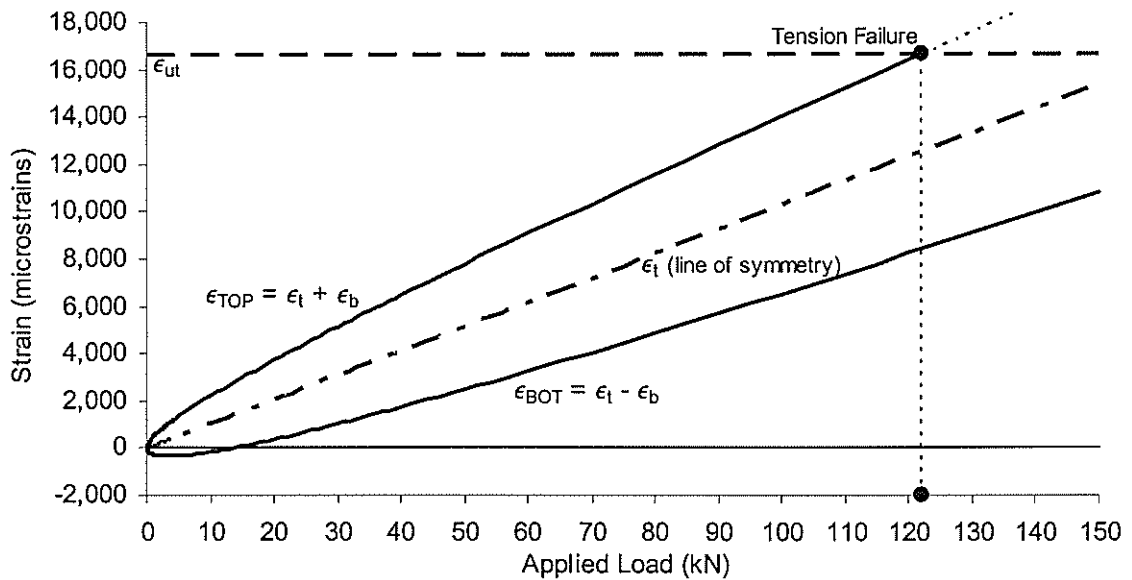


Figure 7-14: Strain vs. Loading Graph for Design Example 2

8 CONCLUSIONS AND RECOMMENDATIONS

8.1 INTRODUCTION

The effect of harping CFRP prestressing tendons on their tensile capacity was investigated both experimentally and through development of an analytical model. Various harping configuration variables were used: tendon size, deviator size and harping angle. A range of practical values for the configuration variables were utilised in the test program – tendon diameter (9.5mm & 6.3mm), deviator radius (50mm, 100mm, 250mm, 500mm & 1000mm) and harping angle (2, 3, 5, 6, 9, 10 & 15). Specimens subject to a total of 24 unique configuration variable combinations were tested to failure under tensile loading, recording the mode of failure and failure load level.

Two analytical models for predicting the tendon capacity reduction due to harping were developed. The primary model was based on classic elastic bending theory and equilibrium. The extended model refined the primary model to include longitudinal shear deformation, by discretizing the tendon into an equivalent spring frame model and analysing it using the matrix stiffness method for structures. The equivalent spring frame model accounts for transition effects or stress discontinuities in the tendon where it transitions from the curved portion to the straight portion. Within this region, plane sections rotate away from perpendicular to the neutral axis to effect a smooth bending stress transition. The transition effects reduce the effective stiffness and can reduce the axial bending strains

Further to the extended model, closed form equations for key values were developed by a regression analysis of the equivalent spring frame model solutions.

Based on the recorded data and the analytical models, harped CFRP prestressing tendon tensile strength design procedures were developed, including a failure mode control and a tensile capacity reduction calculation.

8.2 CONCLUSIONS

The harped CFRP prestressing tendon tensile strength design procedures developed from the experimental program and analytical models performed quite well. Good agreement was seen between the measured data and the predicted strength as determined by the analytical models.

Based on the experimental research program and analytical model development, the following conclusions can be drawn:

Material Properties

- 1) The CFRP tendon material properties, as supplied by the tendon manufacturer, showed a significant scatter, which was reflected in the experimental data from testing harped tendons.
- 2) The guaranteed minimum and laboratory tested maximum properties, as supplied by the tendon manufacturer, provided adequate lower and upper bounds for the expected deviation of the actual versus predicted failure level correlation.

Experimental Test Data – Tendon Behaviour

- 1) Three possible failure modes were observed in the experimental program: bending-tension, bending-compression and bending-shear failure.
- 2) Bending-compression and bending-shear failure modes typically occurred at much lower load levels than bending-tension failure, and should be avoided.

- 3) Bending-compression failures typically occurred at large harping angles.
- 4) Bending-shear failures typically occurred at medium to large harping angles with small deviator sizes.
- 5) Increasing the harping angle decreased the tensile capacity of the harped tendon.
- 6) Decreasing the deviator size decreased the tensile capacity of the harped tendon when the tendon radius of curvature was physically limited by the deviator.

Existing Analytical Models

- 1) The JSCE model for characteristic strength showed a very poor correlation with the test data and was very unconservative.
- 2) The JSCE model for the design strength, including a material coefficient, showed a slightly better correlation with the test data, but was still unconservative for many configurations.
- 3) The Gilstrap model showed a very poor correlation with the test data and was too conservative to allow an efficient use of harped tendons.
- 4) The Ahmad model was unconservative for all the data points when the maximum tensile strain determined in their test program was used as a failure criterion.
- 5) The Ahmad model showed a much better correlation with the test data when the guaranteed minimum tensile strain for the CFRP material used in the current test program was substituted into the model, but was still unconservative for many harping configurations.

- 6) The Ahmad model was difficult to use, as it requires variables to be input in specific units of measure.

Proposed Analytical Models

- 1) A harped CFRP tendon assumes a natural radius of curvature determined by its stiffness, harping configuration variables and the equilibrium of internal and external forces, unless it is physically limited by the deviator radius.
- 2) The primary model developed showed a good correlation with the test data when used with the guaranteed minimum material properties, and was moderately conservative.
- 3) The extended model, an extension of the primary model that included transition effects, also showed a good correlation with the test data.
- 4) The transition effects, as implemented in the extended model, gave only a small change in the calculated tensile strength reduction in comparison to the primary model, especially when the radius of curvature was not physically limited by the deviator.
- 5) The extended model describes the top fibre axial strain distribution along the tendon through the transition zone.
- 6) The extended model allowed longitudinal shear deformation and stress to be approximated.
- 7) Closed form equations to compute the maximum top fibre strain and the maximum longitudinal shear deformation in the extended model, derived by regression analysis, showed a virtually perfect correlation with the full model calculations, and provided a simpler method for the calculation of these values.

Failure Mode Control

- 1) The effective compressive capacity of the tendon was lower than its tensile capacity, which gives rise to the possibility of the occurrence of a bending-compression failure.
- 2) The longitudinal shear deformation and stress, computed using the extended model, was used to determine whether bending-shear failure would take place.
- 3) Effective failure mode control guidelines were developed based on the effective compressive capacity, effective shear capacity and the analytical models.
- 4) The use of multiple deviators can reduce the tensile strength reduction for harped CFRP tendons while maintaining the overall harping angle.

8.3 RECOMMENDATIONS

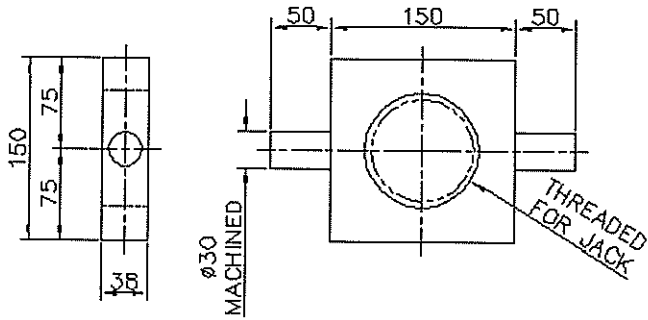
From the experimental program and analytical model development, recommendations can be made for improving CFRP material manufacturing and future research to increase the efficiency of harped CFRP tendons:

- 1) The production of CFRP tendons with more consistent material properties should be considered. Large variations in the material properties result in guaranteed minimum material properties for CFRP tendons that can be substantially lower than their maximum material properties. Since the calculated design strength is based on the guaranteed minimum material properties, tendons with actual material properties that are closer to the maximum values would have calculated design strengths that are much lower than their potential design strengths.

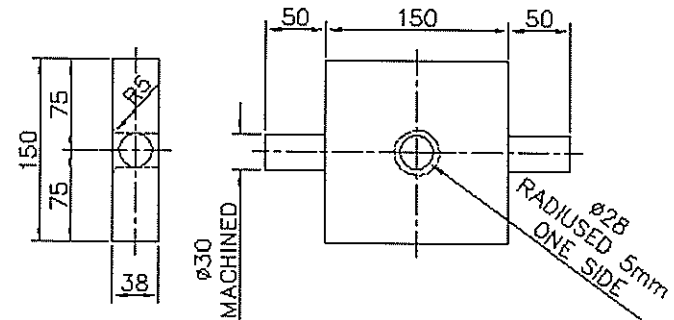
- 2) The development of CFRP tendons with material properties that minimize their strength reduction due to harping should be investigated. This may be achieved by increasing the length of the transition zone, thereby increasing the influence of transition effects on the tendon behaviour. The length of the transition zone may be increased by reducing the magnitude of the longitudinal shear modulus relative to the magnitude of the tensile modulus for the CFRP material.
- 3) Guaranteed minimum compressive strength, longitudinal shear strength and longitudinal shear modulus were shown to have an influence on the calculation of the design strength and failure mode for harped CFRP tendons. Therefore, these material properties need to be tested and published together with the other material properties for manufactured CFRP tendons.
- 4) Failure mode control was shown to be an important aspect of harped CFRP tendon design. However, the design recommendations developed are specific to the particular material used in this research program. Further research should focus on the effects of bending-shear and bending-compression failure. This will facilitate the further development of failure mode control criteria in conjunction with the previous recommendation for additional material property data.

**APPENDIX A: SHOP FABRICATION DRAWINGS FOR
TEST FRAME**

Figure A-1: Anchor Pivot Axle Fabrication



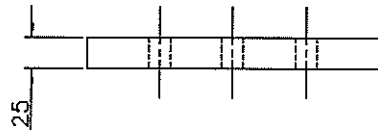
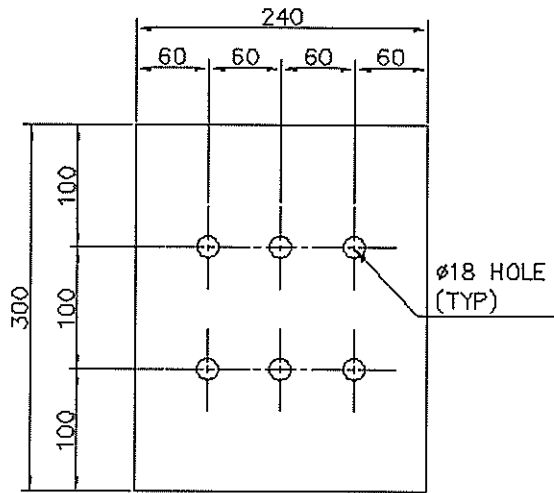
JACK END AXLE
 Mk. No. TGQ01-01
 1 REQ'D
 MATERIAL: 1-1/2" PL



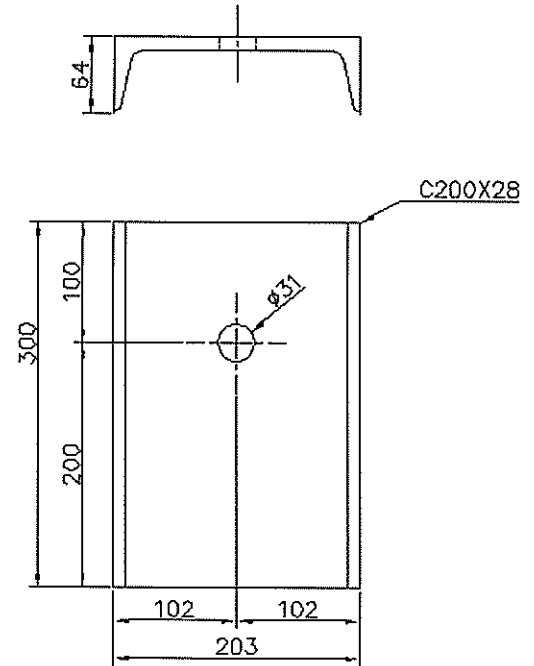
DEAD END AXLE
 Mk. No. TGQ01-02
 1 REQ'D
 MATERIAL: 1-1/2" PL

NOTES: ALL DIMENSIONS IN mm	PROJECT:	DEVIATOR	STUDENT: TREVOR QUAYLE
		MASc EXPERIMENTAL PROGRAMME	ADVISOR: K. SOUDKI/J. WEST
			DATE: JUNE 9, 2003
	JOB No.: 01251		DWG. No.: TGQ01-FD1-R0

Figure A-2: Anchor Pivot Base Fabrication



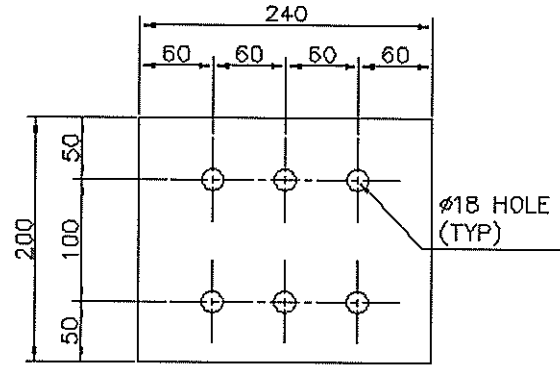
PIVOT BASE PLATE
 Mk. No. TGQ01-03
 2 REQ'D
 MATERIAL: 1" PL



PIVOT SIDE PLATE
 Mk. No. TGQ01-04
 4 REQ'D
 MATERIAL: C200x28

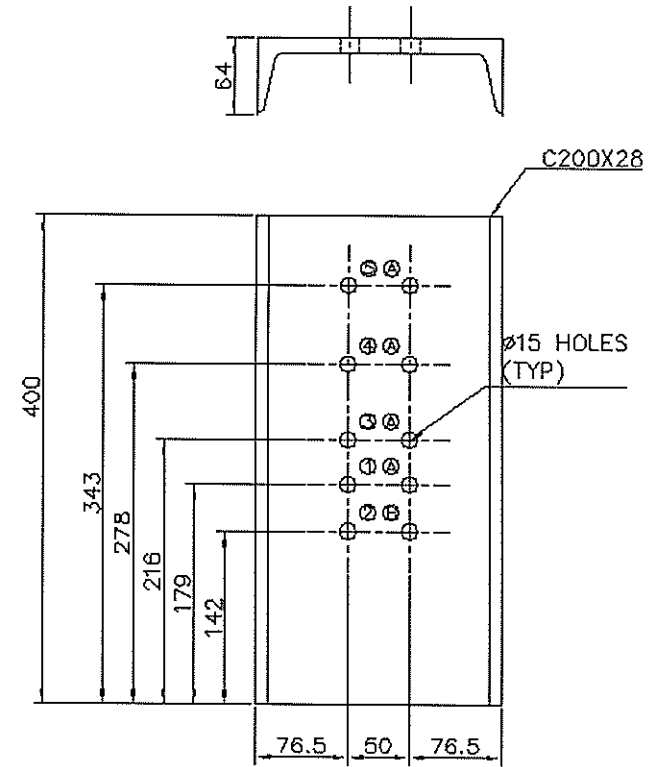
NOTES: ALL DIMENSIONS IN mm	PROJECT:	DEVIA TOR MASc EXPERIMENTAL PROGRAMME	STUDENT: TREVOR QUAYLE
			ADVISOR: K. SOUDKI/J. WEST
			DATE: JUNE 9, 2003
	JOB No.: 01251		DWG. No.: TGQ01-F02-R0

Figure A-3: Deviator Forks Fabrication



PIVOT SIDE PLATE

Mk. No. TGQ01-05
1 REQ'D
MATERIAL: 1" PL



DEVIATOR FORK SIDE PLATE

Mk. No. TGQ01-06
2 REQ'D
MATERIAL: C200x28

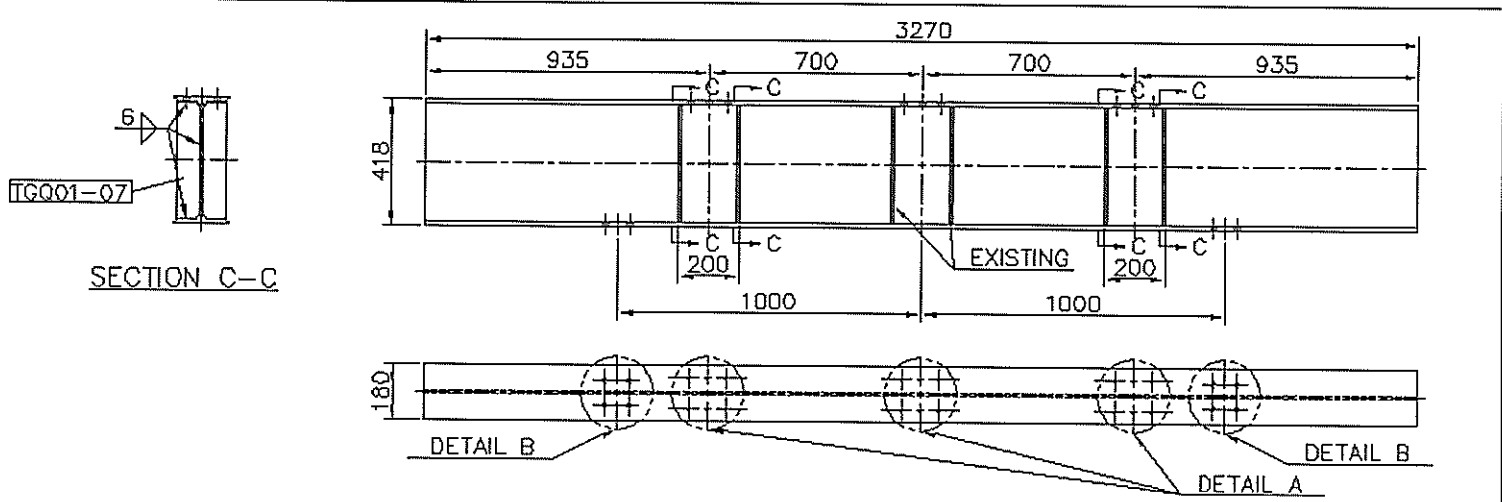
NOTES: ALL DIMENSIONS IN mm

PROJECT: DEVIATOR
MAsc EXPERIMENTAL
PROGRAMME

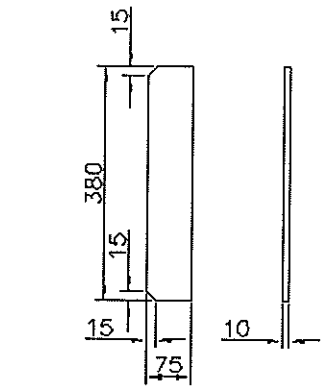
STUDENT: TREVOR QUAYLE
ADVISOR: K. SOUDKI/J. WEST
DATE: JUNE 9, 2003

JOB No.: 01251

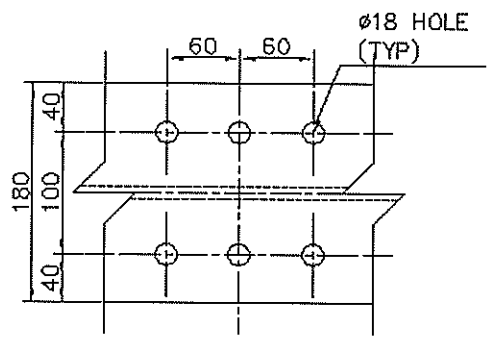
DWG. No.: TGQ01-F03-R0



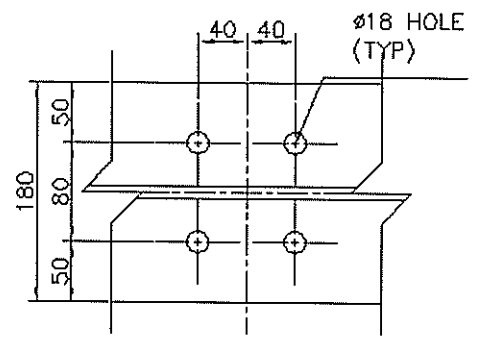
TEST FRAME MAIN BEAM
 Mk. No. TGQD1-08
 1 REQ'D



BEAM STIFFENER
 Mk. No. TGQ01-07
 8 REQ'D
 MATERIAL: 3/8" PL



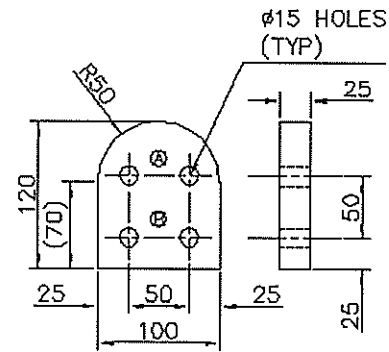
DETAIL A
 (TOP FLANGE)



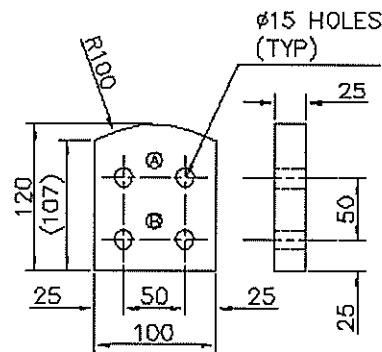
DETAIL B
 (BOTTOM FLANGE)

NOTES: ALL DIMENSIONS IN mm	PROJECT: <u>DEVIATOR</u>	STUDENT: TREVOR QUAYLE
	MASc EXPERIMENTAL PROGRAMME	ADVISOR: K. SOUDKI/J. WEST
	JOB No.: 01251	DATE: JUNE 9, 2003
		DWG. No.: TGQD1-F04-R0

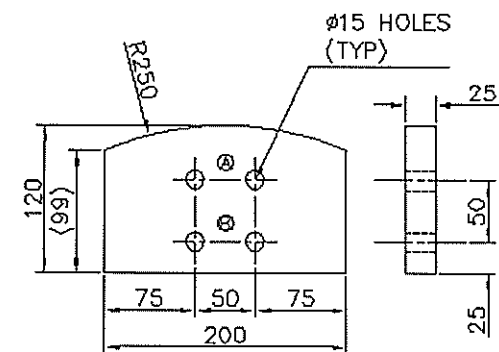
Figure A-4: Main Beam Fabrication



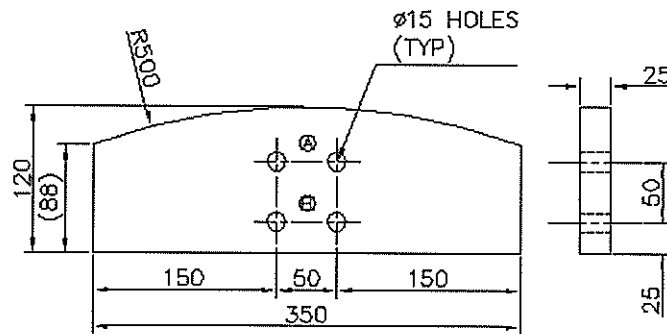
DEVIATOR - 50R
Mk. No. TGQ01-D50R
1 REQ'D
MATERIAL: 1" PL



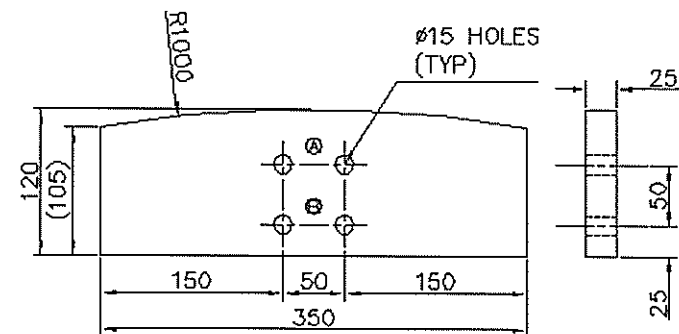
DEVIATOR - 100R
Mk. No. TGQ01-D100R
1 REQ'D
MATERIAL: 1" PL



DEVIATOR - 250R
Mk. No. TGQ01-D250R
1 REQ'D
MATERIAL: 1" PL



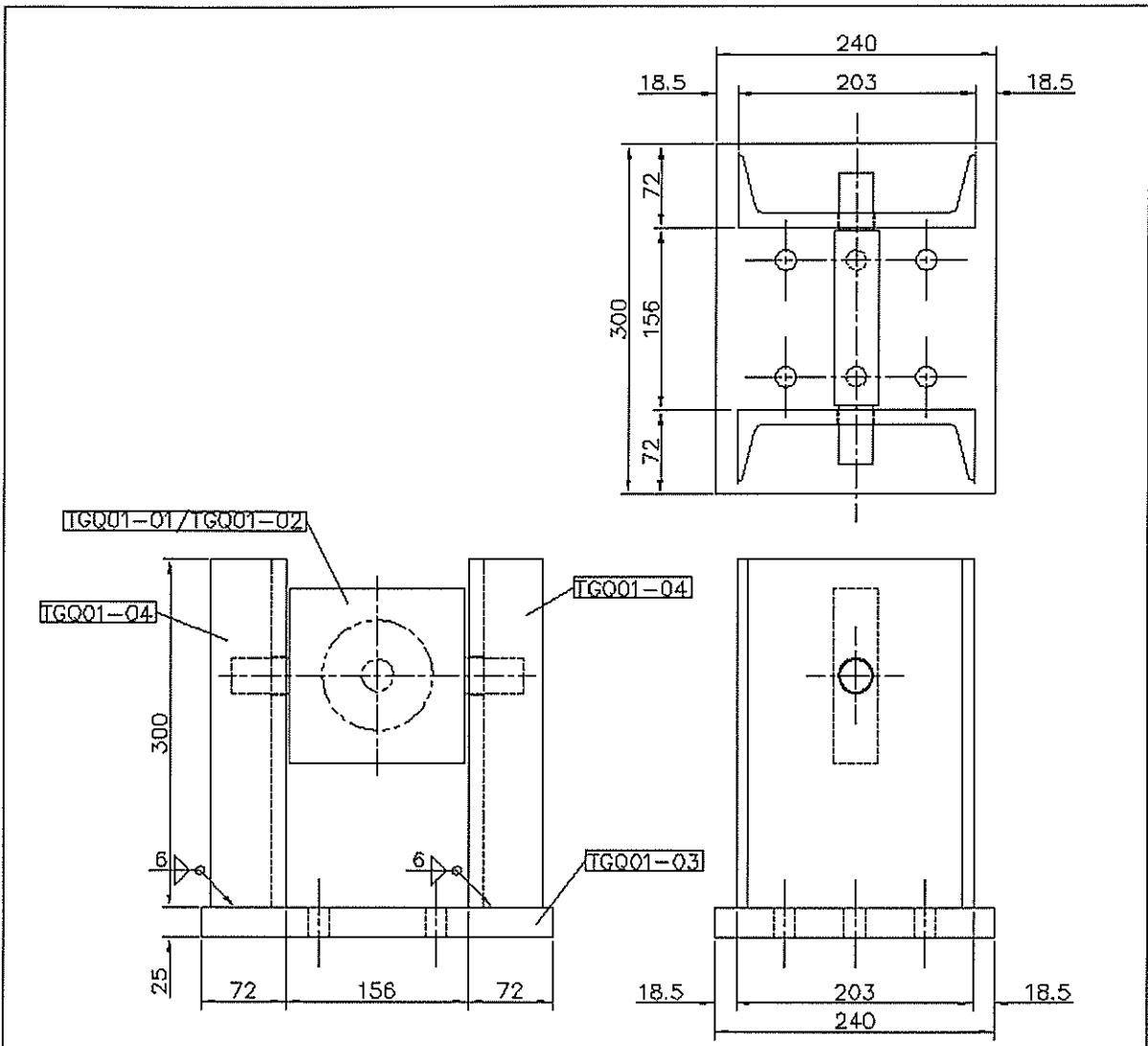
DEVIATOR - 500R
Mk. No. TGQ01-D500R
1 REQ'D
MATERIAL: 1" PL



DEVIATOR - 1000R
Mk. No. TGQ01-D1000R
1 REQ'D
MATERIAL: 1" PL

Figure A-5: Deviator Fabrication

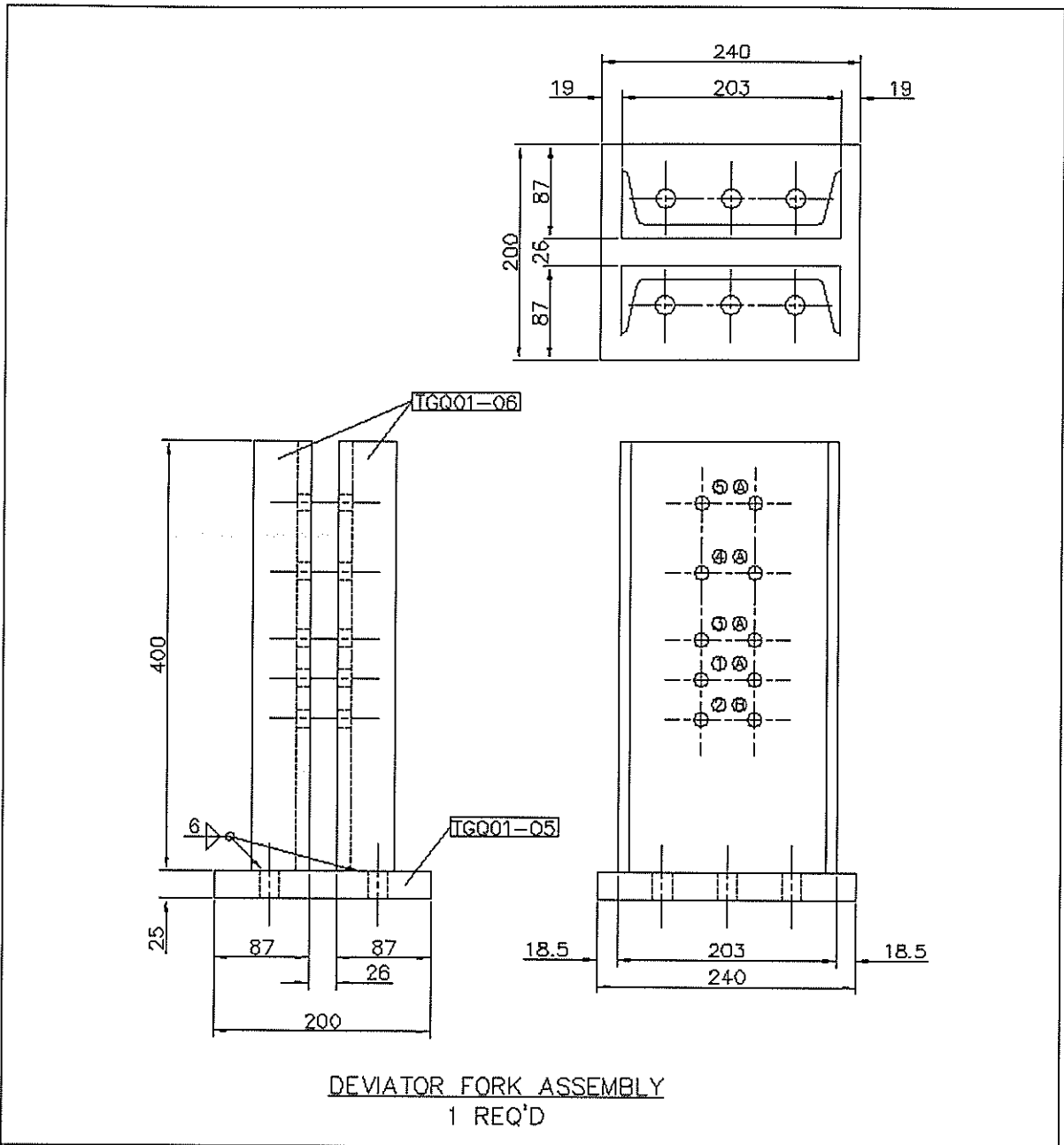
NOTES: ALL DIMENSIONS IN mm	PROJECT: <u>DEVIATOR</u>	STUDENT: TREVOR QUAYLE
	MASc EXPERIMENTAL PROGRAMME	ADVISOR: K. SOUDKI/J. WEST
	JOB No.: 01251	DATE: JULY 28, 2003
		DWG. No.: TGQ01-F05-R0



PROJECT: ANCHOR PIVOT ASSEMBLY
 2 REQ'D - 1 w/TGQ01-01, 1 w/TGQ01-02

PROJECT: <u>DEVIATOR</u> MASc EXPERIMENTAL PROGRAMME	
NOTES: ALL DIMENSIONS IN mm SEE DWGS TGQ01-F01-R0 & TGQ01-F02-R0 FOR PARTS FABRICATION	STUDENT: TREVOR QUAYLE
	ADVISOR: K. SOUDKI/J. WEST
JOB No.: 01251	DATE: JUNE 9, 2003
	DWG. No.: TGQ01-A01-R0

Figure A-6: Anchor Pivot Assembly



PROJECT: DEVIATOR MASc EXPERIMENTAL PROGRAMME	
NOTES: ALL DIMENSIONS IN mm SEE DWG TGQ01-F03-R0 FOR PARTS FABRICATION	STUDENT: TREVOR QUAYLE ADVISOR: K. SOUDKI/J. WEST DATE: JUNE 9, 2003
JOB No.: 01251	DWG. No.: TGQ01-A02-R0

Figure A-7: Deviator Fork Assembly

APPENDIX B: FAILURE DATA FOR CONFIGURATIONS WITH MULTIPLE SPECIMENS

Table B-1: Failure Data for Harping Configurations with Multiple Specimens

Specimen		Tendon Diameter mm	Deviator Radius mm	Harp Angle deg	Failure Stress MPa	% Ultimate ($f_u=2068\text{MPa}$)	Failure Mode ^A
8	A	9.5	500	5	1508.1	72.93%	T
	B	9.5	500	5	1426.0	68.96%	T
	C	9.5	500	5	1071.9	51.83%	T
	Average	9.5	500	5	1335.3	64.57%	-
9	A	9.5	500	5	1115.6	53.95%	T
	B	9.5	500	5	969.8	46.90%	T
	Average	9.5	500	5	1042.7	50.42%	-

^A Failure mode: T = tension, C = compression, S = shear

REFERENCES

- Adachi, Y., Hayashida, M., Sakai, H., Mashima, M. and Miyagawa, T., 1997. Strengthening of Prestressed Concrete Segmental T-Beam Bridge Using FRP External Prestressing Systems, *Proceedings of Non-Metallic (FRP) Reinforcement For Concrete Structures*, pp. 695-702.
- Ahmad, S.H., Jerret, C.V., and Zia, P. 1997. Carbon Fibre-Reinforced Polymer (CFRP) Tendons Subjected to Combined Axial Load and Harping. *High-Performance Concrete: Design and Materials and Recent Advances in Concrete Technology*, ACI, Kuala Lumpur, Malaysia, SP-172, pp. 427-443.
- Al-Mayah, A., 1999. Experimental and Analytical Investigation of Wedge Anchors for CFRP Rods Under Load, MAsc Thesis, University of Waterloo, Waterloo, ON, Canada.
- Al-Mayah, A., 2004. *Interfacial Behaviour of CFRP-Metal Couples for Wedge Anchor Systems*, PhD Thesis, University of Waterloo, Waterloo, ON, Canada.
- Bakis, C.E., Bank, L.C., Brown, V.L., Cosenza, E., Davalos, J.F, Lesko, J.J., Machida, A., Rizkalla, S.H, Triantafillou, T.C., 2002. Fiber-Reinforced Polymer Composites for Construction - State-of-the-Art Review, *Journal of Composites for Construction*, ASCE, 6(2), pp. 73-87
- Beer, F.P., Johnston, E.R.Jr., DeWolf, J.T, 2002. *Mechanics of Materials – Third Edition*, McGraw-Hill, New York, NY.
- Burgoyne, C.J., 1999. Advanced Composites in Civil Engineering in Europe. *Structural Engineering International*, 9(4), pp. 267-273.
- Clarke, J.L., 1993. Alternative Materials for the Reinforcement and Prestressing of Concrete, Blackie Academic & Professional, Glasgow, UK.
- El Refai, A.M., West, J.S, and Soudki, K., 2004. FRP Tendons in Post-Tensioning, *PTI Journal*, 1(3), pp.22-29
- Dolan, C.W., 1999. FRP Prestressing in the U.S.A., *Concrete International*, 21(10), pp. 21-24.

- Dolan, C.W., Bakis, C.E., and Nanni, A., 2001. *Design Recommendations for Concrete Structures Prestressed With FRP Tendons*. Report No. DTFH61-96-C-00019, University of Missouri Rolla, Rolla, Missouri, USA.
- Gilstrap, J.M., Dolan, C.W., and Hamilton, H.R. III., 2001. Characterization of Fiber Reinforced Polymer Prestressing Tendons. *FHWA Contract DTFH61-96-C-00019: FRP Prestressing for Highway Bridges, Volume II*, University of Wyoming, Laramie, WY, USA.
- Grace, N.F., and Abdel-Sayed, G. 1998. Behavior of Externally Draped CFRP Tendons in Prestressed Concrete Bridges. *PCI Journal*, PCI, 48(5), pp. 88-101.
- Grace, N.F., Navarre, F.C., Nacey, R.B., Bonus, W., Collavino, L., 2002. Design-Construction of Bridge Street Bridge – First CFRP Bridge in the United States, *PCI Journal*, 47(5), pp. 20-35
- Grace, N.F., Abdel-Sayed, G., Navarre, F.C., Nacey, R.B., Bonus, W., Collavino, L., 2003. Full-Scale Test of Prestressed Double-Tee Beam, *Concrete International*, 25(4), pp. 52-58
- Hassanain, M.A., and Reda Taha, M. M., 2002. Design Economics of HPC Girder Bridges Prestressed With CFRP Tendons, *4th Structural Specialty Conference of the Canadian Society for Civil Engineering*, CSCE, Montréal, PQ, Canada.
- Hughes Brothers Inc., 2002. Carbon Fibre Reinforced Polymer (CFRP) Rebar: Aslan 200, Product Information Sheet, Seward, NK, USA.
- Japan Society of Civil Engineers (JSCE). 1997. Recommendations for Design and Construction of Concrete Structures Using Continuous Fibre Reinforcing Materials. *JSCE Concrete Engineering Series, No. 23*, JSCE, Tokyo, Japan.
- Machida, A., and Maruyama, K., 2002. Design Code Development for Fibre-Reinforced Polymer Structures and Repairs, *Progress in Structural Engineering and Materials*, 4(2), pp. 149-160, John Wiley & Sons, Ltd.

- Mutsuyoshi, H. and Machida, A. 1993. Behaviour of Prestressed Concrete Beams Using FRP as External Cables. *Fiber-Reinforced-Plastic Reinforcement for Concrete Structures: International Symposium*, ACI, Vancouver, BC, Canada, SP-138, pp. 401-417.
- Piggot, M.R., Harris, B., 1980. Compression Strength of Carbon, Glass and Kevlar-49 Fiber Reinforced Polyester Resins, *Journal of Materials Science*, 15, pp. 2523-38.
- Pisaniu, M.A., 1998. A Numerical Survey on the Behaviour of Beams Pre-Stressed With FRP Cables, *Construction and Building Materials*, 12(4) , pp. 221-232
- Rizkalla, S., Shehata, E., Abdelrahman, A., and Tandros, G., 1998. A New Generation: Design and Construction of a Highway Bridge with CFRP, *Concrete International*, 20(6), pp. 35-38
- Scalzi, J.B., 2000, Will FRP Composites Ever Change Bridge Engineering?, *Concrete International*, 22(4), pp. 56-58.
- Swanson, S.R., 1990. A Model for Compression Failure in Fibre Composite Laminates, *Recent Developments in Composite Materials Structures*, ASME, New York, NY, pp. 81-85.
- Taniguchi, H., Mutsuyoshi, H., Kita, T., and Machida, A., 1997. Flexural Behaviour of Externally Prestressed Concrete Beams Using CFRP and Aramid Rope Under Static and Dynamic Loading, *Proceedings of the Third International Symposium on Non-Metallic (FRP) Reinforcement for Concrete Structures, Vol.2*, Sapporo, Japan.